Personalizing Brain Pathology Analysis Using Temporal Resting State fMRI Signal Complexity Analysis

PERSONALIZING BRAIN PATHOLOGY ANALYSIS USING TEMPORAL RESTING STATE FMRI SIGNAL COMPLEXITY ANALYSIS

BY

OLGA M. DONA LEMUS, B.Sc.,M.Sc.

A THESIS

SUBMITTED TO THE SCHOOL OF GRADUATE STUDIES

OF MCMASTER UNIVERSITY

IN PARTIAL FULFILMENT OF THE REQUIREMENTS

FOR THE DEGREE OF

DOCTOR OF PHILOSOPHY

Doctor of Philosophy (2017) McMaster University

(Biomedical Engineering) Hamilton, Ontario, Canada

TITLE:	Personalizing Brain Pathology Analysis Using Temporal Resting State fMRI Signal Complexity Analysis
AUTHOR:	Olga M. Dona Lemus (Hon) B.Sc., M.Sc., (Medical Physics) McMaster University, Hamilton, Ontario Canada
SUPERVISOR:	Dr. Michael D. Noseworthy
NUMBER OF PAGES:	xvi, 174

To those who have failed and keep trying.

. . . . . .

Fractal geometry will make you see everything differently. There is a danger in reading further. You risk the loss of your childhood vision of clouds, forests, flowers, galaxies, leaves, feathers, rocks, mountains, torrents of water, carpet, bricks, and much else besides. Never again will your interpretation of these things be quite the same.

Michael F. Barnsley, Fractals Everywhere (2000), 1

Abstract

Assessment of diffuse brain disorders, where the brain may appear normal, has proven difficult to translate into personalized treatments. Previous methods based on brain magnetic resonance imaging (MRI) resting state blood oxygen level dependent (rs-BOLD) signal routinely rely on group analysis where large data sets are assessed using region-of interest (ROI) or probabilistic independent component analysis (PICA) to identify temporal synchrony or desynchrony among regions of the brain.

Brain connectivity occurs in a complex, multilevel and multi-temporal manner, driving the fluctuations observed in local oxygen demand. These fluctuations have previously been characterized as fractal, as they auto-correlate at different time scales. In this study we propose a model-free complexity analysis based on the fractal dimension of the rs-BOLD signal, acquired with MRI. The fractal dimension can be interpreted as a measure of signal complexity and connectivity. Previous studies have suggested that reduction in signal complexity can be associated with disease. Therefore, we hypothesized that a detectable differences in rs-BOLD signal complexity could be observed between patients with diffuse or heterogeneous brain disorders and healthy controls.

In this study, we obtained anatomical and functional data from patients with brain disorders where traditional methods have been insufficient to fully assess the

condition. More specifically, we tested our method on mild traumatic brain injury, autism spectrum disorder, chemotherapy-induced cognitive impairment and chronic fatigue syndrome patients. Three major databases from the Neuroimaging Informatics Tools and Resources Clearinghouse (NITRC) project were used to acquire large numbers of age matched healthy controls. Healthy control data was downloaded from the the Autism Brain Imaging Data Exchange (ABIDE), the Alzheimer's Disease Neuroimaging Initiative (ADNI) and the Human Connectome Project specifically matching our experimental design.

In all of our studies, the voxel-wise rs-BOLD signal fractal dimension was calculated following a procedure described by Eke and Herman *et al.*, 2000. This method was previously used to assess brain rs-BOLD signal in small mammals and humans. The method consists of estimating the Hurst exponent in the frequency domain using a power spectral density approach and refining the estimation in the time domain with de-trended fluctuation analysis and signal summation conversion methods. Voxel-wise fractal dimension (FD) was then calculated for every subject in the control and patient groups to create ROI-based Z-scores for each individual patient. Voxel-wise validation of FD normality across controls was studied and non-Gaussian voxels, determined using kurtosis and skewness calculations, were eliminated from subsequent analysis. To maintain a 95% confidence level, only regions where Z-score values were at least 2 standard deviations away from the mean were included in the analysis. In the case of chronic fatigue patients and chemotherapy induced cognitive impairment, DTI analysis was added to also determine whether white matter abnormalities were also relevant. Similar Z-score analysis on DTI metrics was also performed.

Brain microscopic networks, modeled as complex systems, become affected in diffuse

brain disorders. Z-scoring of the fractal rs-BOLD frequency domain delineated patient-specific regional brain anomalies which correlated with patient-specific symptoms. This technique can be used alone, or in combination with DTI Z-scoring, to characterize a single patient without any need for group analysis, making it ideal for personalized diagnostics.

Acknowledgements

I would like to thank my supervisor, Dr. Michael D. Noseworthy, for the patient guidance, encouragement and advice he has provided throughout my time as his student. I have been extremely lucky to have a supervisor who came up with new projects when the original project did not materialize and who believed I could finish this work when I did not believe it myself. I would also like to thank all the members of my thesis committee Dr. Wong, Dr. Hall and Dr. Bock who helped me with patients recruitment, interpretation of neuropychological components and who significantly contributed to the realization of this work.

I would also like to acknowledge and thank my friends and colleagues of the Imaging Research Centre for their support. They have read my work, troubleshot my code, listened to my rants when things were not working or when papers were rejected. Some have already graduated and others have just started and they are: Evan McNabb, Andrew Davis, Alyaa Elzibak, Conrad Rockel (Conradical), Saurabh Shaw, Alireza Akbari (Ali), Michael Behr, David Stillo, Catalina Charles (Caty), Alejandro Santos, Amy Harrison and Julia (Shrimpy), Mitchell (Don P) Doughty, Nick Simard and Diana Harasym. Thanks for the laughs too. This PhD work would not have been possible without the help and support from Norm Konyer and the IRC technologists Cheryl Contant, Julie Lecomte, and Carol Awde. They have taught me

more about MRI than any book could ever do.

Lastly, I would like to thank my family and personal friends for their support during this student period of my life that is finally about to end.

Notation and abbreviations

AD ..... Alzheimer's Disease

AD ..... Axial Diffusivity

ADI-R ..... Autism Diagnostic Interview Revised

ADNI ..... Alzheimer's Disease Neuroimaging Initiative

ADOS ..... Autism Diagnostic Observation Schedule

ASD ..... Autism Spectrum Disorder

BET ..... Brain Extraction Tool

BOLD ..... Blood Oxygen Level Dependent

CBF ..... Cerebral Blood Flow

CC ..... Corpus Callosum

CFS ..... Chronic Fatigue Syndrome

CFS ..... Chronic Fatigue Syndrome

CNS ..... Central Nervous System

CSF ..... Cerebrospinal Fluid

CT ..... Computed Tomography

DBS ..... Deep Brain Stimulation

DFT ..... Discrete Fourier Transform

DMN ..... Default Mode Network

DTI ..... Diffusion Tensor Imaging

EEG ..... Electroencephalography

EPI ..... Echo Planar Imaging

FA ..... Fractional Anisotropy

fBm ..... Fractional Brownian Motion

FD ..... Fractal Dimension

FDT ..... fMRIB Diffusion Toolbox

fGn ..... Fractional Gaussian Noise

FMRI ..... Functional Magnetic Resonance Imaging

FNIRS ..... Functional Near-Infrared Spectroscopy

GABA ..... gamma-Aminobutyric Acid

GM ..... Gray Matter

HIREB ..... Hamilton Integrated Research Ethic Board

IFOF ..... Inferior Fronto Occipital Fasciculus

ILF ..... Inferior Longitudinal Fasciculus

IQ ..... Intelligence Quotient

JHUICBM John Hopkins University and International Consortium of Brain Mapping

LFF ..... Low Frequency Fluctuations

MD ..... Mean Diffusivity

MEG ..... Magnetoencephalography

MPRAGE ..... Magnetization Prepared Rapid Gradient Echo

MRI ..... Magnetic Resonance Imaging

MRS ..... Magnetic Resonance Spectroscopy

mTBI ..... mild Traumatic Brain Injury

myoI ..... myoinositol

NAA ..... N-Acetyl Aspartate

PCC ..... Posterior Cingulate Cortex

PET ..... Positron Emission Tomography

PICA ..... Probabilistic Independent Component Analysis

PPMC ..... Pearson Product Moment Correlation

PSD ..... Power Spectrum Density

RCFT ..... Rey Complex Figure Test and Recognition Trial

RD ..... Radial Diffusivity

ROI ..... Region of Interest

SCAS ..... Spence Children's Anxiety Scale

SPECT ..... Single Photon Emission Tomography

SSCM ..... Signal Summation Conversion Method

SWI ..... Susceptibility Weighted Imaging

SWV ..... Scale Window Variance

TBSS ..... Tract Based Spatial Statistics

TE ..... Echo Time

TFCE ..... Threshold Free Cluster Enhancement

TR ..... Repetition Time

WM ..... White Matter

Contents

List of Figures

Chapter 1

Introduction to Fractal Structures and Fractal Dynamics

Fractals are geometrical or mathematical structures that can be found in countless biological structures such as trees and coral colonies, and also inside animal bodies in the lungs and vascular branching networks. Furthermore, fractals are used in graphics created for movies and video games, on wireless communications and in numerous areas of the medical field. Fractals are most commonly thought of as spatial constructs but can also be used to classify the temporal domain such as with the rhythm of the heart and ultimately the brain.

These mathematical structures mainly differ from others on the way they scale. Unlike a cube where if the face doubles, the volume increases by six, a fractal structure scales by a power that is not necessarily an integer and this power is called the fractal dimension. Fractals are generated by divergent, self similar functions that are un-differenciable and are ideal to characterize complex systems where typical (i.e. Euclidean or integer) dimensions are insufficient.

Although first described by Benoit Bandelbrot in 1975, fractal applications were not developed until 1978 when Loren Carpenter, an engineer for Boeing aircraft, used fractal geometry to create computer generated landscapes. The computer graphics industry rapidly incorporated fractal techniques to generate stunningly realistic natural looking structures. (See Figure1.1)

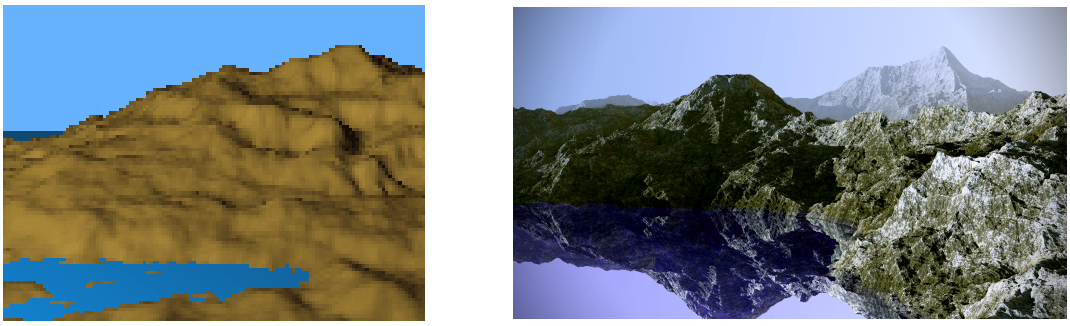

(a) (b)

Figure 1.1: (a). Fractal Surface. (Szeliski and Terzopoulos, 1989). (b). Fractal Landscape. Debian art. (Bezo97, 2016)

In fractals, patterns are replicated at different scales. When the replication is exactly the same at every scale, it is called a self-similar pattern. One of the most familiar examples of self-similarity can be observed in a tree. In each of the branching nodes of a tree, the pattern of branching is very similar and repeats throughout the tree from the base to the top. This fractal characteristic in trees has enabled new methods to calculate, with higher certainty, the amount of oxygen produced by an entire rain forest and its carbon dioxide consumption (Bentley *et al.*, 2013). Figure 1.2 demonstrates how the branches of a tree model can be divided in subsections that are similar at different scales.

Another groundbreaking application of fractals was discovered by Nathan Collen when he introduced fractal geometry in the design of modern antennas (Cohen, 2002).

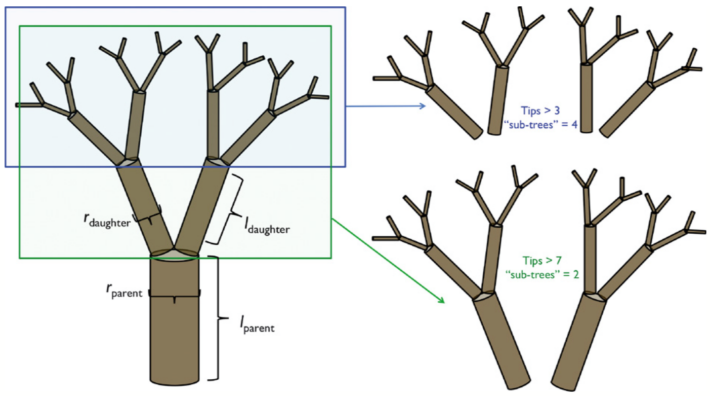

Figure 1.2: Model for fractal tree geometries (Bentley *et al.*, 2013)

A fractal pattern caused the size of the antennas to be drastically reduced and the frequency range to be widened. This discovery has been considered a breakthrough in technological communication and fractal antennas are used in every communication device today.

In addition to the spatial domain, fractal patterns can also be observed in the time domain. A clear fractal pattern can be observed in the frequency of the heart beat. The human heart rate generates fluctuations on different time scales that are statistically self similar (Goldberger, 1996). This dynamic can be observed in Figure 1.4 and it has become an established bio-marker for the diagnosis of heart disease. Additionally, fractal dynamics had been observed in electrocardiogram (ECG) (Bär *et al.*, 2007), in brain electroencephalography (EEG)(Nan and Jinghua, 1988) and more recently in the brain blood oxygen level dependent (BOLD) signal acquired with magnetic resonance imaging (MRI) (Zarahn *et al.*, 1997; Bullmore *et al.*, 1996, 2001).

Many biological systems exhibit fractal dynamics, however the reason behind this behavior is still a mystery. One possible explanation is that, as seen with the fractal antennas, fractal systems are more efficient in storing information, which allows for

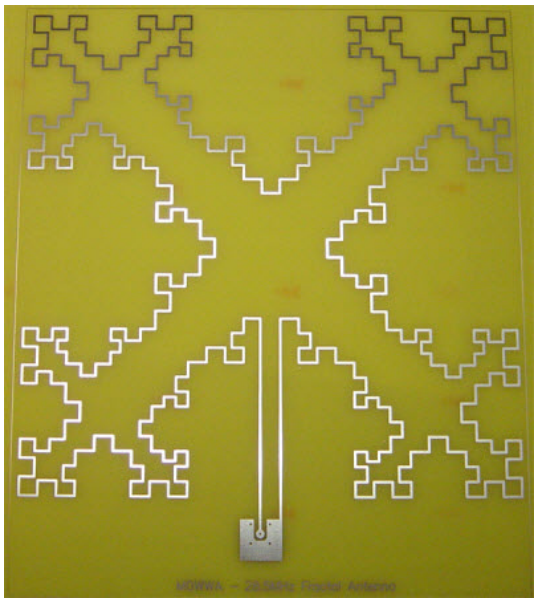

Figure 1.3: Fractal antenna. Reproduced with permission of Juan J de Onate, M0WWA

adaptability and learning (Sharma, 2009). Reduction of the fractal dimension in biological systems has been associated with disease due to a reduced capacity of the system to adapt. In the case of the brain, complexity of brain signals, characterized by the fractal dimension (FD), has been investigated using resting-state EEG (rs-EEG) and rs-BOLD. A recent study by Smits et al. (Smits *et al.*, 2016) showed calculations of FD in resting state EEG recordings from 67 Alzheimer's Disease (AD) patients and 41 healthy controls. They found that the FD and signal complexity decreased with age in normal controls and that it further decreased in AD patients, especially in temporal-occipital regions of the brain. This study supports the concept that brain signal FD correlates with changes in brain connectivity and complexity.

In another study Warsi et al. (Warsi *et al.*, 2012) studied the correlation of rs-BOLD fractal dimension and in vivo proton magnetic resonance spectroscopy (^{1}H-MRS) in the left putamen of AD patients and normal controls. It was shown that decreased

FD was consistent with AD severity, as measured with known biomarkers N-acetyl aspartate (NAA) (r = 0.44, p = 0.015) and myoinositol (myoI) (r = -0.45, p = 0.012) Additionally, a study by Weber et al. (Weber *et al.*, 2014) showed how complexity of the rs-BOLD brain signal decreased as ethanol levels in the brain increased. This was seen particularly in the right basal ganglia at 60 and 90 minutes after ethanol consumption. Furthermore, the rs-BOLD signal complexity returned as the brain ethanol became metabolized. Ethanol directly affects function of the brain GABA-A receptors (Simson *et al.*, 1993) decreasing brain functional connectivity. As ethanol was cleared in the brain, brain connectivity increased and fractal dimension increased. The conclusion from this work was that the temporal complexity of brain resting state was diminished with increased levels of brain alcohol. In other words, the ability of the brain to process information was reduced in an intoxicated state and this effect was observed in the fractal dimension of the BOLD signal.

Despite the early identification of fractals in brain signals and the value of the FD as a biomarker for pathology or disease, there have been very few studies on its clinical applications beyond aging and dementia (Warsi *et al.*, 2012; Maxim *et al.*, 2005; Wink *et al.*, 2006). The complex nature of fractals makes the mathematical concept behind fractals difficult to understand even for mathematicians thus impeding advancement on this field of study. This work is intended to expand the fractal analysis of brain signals to pathologies of the brain where traditional diagnostic methods have been insufficient and will hopefully create a route map for future researchers and clinicians willing to include chaos and complexity in the study of the brain.

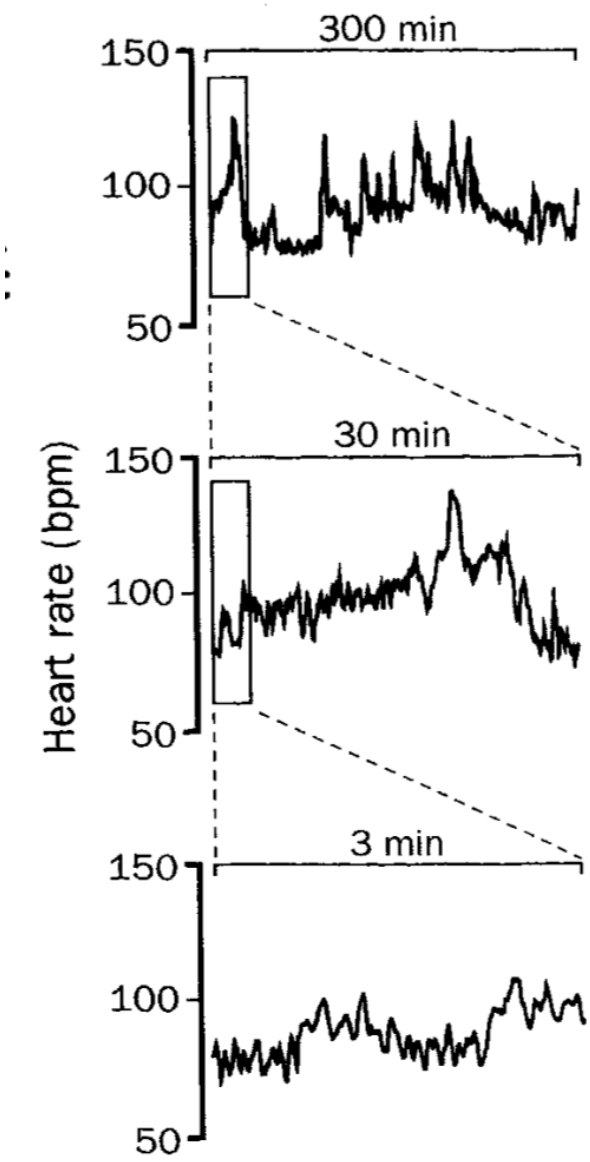

Figure 1.4: Schematic representation of fractal dynamics in the human heart rate (Goldberger *et al.*, 2002).

Chapter 2

Fractal behavior of the brain BOLD signal

2.1 The hemodynamic response

The human brain is the control center of the body. It sends and receives millions of signals every second, in the form of hormones, nerve impulses, and chemical messengers. Changes in brain activity could cause deficits in cognition, consciousness and motor control, hence being able to asses brain activity is fundamental in the diagnosis of several disorders.

In the brain, neuronal activation triggers an increase in cerebral blood flow (CBF). This phenomenon is known as CBF and neuronal activity coupling and it was first observed in 1980 in invasive animal studies (Tsubokawa *et al.*, 1980; Roy and Sherrington, 1890). The mechanism behind the CBF and neuronal activity coupling is still under scrutiny, but it has been suggested that when a region of the brain becomes active in response to a particular stimulus, the metabolic activity of the neurons increase,

demanding more oxygen and glucose, therefore increasing the local blood flow (Nair, 2005). Active neurons do not require much more oxygen compared to inactive neurons. As a result there is a local increase in oxygen in the blood vessels surrounding the active regions. Consequently, by measuring oxygenation, blood flow and neuronal activity can be indirectly determined.

The need for non-invasive methods required in human studies caused an advancement in different imaging modalities aiming at measuring blood oxygenation such as functional positron emission tomography (PET), functional near infrared spectroscopy (fNIRS) and BOLD functional magnetic resonance (fMRI). Out of these modalities, BOLD fMRI is the most common method of measuring brain function. This is because MRI-based techniques provide an ideal balance between spatial and temporal resolution and do not require radioactive contrast agents as PET. Figure 2.1 shows a basic schematic representation of the hemodynamic response function for an activated voxel in the brain. After the stimulus, it takes about 2 seconds before a change can be observed. As the CBF increases, the hemodynamic response gradually increases until it peaks at around 6 seconds and then slowly decays to baseline levels at 15 to 20 seconds. An initial and a final undershot is generally observed although it is not clear what are the mechanisms behind them (Lazar, 2008).

2.2 BOLD fMRI

Oxygen is carried throughout the body by a red blood cell protein know as hemoglobin (See Figure 2.2). The hemoglobin molecule is paramagnetic due to the presence of iron. Paramagnetic materials have permanent magnetic moments (dipoles) due to the spin of unpaired electrons in atomic or molecular electron orbitals. In the presence of

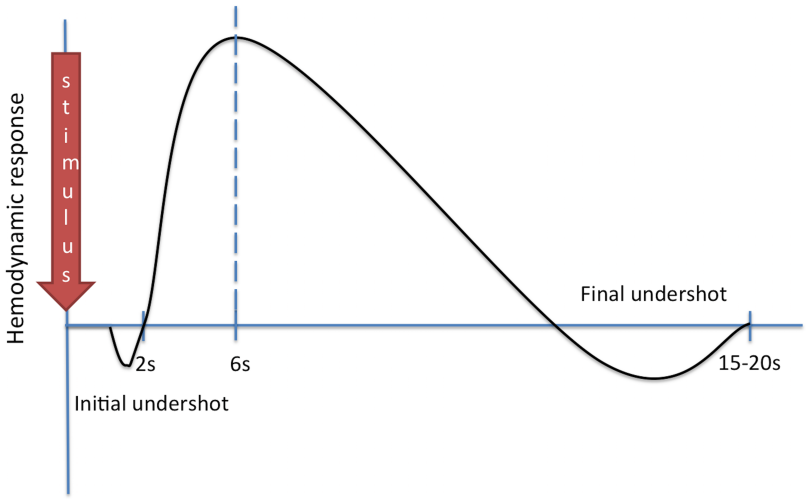

Figure 2.1: Schematic representation of the hemodynamic response.

an external magnetic field, the spins align themselves with the magnetic field, thereby increasing the local field strength. Hemoglobin without bound oxygen molecules, deoxyhemoglobin, is paramagnetic because of the high spin state (S = 2) of the heme iron. In contrast, oxygen-bound hemoglobin, oxyhemoglobin, has low spin (S = 0) and is diamagnetic (Pauling and Coryell, 1936). This affects the MR signal creating the Blood Oxygen Level Dependent (BOLD) contrast effect. More specifically, when oxygen increases the local magnetic field decreases, affecting transverse magnetization, thereby increasing T2* time (slower decay) and therefore the MR signal.

A typical BOLD fMRI experimental setup is a "block design", in which a task is performed and stopped repeatedly for certain lengths of time, with the goal of shifting brain activity between two or more well defined states. This shift should allow the measurement of the relative changes in cerebral blood flow between the states (Friston *et al.*, 1999). A statistical activation map is created based on a comparison between stimulation and rest states. This map is then used to present the activation as a color

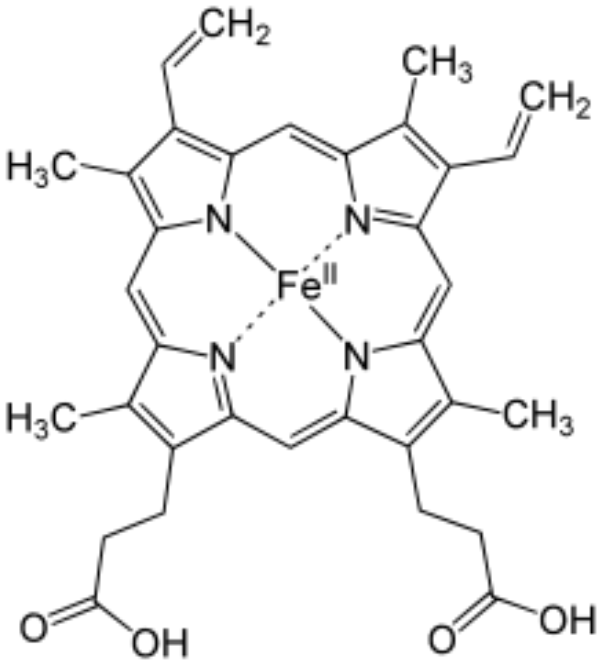

Figure 2.2: Schematic representation of the hemoglobin molecule.

overlay on an higher resolution anatomical T1 weighted image.

The major limitation with task-based fMRI is the ability of the subject to adequately and consistently perform or respond to the task. Furthermore, activation requires appropriate control tasks that may be difficult to determine as they need to cause similar activation across all subjects. Because of these difficulties, assessment of brain connectivity has shifted towards the use of resting state networks (rs-fMRI). rs-fMRI is aimed at mapping resting state functional connectivity in the brain. Resting state networks are brain regions which are temporally-correlated in BOLD response in the absence of a specific task. Brain networks may or may not be physically adjacent to one another, but have consistently similar patterns during rest. More specifically, the default mode network (DMN) is active during wakeful rest with the subject not performing any tasks. These networks are known to be consistent across healthy

subjects and do not rely on subject performance. However, a limitation of using rs-fMRI to assess brain connectivity is that they heavily rely on group analysis, which is generally unsuitable when drawing conclusions on heterogeneous disorders. Large datasets of rs-fMRI are assessed using probabilistic independent component analysis (PICA) to find temporal synchrony among regions of the brain. This determines the brain networks and the correlation coefficients, where the latter represents the connectivity strength within each network. This approach is generally unsuitable to assess the condition of an individual patient. As a result, the aim of this work consists in exploring an alternative single-subject approach, using a model-free complexity analysis based on the fractal nature of the rs-BOLD signal acquired with magnetic resonance imaging.

2.3 Fractal behavior in the BOLD signal

From the previous section we know that the rs-BOLD signal is produced by temporal fluctuations of blood oxygen in the brain. At rest, these fluctuations are caused by complex neuronal connective functions, that demand an increase in local oxygen consumption. When the deoxyhemoglobin to oxyhemoglobin ratio decreases, the local magnetic field is perturbed due to changes in magnetic properties, which cause the MR signal to increase.

Studies on the brain rs-BOLD signal have shown that the signal contains spontaneous low frequency fluctuations (LFF) (Fox and Raichle, 2007) that originate from physiological functions such as cerebral blood oxygenation and cerebral blood flow and volume as well as from a a small component of instrument noise added during fMRI acquisition (Zarahn *et al.*, 1997; El Boustani *et al.*, 2009; Herman *et al.*, 2011; Eke

et al., 2000, 2002). These LFF follow the inverse power law scaling in the frequency domain, which is a defined indication of fractality. Figure 2.3 shows the raw signal and the corresponding power spectrum analysis of a 4x4x3mm voxel in the right hippocampus of a healthy subject. The power spectrum shows the power-law decay on a log-log scale in the frequency range of 0.08 - 0.16 Hz. Magnet and instrument noise usually appears on the lower frequencies (<0.02Hz) and the high frequencies are filtered where the power is equally distributed across frequencies (random or white noise) (Herman *et al.*, 2011).

Time signals are considered fractals when they are self-similar and auto-correlate across different time scales. The fractal dimension (FD) is considered a metric of signal complexity, and has been previously used as a descriptor of the neural activity based on hemodynamics and metabolic response (Herman *et al.*, 2011; Bullmore and Sporns, 2009).

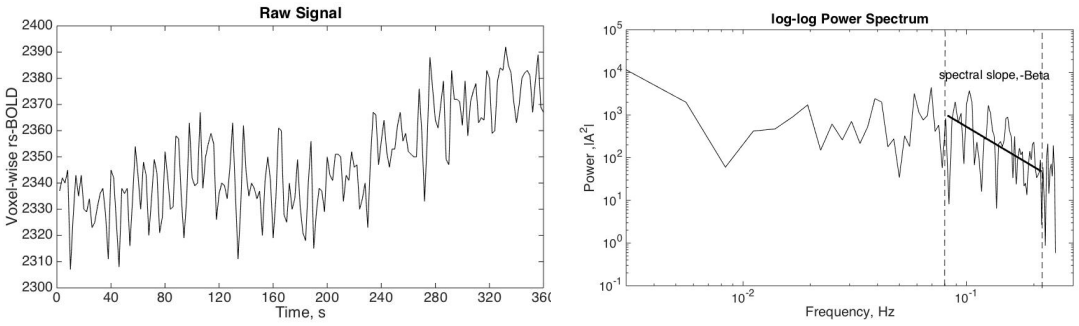

(a) (b)

Figure 2.3: (a). Raw BOLD signal .(b) Power spectrum analysis showing the power law decay in the frequency range of 0.08 - 0.16 Hz

2.4 BOLD fMRI acquisition

The effectiveness of the fractal analysis is based on the ability of the signal to capture the true dynamics of the processes being studied. Ideally the sampling frequency should be one order of magnitude higher than the highest frequency of the hemodynamic response to neuronal activation. However, in the case of the BOLD signal, the sampling frequency is determined by the repetition time (TR). The minimum TR (frequency = 1/TR) is limited by the number of slices that are acquired on a single shot. To cover the human brain at a resolution of 3mm per slice, the MR system requires acquisition of 30 slices on a single shot, which limits the minimum TR to 1.7 s (0.58 Hz). The need for a fast acquisition requires a fast MRI imaging technique. BOLD fMRI commonly uses Echo Plannar Imaging (EPI) to fill in the k-space which is considered one of the fastest imaging methods. All the k-space is filled-in following a single RF pulse. Since all the space must be acquired before there is a significant decay in T2*, this techniques introduces a trade off in spacial resolution. Typical EPI images will produce at most 128x128 voxels in a slice. In summary, in order to increase the temporal resolution, spatial resolution must be sacrificed. The k-space trajectory for a single shot EPI can be observed in Figure 2.4

2.5 Fractal Analysis

Because the rs-BOLD signal has been associated with post-synaptic potentials, which are mainly localized in gray matter as opposed to action potentials more common in the white matter, calculation of the FD must be performed using a gray matter mask. There are several methods to estimate the fractal dimension, however the method

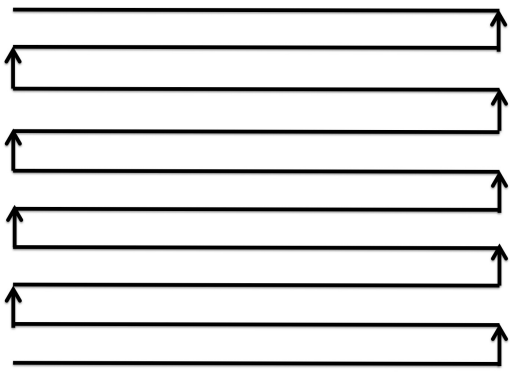

Figure 2.4: Schematic representation k-space trajectory for a single shot EPI

proposed by Eke et al. Eke *et al.* (2002) has been the most successful in the analysis of the BOLD signal. The methodology proposed by Eke et al. suggests estimating the fractal dimension (FD) by calculating a voxel-wise Hurst exponent (H). For self-affine processes in an n-dimensional space, the Hurst exponent is related to the fractal dimension (FD) such as $FD + H = n + 1$, where $n = 1$ for a time domain signal. The rs-BOLD raw signal is initially normalized, end matched and bridge de-trended following Eke's procedure. The raw data is normalized by subtracting the mean from every data point while end matching and bridge detrending is achieved by subtracting from the data the line that connects the first and the last point and multiplying the data by a parabolic window Equation (2.1).

$$W(j) = 1 - \left(\frac{2j}{N+1} - 1 \right), j = 1 \rightarrow N, \tag{2.1}$$

Where N is the number of time points.

The series are Fourier transformed to the frequency domain and the scaling exponent (beta) of the inverse power law Equation (2.2) calculated. Where A is the amplitude of the discrete Fourier transform (DFT) at frequency f; β is the spectral index and c is a constant.

The spectral index is calculated in a frequency range where the power-law scaling behavior is consistently observed across all voxels and subjects. The spectral regions known to display magnet and instrument noise and uncorrelated noise are generally removed from the analysis. A previous study (Herman *et al.*, 2011) have suggested excluding low frequency regions below 0.02 Hz due to the presence of MRI system noise in that region (Zarahn *et al.*, 1997). It is also recommended that an isolated vasomotion peak that often appears at 0.1 Hz be removed in order to avoid bias in estimating the spectral index when fitting the linear trendline across the spectral estimates of the spectrum. However, the same study by Herman *et al.* (Herman *et al.*, 2011) demonstrated that this peak only appears in about 2% of the voxels and that the impact in the results was negligible.

Following the dichotomous model proposed by Mandelbrot and Van Ness (Mandelbrot and B., 1967) the signals are then classified as fractional Brownian motion (fBm) for $\beta > 1$ and fractional Gaussian noise (fGn) for $\beta < 1$.

$$|A(f)^2| \propto cf^{-\beta}, \tag{2.2}$$

The Hurst exponent on fGn signals is calculated by using the dispersional analysis proposed by Bassingthwaighte ((Bassingthwaighte and Raymond, 1995)), which is based on the variability of the local averages of the signal over different time windows

(τ) Equation (2.3). However, a scaled window variance analysis is used to calculate H on the fBM signals when the series are divided in non-overlapping windows.

$$SD(\tau) = SD(\tau_0)\left(\frac{\tau}{\tau_0}\right)^H, \tag{2.3}$$

Signals where β is near 1 produced ambiguous results, therefore the classification method must be refined using the signal summation conversion method (SSCM) described by (Eke *et al.*, 2002).

Chapter 3

Hypothesis, Methods and Experimental Design

3.1 Hypothesis

It is well known that the brain is best modeled as a complex system (Kannathal and Puthusserypady, 2004) and therefore it is hypothesized that a measure of complexity using FD could provide an alternative method to assess brain disorders. Brain connectivity is best described as a multilevel model that takes into account three distinctive levels of interaction: synaptic connections that link independent neurons, networks that connect neuronal populations and brain regions linked by fiber pathways. A measure of complexity of this model constitutes an ideal indicator of multilevel and multitemporal connectivity within different brain regions. Tentatively, a healthy brain is associated with more complex signals and high FD, while a diseased or dysfunctional brain is associated with less complex signals and low FD (Warsi *et al.*, 2012; Weber *et al.*, 2014; Smits *et al.*, 2016; Goldberger *et al.*, 2002). The capacity of the brain to

perform real-time adaptation and processing of these connections is reflected in the local demand of glucose and oxygen consumption, which drives the brain metabolic fluctuation observed in the rs-BOLD signal.

At the same time, the BOLD signal is also a complex mixture of blood flow, metabolism, fluctuating oxygenated and deoxygenated hemoglobin, blood volume, and external sources of noise. Linear models generally fail in taking into account the complexity of the phenomenon that is being studied and are challenged when making conclusions on results where many levels of complexity are convoluted. The objective of this work consist in demonstrating how the rs-BOLD fractal dimension could provide additional patient-specific brain focal information that can be used to assess and possibly monitor patients.

In order to demonstrate the applicability of the FD in assessing brain disorders where traditional diagnostic methods have been insufficient, four different disorders were tested: Mild Traumatic Brain Injury (mTBI), Autism Spectrum Disorder (ASD), Chemotherapy-related Cognitive Impairment (Chemo-Brain) and Chronic Fatigue Syndrome (CFS). These disorders have in common a noticeable heterogeneity among their subjects.

For instance, ASD patients show a variety of clinical presentations, where each individual will display unique difficulties in the three autism domains: verbal and non-verbal communication, social interaction and restricted and repetitive behaviors. Additionally, different classes of psychotropic medication are prescribed to treat the symptoms which create additional confounding while investigating this disease.

In the case of mTBI, the injury unlikely occurs under the same conditions for each patient. Location of the direct impact in the brain, and strength of the rotational and

shearing forces experienced varies significantly from subject to subject.

Chemo-brain patients are also significantly heterogeneous. patients are prescribed a cocktail of chemotherapy drugs depending on type and stage of the tumor and also the general health of the patient. This is very specific to every patient. Additionally, many confounding factors arise with respect of cognition in these patients as patients undergoing chemotherapy are usually under psychological distress which affects their cognitive performance. Furthermore, many patients are under the influence of medication prescribed to attenuate side effects of chemotherapy, such as anti-nauseates and anti-inflammatories. In cases in which estrogen or progesterone receptors are detected in the tumor, hormone therapy can be prescribed to the patients, which may also cause an effect in cognition.

A design of a single subject approach, independent of group analysis, is fundamental in these disorders. Hence, estimation of the FD of the voxel wise BOLD signal could potentially arise as new metric in assessing complex brain pathologies.

3.2 Methods

Mild TBI (15 subjects), Chemobrain (5 subjects) and CFS patients (1 subject) were recruited for this study. The study was approved by our Institutional Research Ethics Board, (Hamilton Integrated Research Ethic Board (HIREB)) and all patients gave written informed consent. In the case of mTBI patients, parental assent was also obtained in writing as these patients were paediatric. All the studies were conducted according to the principles expressed in the Declaration of Helsinki. Healthy control data and ASD patients data (55 subjects) were acquired throughout the NITRC data base directly from the Human Connectome Project (180 subjects), The Alzheimer's

Disease Neuroimaging Initiative (ADNI)(32 subjects), and the ABIDE-1 data-base (55 subjects).

Resting state BOLD fMRI and anatomical data of the patients were acquired on a 3T GE Signa scanner using a 32-channel RF-coil (General Electric Healthcare, Milwaukee, WI). The anatomical data were acquired following a 3-plane localizer and a calibration scan designed for parallel imaging using a 3D inversion recovery-prepped T1-weighted pulse sequence (fSPGR, axial acquisition, TE/TR/flip angle = 1.8/15.63/15deg, 256x256 matrix with 1.2 mm slice thickness with 26 cm FOV). Resting state functional BOLD data was acquired in 10 min using an echo planar imaging (EPI) sequence with FOV = 22cm, image matrix = 64x64; flip angle = 90deg; echo time (TE) = 35 ms; repetition time (TR) = 2000ms (i.e, 0.5Hz temporal sampling frequency); slice thickness of 3mm; and 180 temporal points. At the beginning of every scan, 4 additional data points were acquired but automatically discarded to allow the system to reach steady state. The rs-BOLD data were corrected for motion artifacts using a time series general affine registration for 12 parameters (3dWarpDrive/AFNI). Posterior ROI analysis required the rs-BOLD data to be transformed into a standard space where statistical maps of anatomically defined brain regions have been defined. Skull stripped anatomical data were aligned to the TT_N27 Tailarach standard space then warped with the rs-BOLD data using a 12-point affine transformation to obtain our final dataset. The regions of interest (ROIs) were extracted from the TT_Daemon human brain atlas (Eickhoff S, Stephan KE, Mohlberg H, Grefkes C, Fink GR, Amunts K, 2005) provided with the AFNI package (Cox, 1996).

Although all control data were scanned using a similar GE Healthcare 3T MR scanner and similar pulse sequence and parameters as in the patients data, some

differences existed. For instance, the data from ABIDE-1 database was collected with 300 data points while the data from the human connectome project was acquired on 180 data points. These differences were accounted for in the analysis.

3.3 Statistical analysis

A voxel-based Z-scoring methodology was used for statistical analysis. The Z-score is the number of standard deviations (σ) a data point is above ($Z > 0$) or below the mean ($Z < 0$). The Z-score of the voxel-wise fractal dimension was calculated as: $Z_{FD} = (x - \mu)/\sigma$. Where x is the localized voxel rs-BOLD FD and μ and σ are the voxel mean and standard deviation of that same voxel from the control group respectively.

Prior to application of Z-scoring, voxel-wise validation of normality was performed on the control group data (i.e. voxel-wise skewness and kurtosis was investigated). Failure to satisfy normality indicated voxels that were not classifiable based on this approach. Also, due to inaccurate spatial warping of all control subjects some voxels had the possibility of not existing (i.e. unable to classify) simultaneously over all control subjects.

To achieve a statistical power of at least 0.9, only voxels that existed simultaneously in at least 11 subjects were included in the final Z-score maps. Control data was tested for normality using the Kolmogorov-Smirnov test in every study (Smirnov, 1948) (Figure 3.1a), and kurtosis and skewness calculations (Figure 3.1b,c). Based on the Kolmogorov-Smirnov test control data was considered normal within the gray matter mask. However, a more detailed analysis of skeweness and kurtosis usually revealed voxels that deviated from the univariated normal distribution, which were

subsequently removed from the final Z-score map. This approach removed only around 3% of the voxels in the mean mask for normal controls. Thus the final mask was deemed acceptable for use as a Z-score featurespace.

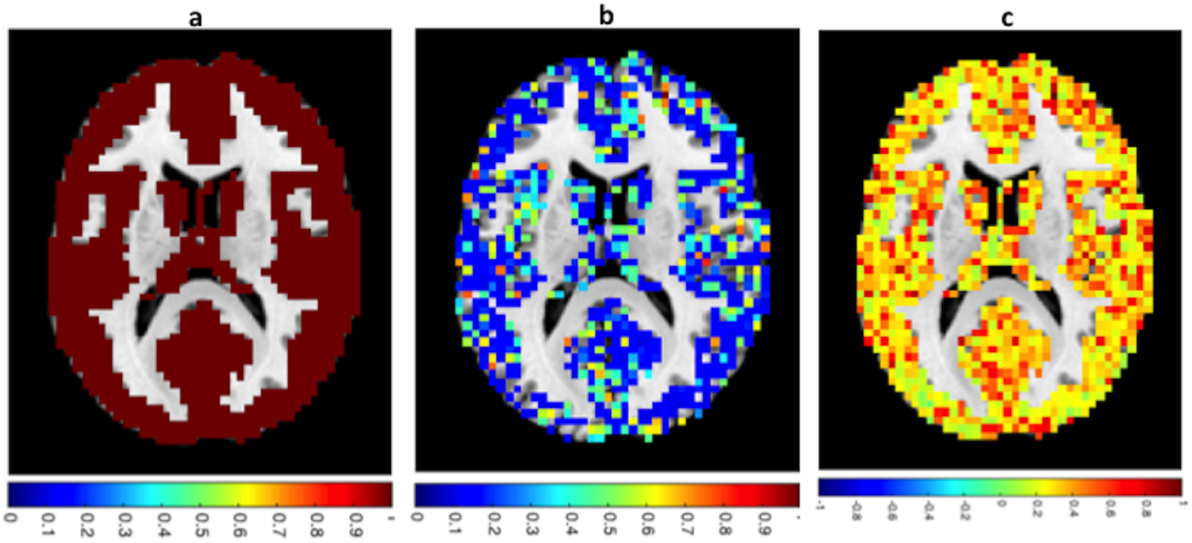

Figure 3.1: Analysis of normality.(a) Kolmogorov- Smirnov normality test. h=1 indicates rejection of the null hypothesis at a 5% significance level. (b) Kurtosis map. Voxels where $k \neq 3.0 \pm 0.5$ were removed from analysis. The map was centered at k=3. (c) Skewness map. Skewness measures asymmetry of the distribution. Positive skew(sk) indicates more data points above the mean while negative skew indicates more data points below the mean. Voxels where $sk \neq 0.0 \pm 0.5$ were removed from the analysis and the sk map was normalized.

3.4 Experimental Design

The first study focused on the fractal analysis of the BOLD signal from children with mTBI. mTBI is defined as a range of microstructural neurological injuries coupled with functional disturbances that are rarely detectable with traditional MRI or Computed Tomography (CT) scans. Post-injury symptoms are generally grouped into three categories: cognitive, physical and behavioral anomalies. Symptoms include headache,

difficulty concentrating, sleep impairment, memory deficit, depression and anxiety. In this study, the voxel-wise FD was calculated in every subject and normalized with the healthy control data to produce a Z-score map. The regions were $|Z| > 2$, were reported as abnormal and the results were correlated with the individual post-concussion symptom scale, (PCSS).

The second study explored the fractal dimension of ASD patients compared with healthy controls. Neuroimaging research has previously explored anatomical and functional disturbances in ASD patients. However, given the heterogeneous nature of ASD, the results have been inconsistent or inconclusive. We hypothesized that patients with ASD could show changes in the FD of the rs-BOLD signal and that theses changes would reflect underlying alterations of neural structural organization and functional connectivity. Furthermore, FD analysis would open the possibility of single subject assessment. Diagnosis and severity of the symptoms was quantified in this study using the scores of the Autism Diagnostic Observation Schedule (ADOS) (Lord *et al.*, 2000), the Autism Diagnostic Interview Revised (ADI-R) (Lord *et al.*, 1994) as well as clinical consensus. The data was IQ matched to eliminate the confounding from IQ differences between the diseased and healthy groups.

To determine regions of the brain of ASD patients with increased or decreased signal complexity respect to a typical control group, the voxel-wise FD was estimated on every subject of both groups and normalized using the Z score methodology. Only Z-score values were $|Z| > 2$ were considered statistically significant for a 0.95 confidence level. Finally, the Pearson Product Moment Correlation (PPMC) method was used to establish correlation between ROI-based Z-score values and ADI-R and ADOS questionnaires.

The third study examined the fractal dimension of the BOLD signal in cancer patients experiencing chemotherapy-related cognitive impairment. Chemotherapy is known to be one of the most efficacious and aggressive treatments for cancer. It causes many side effects including what is known as chemo-brain. The symptoms associated with this condition are: memory lapses, concentration problems, disorganized thinking and slower mental processing, none of which are easily detected on traditional MRI or CT imaging modalities. Gray matter and white matter changes have been previously reported for chemo-brain patients. Because the rs-BOLD signal has been associated with post-synaptic potentials, which are mainly localized in gray matter as opposed to action potentials more common in the white matter, diffusion tensor image (DTI) was added in this study to assess the white matter integrity. Five subjects with chemo-brain symptoms were recruited for this study. Healthy control data were acquired throughout the NITRC data base directly from the Human Connectome Project and the ADNI database. Although the data was not age matched, patients above 70 years old were only matched with healthy controls from the ADNI data base due to normal aging brain atrophy occurring at higher rates after this age (Peters, 2006; Scahill *et al.*, 2003). Additionally, patients were administered the following neuropsychological tests: Hopkins Verbal Learning Test Revised (HVLT-R) (Benedict and Brandt, 2001), Rey Complex Figure Test and Recognition Trial (RCFT) (Meyers and Meyers, 1995), Digit Span - Wechsler adult intelligence scales (WAIS-III) (Wechsler, 2014), Cognitive Failures Questionnaire (Broadbent *et al.*, 1982) and the Edinburgh Handedness Inventory(Oldfield, 1971). To determine regions of the brain of chemo-brain patients with increased or decreased signal complexity respect to a typical control group, the voxel- wise FD for gray matter and DTI measures for white

matter were estimated on every subject of both groups and normalized using the Z score methodology. Only Z score values were $|Z| > 2$ were considered statistically significant for a 0.95 confidence level.

The fourth and final study implemented a case study on a single subject suffering from CFS. The goal of this study was to explore the capabilities of the fractal analysis on a single subject compared to healthy controls. CFS is a particular case of myalgic encephalomyelitis, where clear inflammation of the brain or spinal cord cannot be detected. Patients diagnosed with CFS experience marked fatigue and weakness in the absence of physical activity. A variety of other symptoms usually accompany this disease such as muscle pain, headaches, impaired memory and concentration and mental fog. Some evidence suggest that the damage in CFS occurs mainly in white matter, therefore DTI was also added on this study to account for white matter abnormalities. To determine regions of the brain of the CFS patient with increased or decreased signal complexity respect to a typical control group, the voxel- wise FD for gray matter and DTI measures for white matter were estimated and normalized using the Z score methodology.

The next four chapters provide further details on the experimental design as well as a discussion of the results. Each following chapter is a published or submitted paper and contains all the information required to replicate the experiments or to be used as a guide for future applications.

Chapter 4

Fractal Analysis of rs-BOLD Signals in Mild Traumatic Brain Injury (mTBI)

Regional Fractal Analysis of Brain Blood Oxygenation Level Dependent (BOLD) Signals from Children With Mild Traumatic Brain Injury (mTBI).

Olga Dona, Michael D. Noseworthy , Carol DeMatteo and John F. Connolly

4.1 Context of the paper

In this study, we applied the fractal dimension methodology combined with Z scoring statistics to detect abnormalities in the brain following mild traumatic brain injury (mTBI). Fractal dimension of the brain resting state blood oxygen level dependent (rs-BOLD) signal represents complexity and therefore the level of connectivity or activity certain brain region possess. While a single value of fractal dimension assigned to a brain region have not intrinsic meaning, in a Z scoring or normalized model, we were able to differentiate whether certain value was considered normal for that region or if it was above or below the local mean. Furthermore, we hypothesized healthy brains would show higher temporal complexity when compared with mTBI patients.

After implementing this methodology, we were able to find regions in the brain of mTBI patients with decreased connectivity using FD methodology despite not showing any abnormality in an anatomical scan. These regions have been previously reported in the literature as dysfunctional for mTBI patients. We concluded from this paper that the method we have proposed is able to provide additional information of mTBI in a non-invasive and fast manner and could potentially aid in the design of future treatment plans.

4.2 Declaration Statement

Olga M. Dona, as first author, acquired the data, performed the data analysis and interpretation of the results and drafted the article including tables and figures. Contributions by Olga M. Dona warranted her name as first author.

Dr. Michael D. Noseworthy, as corresponding author, designed and conceptualized

this project which is part of a his long trajectory on developing applications based on the fractal analysis in human brain signals. He performed the critical revision of the article and the final approval of the version to be published. Furthermore, Dr. Noseworthy provided constant guidance and advice through out the duration of this study and secured substantial funds.

Dr. Carol DeMatteo actively recruited mTBI patients for this project and participated in the final revision of the article, providing insightful understanding in the correlation between some detected areas and the reported symptoms. She also contributed by securing funding towards patients scanning time.

Dr. John F. Connolly contributed to the design of this study and collaborated in securing the funds required to guarantee appropriate scanning time per patient.

This paper has been published in the journal PLOS ONE on January 10^{th}, 2016. Citation: Dona O, Noseworthy MD, DeMatteo C, Connolly JF (2017) Fractal Analysis of Brain Blood Oxygenation Level Dependent (BOLD) Signals from Children with Mild Traumatic Brain Injury (mTBI). PLoS ONE 12(1): e0169647. doi:10.1371/journal.pone.0169647

4.3 Paper

Fractal Analysis of Brain Blood Oxygenation Level Dependent (BOLD) Signals from Children With Mild Traumatic Brain Injury (mTBI)

Olga Dona[1,2], Michael D. Noseworthy[1,2,3,4,¤*] , Carol DeMatteo[5] and John F. Connolly[1,6]

1 McMaster School of Biomedical Engineering, McMaster University, Hamilton, Ontario, Canada.
2 Imaging Research Centre, St. Joseph's Healthcare, Hamilton, Ontario, Canada.
3 Department of Electrical and Computer Engineering, McMaster University, Hamilton, Ontario, Canada.
4 Department of Radiology, McMaster University, Hamilton, Ontario, Canada.
5 School of Rehabilitation Medicine, McMaster University, Hamilton, Ontario, Canada.
6 Department of Linguistics, McMaster University, Hamilton, Ontario, Canada.
¤Current Address: Department of Electrical and Computer Engineering, McMaster University. Engineering Technology Building, ETB-406. 1280 Main St. West, Hamilton, Ontario. Canada L8S 4K1.

* Corresponding author
E-mail: nosewor@mcmaster.ca (MDN).

Abstract

Background

Conventional imaging techniques are unable to detect abnormalities in the brain following mild traumatic brain injury (mTBI). Yet patients with mTBI typically show delayed response on neuropsychological evaluation. Because fractal geometry represents complexity, we explored its utility in measuring temporal fluctuations of brain resting state blood oxygen level dependent (rs-BOLD) signal. We hypothesized

that there could be a detectable difference in rs-BOLD signal complexity between healthy subjects and mTBI patients based on previous studies that associated reduction in signal complexity with disease.

Methods

Fifteen subjects (13.4±2.3 y/o) and 56 age-matched (13.5±2.34 y/o) healthy controls were scanned using a GE Discovery MR750 3T MRI and 32-channel RF-coil. Axial FSPGR-3D images were used to prescribe rs-BOLD (TE/TR=35/2000ms), acquired over 6 minutes. Motion correction was performed and anatomical and functional images were aligned and spatially warped to the N27 standard atlas. Fractal analysis, performed on grey matter, was done by estimating the Hurst exponent using de-trended fluctuation analysis and signal summation conversion methods.

Results and Conclusions

Voxel-wise fractal dimension (FD) was calculated for every subject in the control group to generate mean and standard deviation maps for regional Z-score analysis. Voxel-wise validation of FD normality across controls was confirmed, and non-Gaussian voxels (3.05% over the brain) were eliminated from subsequent analysis. For each mTBI patient, regions where Z-score values were at least 2 standard deviations away from the mean (i.e. where $|Z| > 2.0$) were identified. In individual patients the frequently affected regions were amygdala (p=0.02), vermis(p=0.03), caudate head (p=0.04), hippocampus(p=0.03), and hypothalamus(p=0.04), all previously reported as dysfunctional after mTBI, but based on group analysis.It is well known that the brain is best modeled as a complex system. Therefore a measure of complexity using rs-BOLD signal FD could provide an additional method to grade

and monitor mTBI. Furthermore, this approach can be personalized thus providing unique patient specific assessment.

Introduction

Mild traumatic brain injury (mTBI), commonly referred to as concussion, is a significant medical condition with serious implications for those affected, particularly where the extension of the injury is not easily assessed or even detected. It represents 75% of all head injuries [1] and disproportionally affects young men and athletes. Furthermore, the elderly are also a significant group because of increased incidence of falls and subsequent head trauma [2, 3].

All mTBIs are neurological injuries, which occur from rapid accelerative and/or decelerative linear and rotational forces applied to the head. These result in rapid velocity changes leading to the brain hitting the inside surface of the skull on the side nearest the origin of the force. Subsequently, milliseconds later, the brain also collides with the opposite side of the skull (contra-coup injury). In addition to direct translational forces there are also rotational and shearing forces making mTBI a highly complex injury. The occurrence of these forces does not necessarily come from direct impact. The subsequent pathology is thought to be the result of a primary mechanism (i.e. shearing and compression) occurring at the time of injury and from a secondary mechanism involving edema and hypoxia, which occur in a time window of hours to days after the incident [4]. Post-concussive symptoms are generally grouped into three categories: cognitive, physical and behavioral anomalies. Symptoms include headache, difficulty concentrating, sleep impairment, memory deficit, depression and anxiety [5, 6]. These clinical symptoms are persistent in 10% of cases,

lasting for months to years after the injury [7].

mTBI can be defined as a range of microstructural injuries coupled with functional disturbances, rather than major structural injury, and thus have minimal detectable anatomic pathology [8]. Consequently, conventional magnetic resonance imaging (MRI) and computed tomography (CT) techniques are ineffective for mTBI assessment, whether the patient has persistent post-concussive symptoms or not. Therefore, the main objective of our work was to focus on developing a new approach to assess brain functional disturbances. To do this we exploited the functional capabilities of the resting state blood level oxygen dependent (BOLD) signal obtained with magnetic resonance imaging (MRI).

The BOLD effect results from differences in magnetic properties between oxyhemoglobin and deoxyhemoglobin in blood vessels. The magnetic susceptibility difference between these two results in a T2*-weighted signal change. Under an external stimuli, neuronal activity increases, creating a demand for oxygen delivery and therefore increasing the BOLD signal. Furthermore, in the absence of a specific task or stimuli, BOLD signals show fluctuations as a result of complex brain interactive and connective function and this is known as resting state BOLD (rs-BOLD). The rs-BOLD signal is a complex signal, where the effects of cerebral blood oxygenation and cerebral blood flow and volume are convoluted. The rs-BOLD signal shows spontaneous low frequency fluctuations [9], that exhibit inverse power-law scaling in the frequency domain [10]. It has been suggested, that these fluctuations and the inverse power-law behavior they follow originate from physiological functions as well as from instrument noise added during fMRI acquisition [10–14]. The inverse power-law scaling is a fundamental characteristic of

signals or structures considered as fractals. Fractals are infinitely complex patterns that are self-similar across different scales and their estimated dimension is a measure of the complexity of the system [15]. Complexity of the BOLD signal has been previously used as a descriptor of the neural activity based on hemodynamics and metabolic response [12, 16]. The brain, when healthy, is best described as a complex system and thus could display regional changes in the fractal dimension (FD) of the rs-BOLD signal as a result of a mTBI. A direct injury to the white matter tracts and demyelination due to chronic inflammation could affect structural connectivity among certain regions and inflammation around deep brain structures could also affect neuronal activity [17]. We hypothesized that FD could be a measure of brain local neural activity and therefore be a metric for identifying subtle functional changes in mTBI patients that are not appreciable at the anatomical level.

Materials and Methods

Patients and controls.

Fifteen subjects (13.4±2.3 y/o) with a diagnosis of concussion (post-concussion symptom scale, PCSS = 29.9±23.8) and 56 age-matched (13.7±7.8 y/o) healthy controls were scanned at rest with eyes open. For the mTBI patients the average time between MRI scanning and the date of injury was 33.0±43.8 days. The study was approved by our Institutional Research Ethics Board, (Hamilton Integrated Reaseach Ethic Board (HIREB)) and all patients gave written informed consent. As these patients were paediatric, parental assent was also approved in writing. The study was conducted according to the principles expressed in the Declaration of Helsinki.

Data acquisition and pre-processing

Patients were scanned using a GE MR750 Discovery 3T MRI scanner, while all control data were scanned using a similar GE Healthcare 3T MR scanner. Both systems used a 32-channel RF receiver coil (General Electric Healthcare, Milwaukee, WI). Healthy control data were obtained from the NIH database (ABIDE-Michigan_S1) [18]. Control data were acquired in a similar MRI scanner, using the same pulse sequence and parameters as in the patients data.

Following a routine 3-plane localizer and calibration scan for parallel imaging, a 3D inversion recovery-prepped T1-weighted anatomical data set was acquired (fSPGR, axial acquisition, TE/TR/flip angle = 4.25/11.36/12°, 256x256 matrix with 1mm slice thickness with 25.6cm FOV, 1mm isotropic acquisition). Resting state functional BOLD data was acquired using an echo planar imaging (EPI) sequence with FOV = 22cm, image matrix = 64x64; flip angle = 90°; echo time (TE) = 35ms; repetition time (TR) = 2000ms (i.e, 0.5Hz temporal sampling frequency); slice thickness of 3mm; and 180 temporal points. At the beginning of every scan, 4 additional data points were acquired but automatically discarded (allowing the system to reach steady state), making the final scan time 6 minutes and 8 seconds.

Motion correction was performed on resting state data, using a 6 point affine transformation, with the AFNI tool `3DVolreg`. Images were spatially registered to the first volume of the rs-BOLD data. Then anatomical and motion corrected rs-BOLD data were aligned and spatially warped using a 12-point affine transformation to the TT_N27 atlas using AFNI [19]. Because functional information is assumed to be processed predominantly in gray matter a binary mask was created from the TT_N27 atlas and multiplied through all functional rs-BOLD volumes.

Fractal analysis

Fractal analysis, performed over the mask on a voxel-wise basis, was done by calculating the Hurst exponent according to the procedure described by Eke et al. [13], using Matlab (v.8.3.0, The Mathworks, Natick MA). According to the rs-BOLD acquisition parameters, the time signal was sampled at 0.5 Hz for 360 seconds (180 time points x TR). Fractality or self-similarity of the time signal was assessed using a power spectral density (PSD) analysis. Low frequency fluctuation (LFF) of the BOLD signal follows an inverse power law scaling according to Eq (1) [14]:

$$|A(f)^2| \propto cf^{-\beta}, \tag{1}$$

Where A is the amplitude of the discrete Fourier transform (DFT) at frequency f; β is the spectral index and c is a constant. Following the dichotomous model proposed by Mandelbrot and Van Ness [20] the signal can be classified as fractional Brownian motion (fBm) for $\beta > 1$ and fractional Gaussian noise (fGn) for $\beta < 1$, with the Hurst exponent (H) calculated as $H = (\beta - 1)/2$ and $H = (\beta + 1)/2$ respectively for classification purposes. H is a measure of the correlation or anti-correlation of the signal. When H is close to 1.0 this indicates high correlation while H closer to 0 indicates anti-correlation. The long-memory dependence characterized by the Hurst exponent is a global characteristic while the fractal dimension is a local property. Local properties are reflected in the global characteristics, for self-affine processes in an n-dimensional space which result in the relationship $FD + H = n + 1$ where $n = 1$ for a time domain signal.

Following temporal co-registration, the raw BOLD signal Fig 1a was normalized (voxel-wise), end matched and bridge de-trended based on the procedure described by

Eke et al. [14]. The log-log representation of the power spectrum Fig 1b contained multiple characteristic regions, which could be a sign of multi-modality [12]. However, for the purpose of our study, we selected a frequency range from 0.08 - 0.16 Hz where power-law scaling behavior was consistently observed across all voxels and subjects. We followed recommendations from Herman et al. [12] about excluding low frequency regions of below 0.02 Hz due to the presence of MRI system noise in that region [10]. The peak at 0.1 Hz caused by synchronized vasomotion was not excluded as a previous study suggested in only appears in about 2% of the acquisitions [12]. The same study reported that arterial blood pressure does not affect the fractal analysis as it is uncorrelated with the rs-BOLD fluctuations.

The final Hurst coefficient was calculated by applying dispersional analysis on the fGn signals; scale windowed variance (SWV) analysis on the fBm signals and signal summation conversion (SSC) methods for the un-classified signals. FD maps were generated using the estimated voxel-wise Hurst exponent for the 15 patients and the 56 controls.

Statistical analysis

A voxel-based Z-scoring methodology was used for statistical analysis. The Z-score is the number of standard deviations (σ) a data point is above ($Z > 0$) or below the mean ($Z < 0$). The Z-score of the voxel-wise fractal dimension was calculated as: $Z_{FD} = (x - \mu)/\sigma$. Where x is the localized voxel rs-BOLD FD and μ and σ are the voxel mean and standard deviation of that same voxel from the control group respectively. Prior to application of Z-scoring, voxel-wise validation of normality was performed on the control group data (i.e. voxel-wise skewness and kurtosis was investigated). Failure to satisfy normality indicated voxels that were not classifiable

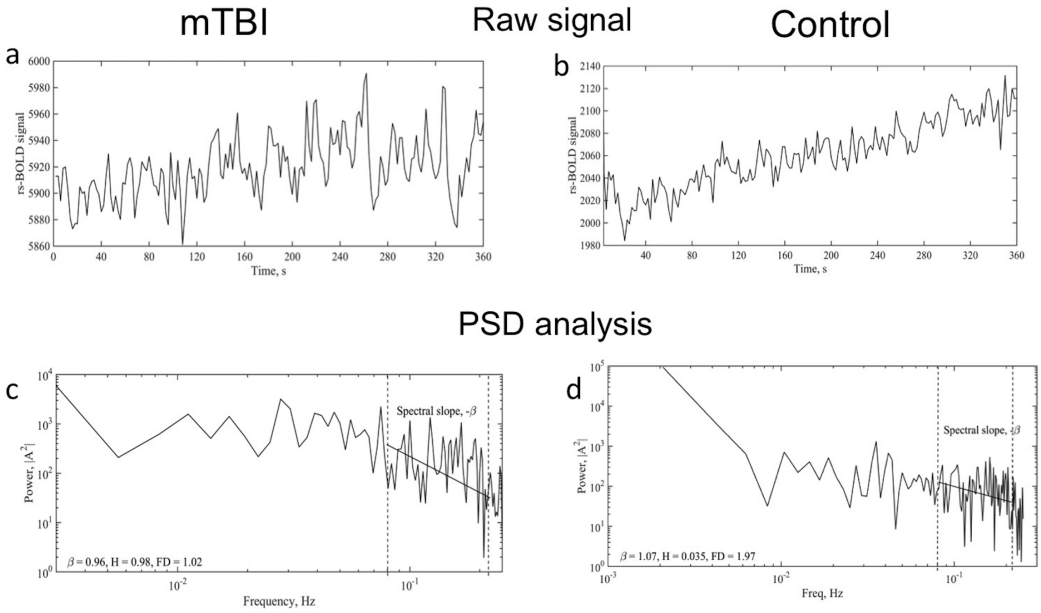

Fig 1. Raw signal and power spectrum analysis. (a) Sample raw rs-BOLD signal from grey matter of an mTBI patient(a) and a healthy control brain(b). These time courses were specifically from a 4x4x3mm voxel in the right hippocampus, located at 24.0[L],5.0[P],15.0[S] mm in the N27 atlas. (c,d) Power spectrum, from the same voxel from Fig.1a and Fig.1b respectively, showing power-law decay on a log-log scale. A frequency range of 0.08 - 0.16 Hz was fit because of the consistency in power law scaling behavior (between and within subjects) of this spectral region.

based on this approach. Also, due to inaccurate spatial warping of all control subjects some voxels had the possibility of not existing (i.e. unable to classify) simultaneously over all control subjects. To achieve a statistical power of at least 0.9 only voxels that existed simultaneously in at least 11 subjects were included in the final Z-score maps. Control data was tested for normality using the Kolmogorov-Smirnov test [21] Fig 2a, and kurtosis and skewness calculations Fig 2b,c. Based on the Kolmogorov-Smirnov test control data was considered normal within the gray matter mask. However, a more detailed analysis of skeweness and kurtosis revealed voxels

that deviated from the univariated normal distribution, which were subsequently removed from the final Z-score map. This approach removed only 3.06% of the voxels in the mean mask for normal controls. Thus the final mask was deemed acceptable for use as a Z-score featurespace.

Regions of interest(ROIs)

The Z-score maps from patients were co-registered to the TT_Daemon [22] human brain atlas and the mean Z-score was calculated for each of the 240 regions included in the atlas Fig 3.

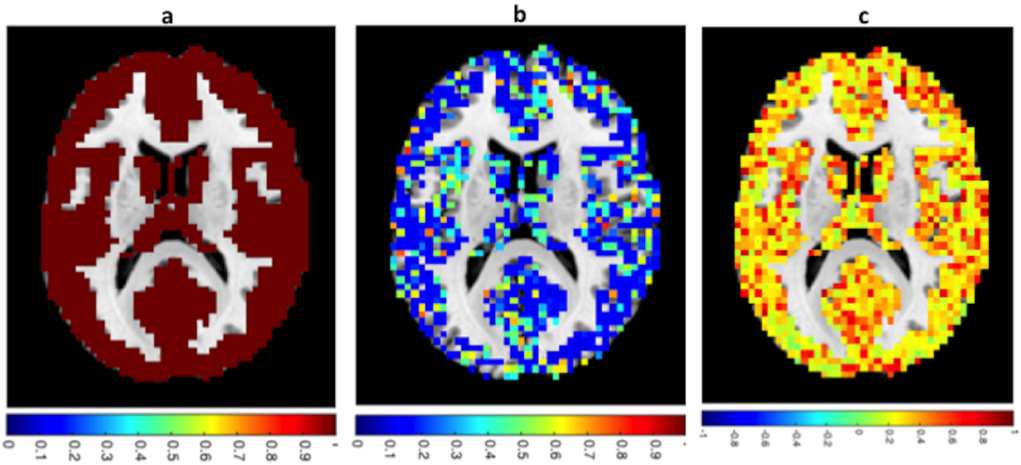

Fig 2. Analysis of normality. (a) Kolmogorov – Smirnov normality test. h=1 indicates rejection of the null hypothesis at a 5% significance level. (b) Kurtosis map. Voxels where $k \neq 3.0 \pm 0.5$ were removed from analysis. The map was centered at k=3. (c) Skewness map. Skewness measures asymmetry of the distribution. Positive skew(sk) indicates more data points above the mean while negative skew indicates more data points below the mean. Voxels where $sk \neq 0.0 \pm 0.5$ were removed from the analysis and the sk map was normalized.

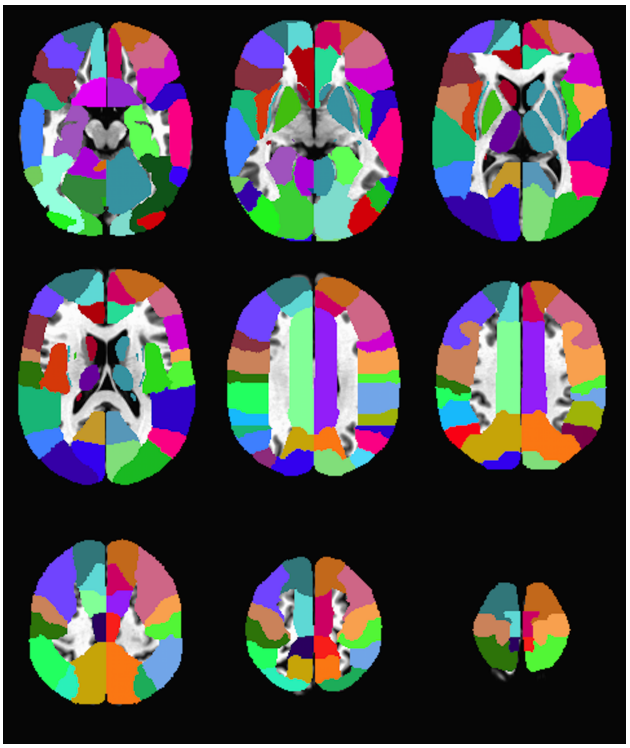

Fig 3. Regions of interest. Montage showing 9 axial slices (taken every 5mm) through the TT_Daemon human brain atlas [22] with a selection of the 240 colour-coded brain structures identified.

Results

Fractal dimension maps

Voxel-wise FD values were calculated for each of the 15 patients and 56 controls from the gray matter mask Fig 4. The mean gray matter FD for TBI patients was 1.58 $\pm$ 0.03 while the mean gray matter FD for controls was 1.61 $\pm$ 0.01. Using an unpaired t-test with unequal sample sizes, overall brain gray matter FD in patients was significantly lower compared to control ($p < 0.05$).

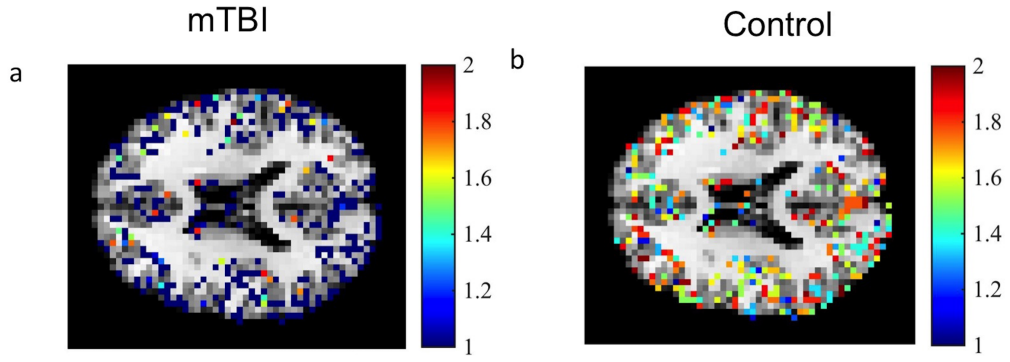

Fig 4. FD map. FD map over a gray matter mask for an mTBI patient(a) and a healthy control(b). FD values closer to 2 show increased signal complexity while FD values closer to 1 show decreased signal complexity in that region

Z-score and ROI analysis

Voxel-wise Z-score maps were calculated for every patient Fig 5 on the 240 defined regions. Ten regions that deviated the most from the control group mean were extracted for each subject and the 11 regions with higher frequency of abnormal fractal behavior were selected as the final regions of interest Fig 6. Table1 shows mean Z-score, standard deviation and p values calculated for those regions of interest that deviated greatest from control mean values.

The PCCS score was collected for every mTBI patient. This is a self-reported questionnaire where patients report, using a scale from 0-6 (no symptoms to severe), symptoms as headache, nausea, vomiting, balance problems, dizziness, fatigue, trouble falling to sleep, excessive sleep, loss of sleep, drowsiness, light sensitivity, noise sensitivity, irritability, sadness, nervousness, more emotional, numbness, feeling slow, feeling foggy, difficulty concentrating, difficulty remembering and visual problems.

Z-scores were calculated for all the regions of interest and correlated with the

Table 1. Mean Z-score, standard deviation and p-values for ROI FD values that deviated greatest from healthy controls.

ROIs	μ	σ	p
Right Amygdala	-2.28	0.90	0.02
Right Culmen of Vermis	-2.40	1.07	0.02
Left Uvula of Vermis	-2.14	1.09	0.03
Right Caudate Head	-2.06	0.70	0.04
Left Hippocampus	-2.28	0.65	0.02
Right Nucleus Accumbens	-1.99	1.11	0.05
Left Amygdala	-2.06	0.68	0.05
Right Brodmann area 23	-2.06	0.52	0.05
Right Hypothalamus	-2.01	0.79	0.04
Right Uvula of Vermis	-1.73	1.24	0.08
Right Hippocampus	-2.04	0.85	0.04
Mean_Z (whole brain GM)	-2.85	0.38	0.004

PCSS score, using the Pearson Product Moment Correlation or PPMC (Table2), to show whether there is any relationship between the two variables. For the purpose of this study the strength of the correlation was classified in low, moderate and high, following the criteria proposed on Table3. The p-values reported tested the hypothesis of no correlation against the alternative that there is nonzero correlation. A smaller p-value indicates greater significant difference from zero.

Discussion

Deoxyhemoglobin, because of its paramagnetic properties compared to diamagnetic oxyhemoglobin, has a shorter T2* relaxation time and hence reduced MR signal. When an area of brain is activated, the local neuronal oxygen consumption increases leading to a requirement for increased oxygen delivery (i.e. oxyhemoglobin). This is accomplished by a disproportionate increase in blood flow and volume, in other words more oxygen is delivered during activation than what is metabolically required. This

Table 2. Pearson correlation coefficients and p-values of PCSS compared against regional rs-BOLD Z-score.

Pearson correlation coefficient /ROIs	r	p
Right Amygdala	0.42	0.14
Right Culmen of Vermis	0.46	0.10
Left Uvula of Vermis	0.26	0.37
Right Caudate Head	0.41	0.15
Left Hippocampus	0.39	0.17
Right Nucleus Accumbens	0.31	0.29
Left Amygdala	0.11	0.70
Right Brodmann area 23	0.29	0.32
Right Hypothalamus	0.10	0.74
Right Uvula of Vermis	0.45	0.11
Right Hippocampus	0.25	0.40
Mean_Z (whole brain GM)	0.54	0.05

Table 3. Qualitative criteria used to determine strength of the correlation between FD and PCSS.

Strength of Correlation	Pearson correlation coefficient, r
Low	0.1-0.3
Moderate	0.3-0.5
High	0.5-1.0

leads to a downstream decrease in deoxyhemoglobin and corresponding elevation in T2* and MR signal. Because the signal change is due to an increased ratio of oxy to deoxyhemoglobin it is called the blood oxygen level dependent BOLD signal. During a specific task BOLD increases [23]. However, in the absence of a task, BOLD signal fluctuates as a result of complex brain interactive and connective function. This is referred to as rs-BOLD.

Based on time-domain correlation analysis, rs-BOLD has shown how parts of the brain are regionally in temporal synchrony. These so called resting state networks are robust and seen in all healthy brains. A number of networks are easily found using region-of-interest (ROI) based localization. For example, the default mode network

(DMN), the most dominant resting state network in the brain, is assessed through probing time domain correlation between the posterior cingulate and all other areas of the brain [24]. The problem with typical rs-BOLD analysis is that concurrent assessment of a large number of networks, especially the more subtle ones, requires a large number of concatenated 4D brain data sets and subsequent assessment via probabilistic independent component analysis (PICA). Such an approach is thus only for group-based analysis and single subject evaluation is impossible. An alternative single-subject approach, using rs-BOLD, is using model-free complexity analysis. Measurement of the rs-BOLD fractal dimension is the most frequently avenue for complexity analysis. This method can be used for single subject analysis and is temporally stable within, and between, healthy subjects [25].

Previous analysis of rs-BOLD signals using complexity analysis, based on fractals, has been done to assess early onset Alzheimer's disease (AD). In this work Warsi et al. [26] studied the correlation of rs-BOLD fractal dimension and in vivo proton magnetic resonance spectroscopy (^{1}H-MRS) in the left putamen of AD patients and normal controls. It was shown that decreased FD was consistent with AD severity, as measured with known biomarkers N-acetyl aspartate (NAA) ($r = 0.44$, $p = 0.015$) and myoinositol (myoI) ($r = -0.45$, $p = 0.012$). Additionally, a study by Weber et al. [27] showed how complexity of the rs-BOLD signal decreased as ethanol levels in the brain increased. This was seen particularly in the right basal ganglia at 60 and 90 minutes after ethanol consumption. Furthermore, the rs-BOLD signal complexity returned as the brain ethanol became metabolized. Ethanol directly affects function of the brain GABA-A receptors [28] decreasing brain connectivity. As ethanol was cleared in the brain, brain connectivity increased and fractal dimension increased.

The conclusion from this work was that the temporal complexity of brain resting state was diminished with increased levels of brain alcohol. In other words, the ability of the brain to process information was reduced in an intoxicated state and this effect was observed in the fractal dimension of the BOLD signal.

Complexity of brain signals, characterized by the fractal dimension, has also been investigated in resting-state electroencephalography (rs-EEG). A recent study by Smits et al. [29] showed calculations of FD in resting state EEG recordings from 67 AD patients and 41 healthy controls. They found the FD and signal complexity decreased with age in normal controls and that it further decreased in AD patients, especially in temporal-occipital regions [29]. This study supports the concept that brain signal FD correlates with changes in brain connectivity and complexity.

Based on previous studies [12, 26, 27], it can be inferred that the FD of rs-BOLD represents brain temporal complexity at rest. Ideally, a healthy brain could be associated with more complex signals, due higher multi-level and multi-time connectivity within different brain regions. Furthermore, FD could be an indicator of the brain's ability to perform real-time adaptation and processing of the multitude of external stimuli that subsequently lead to the continuous driving of brain metabolic fluctuation. Low FD characterizes less complex signals, which has been associated with pathologies of the brain [26–28, 30]. Therefore, a decrease in signal complexity could be associated with lack of adaptability and decreased brain connectivity.

The fractal dimension maps produced for mTBI and control subjects showed that overall, grey matter rs-BOLD FD in mTBI patients decreased compared to controls. This indicates reduction in temporal complexity of the rs-BOLD leading us to our hypothesis that patients with mTBI experience a decrease in brain connectivity and

that this could be observed with the FD approach. Z-score and subsequent regional ROI analysis revealed a group of brain regions where FD values were observed to deviate the greatest from mean values, as calculated from a population of healthy controls. On average these regions had Z-scores values of -2.09 $\pm$ 0.18, or 2.09σ below the mean. Table 1 shows 11 brain regions where FD significantly decreased for mTBI patients.

In nine out of fifteen mTBI patients, the right amygdala was among the ten regions with lower Z-score values, however the right culmen of vermis reported the lowest values among the all the studied ROIs. The amygdala is a brain structure known to be highly involved in the processing of emotions. Animal studies have shown decreased excitability, decreased activation and inflammation in the amygdala after mTBI [31, 32]. The reported effects of mTBI in the amygdala also validate neuropsychological symptoms commonly reported by TBI patients. Our study showed decreased FD in the amygdala (Z-score = -2.28$\pm$0.90), which is consistent with decreased neural activity in the region.

The culmen and the uvula of vermis, both cerebellar structures had decreased FD values (Z-score = -2.40$\pm$1.07 and Z-score = -1.93$\pm$1.16 respectively), supporting previous studies that suggested a link between mTBI and cerebellar dysfunction. A recent diffusion tensor imaging (DTI) study of mTBI patients showed decreased fractional anisotropy (FA) in the vermis compared to normal controls [33]. Lower FA has been implicated in reduction of myelin integrity, which for mTBI likely would be due to shearing forces causing micro tears in the axons. [33]. They suggested that damage on these cerebellar regions could be associated with a dysfunction in primitive fear conditioning circuits [34]. Additionally, a longitudinal study based on

brain volume changes, showed a significant decrease in cerebellar volume of mTBI patients [35].

The caudate nucleus and nucleus accumbens are regions of the basal ganglia. They have been implicated with voluntary movement, learning, memory, sleep, and social behavior and cognitive processing of aversion, motivation, pleasure, reward and reinforcement learning respectively [36, 37]. We found decreased FD for these two regions and Z-scores were -2.06±0.7 and -1.99±1.11 respectively. Decreased signal complexity in these regions agrees with neuropsychological symptoms commonly reported by mTBI patients. A previous study correlated iron deposition in these regions, through susceptibility weighted imaging (SWI), to cognitive impairment in mTBI patients. A significant increase in caudate nucleus iron deposition has been found to be positively correlated with the mini-mental state examination [38].

There is increasing evidence that cognitive and memory dysfunction of mTBI patients is related to neuro-physiological changes that occur in the hippocampus. Recent studies have shown changes in important neurotransmitters such as glutamate and γ-aminobutyric acid (GABA) in the hippocampus following mTBI [39, 40]. We found that FD decreased for mTBI patients when compared with the uninjured control group in both these areas. The mean Z-score value for hippocampus was -2.16 ± 0.75. Decreased signal complexity in the hippocampus after mTBI is consistent with changes in neuronal firing patterns reported by Witgen et al. [41].

ROI-based Z-scores were correlated with PCSS scores using the Pearson Product Moment Correlation (PPMC). The correlation coefficients (r) paired with the respective p-values (Table2) showed high correlation for GM; moderate correlation for the right nucleus accumbens, right uvula of vermis, left hippocampus, right caudate

head, right culmen of vermis and right amygdala; and low correlation for left uvula of vermis, left amygdala, right Brodmann area 23, right hypothalamus and right hippocampus. Negative correlation was expected because we hypothesized that as symptoms worsen the FD should decrease. However, all ROIs and GM showed positive correlation Table2 with PCSS. This implies that as symptoms worsen the FD Z-score increases (absolute value of Z-score decreases). The absence of significant correlation with the PCSS score was expected because this metric does not characterize symptoms associated with unique brain regions. Still, PCSS is the most common test used clinically to characterize mTBI. This study, highlights the issues related with the use of a self reported metric while trying to characterize a complex phenomenon.

The effectiveness of PCSS in the assessment of cerebral concussion remains unclear given that such symptoms are non-specific. A study by Iverson et al. indicated that non-concussed normal controls have reported identical symptom scores than those used on the PCSS score [42]. Therefore, using PCSS as a metric to establish correlation with mTBI FD data may be considered unsatisfactory. Neuropsychological tests specifically designed to measure a psychological function, related to a particular brain structure or pathway would be of greater interest for future studies.

The main limitation of this study arises from our relatively low sampling frequency. The effectiveness of the fractal analysis is based on the ability of the signal to capture the true dynamics of the processes being studied. Ideally the sampling frequency should be one order of magnitude higher than the highest frequency of the hemodynamic response to neuronal activation. The BOLD responses are delayed by 1–2 s and have a temporal width on the order of 4–6 s [43], therefore we need to be

able to sample the signal at 0.125 Hz (ideally 1.25 Hz). In order to acquire the rs-BOLD signal for the entire brain in a reasonable time for the patients we were only able to sample at a frequency of 0.5 Hz which significantly limited the scope of our study. New techniques such as multi-band EPI would be ideal to overcome this issue as they are able to achieve full brain sampling rates up to 2.5 Hz [44].

Conclusions

This study shows how rs-BOLD fractal dimension appears to provide additional patient-specific brain focal information that can be used to assess and possibly monitor mTBI patients. Traditional functional imaging approaches, based on linear models, are able to show differences between normal and mTBI patients, but only based on group-based statistics. It is well known that the brain is best modeled as a complex system [45] and therefore a measure of complexity using FD could provide a method to approach the mTBI problem. In this study, we were able to find regions in the brain that despite not showing any abnormality in an anatomical scan, reported decreased signal complexity using FD methodology. These regions have been previously reported as dysfunctional for mTBI patients. The method we have proposed is able to provide additional information of mTBI in a non-invasive and fast manner and could hopefully help in the design of future treatment plans.

Acknowledgments

This project was supported by the Canadian Institutes of Health Research(www.cihr-irsc.gc.ca).

References

1. Faul MXL, Wald M, and Coronado V. Traumatic Brain Injury in the United States: Emergency Department Visits, Hospitalizations and Deaths, 2002–2006. Atlanta, GA: Centers for Disease Control and Prevention; 2010.

2. Susman M, DiRusso SM, Sullivan T, Risucci D, Nealon P, Cuff S, et al. Traumatic brain injury in the elderly: increased mortality and worse functional outcome at discharge despite lower injury severity. J Trauma. 2002;53:219–224. doi: 10.1097/00005373-200208000-00004.

3. Jordan DB The clinical spectrum of sport-related traumatic brain injury. Nat Rev Neurol. 2013 ;9(4):222–230.

4. Greve MW, and Zink BJ. Pathophysiology of traumatic brain injury. Mt. Sinai J Med. 2009;76:97–104. doi: 10.1002/msj.20104.

5. Levin HS, Mattis S, Ruff RM, Eisenberg HM, Marshall LF, Tabaddor K, et al. Neurobehavioral outcome following minor head injury: a three-center study. J. Neurosurg. 1987;66:234–243. doi: 10.3171/jns.1987.66. 2.0234.

6. Park, E., Bell, J. D., and Baker, A. J. Traumatic brain injury: can the consequences be stopped? CMAJ. 2008;178:1163–1170. doi: 10.1503/cmaj.080282

7. Greig NH, Tweedie D, Rachmany L, Li Y, Rubovitch V, Schreiber S, et al. Incretin mimetics as pharmacologic tools to elucidate and as a new drug strategy to treat traumatic brain injury. Alzheimers Dement. 2014;10(12):S62–S75.

8. McCrory P, Meeuwisse WH,Aubry M, et al. Consensus statement on concussion in sport. Br J Sports Med. 2013;47:250–258.

9. Fox M, Raichle M. Spontaneous fluctuations in brain activity observed with functional magnetic resonance imaging. Nat Rev Neurosci. 2007;8:700–711.

10. Zarahn E, Aguirre G, D'Esposito M. Empirical analyses of BOLD fMRI statistics. I. Spatially unsmoothed data collected under null-hypothesis conditions. . Neuro-image. 1997;5:179–197.

11. El Boustani S, Marre O, Behuret S, Baudot P, Yger P, Bal T, Destexhe A, Fregnac Y. Network-state modulation of power–law frequency-scaling in visual cortical neurons. PLoS Comput. Biol. 2009;5.e1000519.

12. Herman P, Sanganahalli BG, Hyder F , Eke A. Fractal analysis of spontaneous fluctuations of the BOLD signal in rat brain. NeuroImage. 2011;58:1060—1069.

13. Eke A, Herman P, Bassingthwaighte J, Raymond G, Percival D, Cannon M, Balla I, Ikrenyi C. Physiological time series: distinguishing fractal noises from motions. Pflugers Arch. 2000;439:403–415.

14. Eke A, Herman P, Kocsis L, Kozak L, Fractal characterization of complexity in temporal physiological signals. Physiol Meas. 2002;23:R1–R38.

15. Mandelbrot BB (1985) Self-affine fractals and fractal dimension. Phys Sci. 1985;32:257-–260

16. Bullmore E, Barnes A, Bassett D, Fornito A, Kitzbichler M, Meunier D, Suckling J. Generic aspects of complexity in brain imaging data and other biological systems. Neuroimage. 2009; 47: 1125-–1134.

17. Felger JC, Li Z, Haroon E, Woolwine BJ, Jung MY, Hu X, Miller AH. Inflammation is associated with decreased functional connectivity within corticostriatal reward circuitry in depression. Mol Psychiatry. Oct 2016;21(10):1358–65. doi: 10.1038/mp.2015.168.

18. Di Martino A, Yan CG, Li Q, Denio E, Castellanos FX et al. The autism brain imaging data exchange: towards a large-scale evaluation of the intrinsic brain architecture in autism. Molecular Psychiatry. Jun 2014;19:659–667. doi:10.1038/mp.2013.78.

19. Cox RW. AFNI Computers and Biomedical Research. 1996;29(3):162–173.

20. Mandelbrot B, van Ness J. Fractional Brownian motions, fractional noises and applications. SIAM Rev. 1968;10:422–437.

21. Smirnov N. Table for estimating the goodness of fit of empirical distributions. Annals of Mathematical Statistics. 1948 ;19:279-281. doi:10.1214/aoms/1177730256.

22. Eickhoff et al. Anatomy Toolbox. Neuroimage 25. 2005; $http://www.fzjuelich.de/ime/spm_anatomy_toolbox$.

23. DeYoe EA, Bandettini P, Neitz J, Miller D, Winans P. Functional magnetic resonance imaging (FMRI) of the human brain. J Neurosci Methods. 1994; 54(2):171–187.

24. Rosazza C, Minati L. Resting-state brain networks: literature review and clinical applications. Neurol Sci. 2011; 32(5):773–785.

25. Warsi MA, Weber AM, Noseworthy MD. Brain Fractal Blood-Oxygen Level Dependent (BOLD) Signals: The Effect of MRI Acquisition Parameters on Temporal Fractal Dimension (FD) Stability. Visualization, Image Processing and Computation in Biomedicine. 2013;2(1). doi: 10.1615/VisualizImageProcComputatBiomed.2013006007

26. Warsi MA, Molloy W, Noseworthy MD. Correlating brain blood oxygenation level dependent (BOLD) fractal dimension mapping with magnetic resonance spectroscopy (MRS) in Alzheimer's disease. MAGMA. 2012 Oct;25(5):335–44. Epub 2012 Mar 24.

27. Weber AM, Soreni N, Noseworthy MD. A preliminary study on the effects of acute ethanol ingestion on default mode network and temporal fractal properties of the brain. MAGMA. 2014 Aug;27(4):291–301. doi: 10.1007/s10334-013-0420-5. Epub 2013 Nov 28.

28. Simpson PE, Criswell HE, Breese GR. Inhibition of NMDA-Evoked Electrophysiological Activity by Ethanol in Selected Brain Regions: Evidence for Ethanol-Sensitive and Ethanol-Insensitive NMDA-Evoked Response. Brain Research. 1993; 607:9–16.

29. Smits FM, Porcaro C, Cottone C, Cancelli A, Rossini PM, Tecchio F. Electroencephalographic Fractal Dimension in Healthy Ageing and Alzheimer's Disease. PLoS One. 2016 Feb 12;11(2):e0149587. doi: 10.1371/journal.pone.0149587.

30. Goldberger et al. Fractal dynamics in physiology: Alterations with disease and aging Proc Natl Acad Sci USA. 2002;99(Suppl):2466-–2472. doi: 10.1073/pnas.012579499

31. Palmer CP, Metheny HE, Elkind JA, Cohen AS. Diminished amygdala activation and behavioral threat response following traumatic brain injury. Experimental Neurology. 2016; 277:215–226:ISSN 0014-4886.

32. Vállez García D, Otte A, Dierckx RA, Doorduin J. Three months follow-up of rat mild traumatic brain injury: a combined [18F]FDG and [11C]PK11195 PET study. J Neurotrauma. 2016. doi:10.1089/neu.2015.4230.

33. Tu T, Williams RA, Lescher JD, Jikaria N et al. Radiological-pathological correlation of diffusion tensor and magnetization transfer imaging in a closed head traumatic brain injury model. Annals of Neurology. 2016; 79(6):907–920. doi:10.1002/ana.24641

34. Alhilali LM, Delic JA, Gumus S, Fakhran S. Evaluation of White Matter Injury Patterns Underlying Neuropsychiatric Symptoms after Mild Traumatic Brain Injury. Radiology. 2015;277(3):793-800. doi: 10.1148/radiol.2015142974.

35. Munivenkatappa A, Bhagavatula ID, Shukla DP, Rajeswaran J. Three time point view of mild brain injuries' structural alteration and their association with cognitive domains. J Neurosurg Sci. 2015 Sep 9;

36. Wenzel JM, Rauscher NA, Cheer JF, Oleson EB. A role for phasic dopamine release within the nucleus accumbens in encoding aversion: a review of the

neurochemical literature. ACS Chem Neurosci. 2015;6 (1):16—26. doi:10.1021/cn500255p.PMID 25491156

37. Malenka RC, Nestler EJ, Hyman SE, Sydor A, Brown RY Molecular Neuropharmacology: A Foundation for Clinical Neuroscience (2nd ed.). New York: McGraw-Hill Medical:147–148, 367, 376. ISBN 978-0-07-148127-4.

38. Liyan Lu, Heli Cao, Xiaoer Wei, Yuehua Li, and Wenbin Li. Iron Deposition is Positively Related to Cognitive Impairment in patients with chronic mild traumatic brain injury: Assessment with susceptibility Weighted imaging BioMed Research International. 2015;2015:id470676. doi:10.1155/2015/470676

39. Harris JL, Yeh HW, Choi IY, Lee P, Berman NE, Swerdlow RH, et al. Altered neurochemical profile after traumatic brain injury: (1)H- MRS biomarkers of pathological mechanisms. J Cereb Blood Flow Metab.2012; 32:2122—2134. doi: 10.1038/jcbfm.2012.114.

40. Almeida-Suhett CP, Prager EM, Pidoplichko V, Figueiredo TH, Marini AM, Li Z, et al. GABAergic interneuronal loss and reduced inhibitory synaptic transmission in the hippocampal CA1 region after mild traumatic brain injury. Exp Neurol. 2015;273:11—23. doi: 10.1016/j.expneurol.2015.07.028

41. Witgen BM, Lifshitz J, Smith ML, Schwarzbach E, Liang SL, Grady MS, et al. Regional hippocampal alteration associated with cognitive deficit following experimental brain injury: a systems, network and cellular evaluation. Neuroscience. 2005; 133:1—15. doi:10.1016/j.neuroscience.2005.01.052

42. Iverson GL, Lange RT. Examination of "postconcussion-like" symptoms in a healthy sample. Appl Neuropsychol. 2003;10:137–44.

43. Bandettini PA, Wong EC, Hinks RS, Tikofsky RS, Hyde JS. Time course EPI of human brain function during task activation. Magn. Reson. Med. 1992; 25:390-–397.

44. Feinberg DA, Moeller S, Smith SM, Auerbach E, Ramanna S, Gunther M, Glasser MF, Miller KL, Ugurbil K, Yacoub E. Multiplexed echo planar imaging for sub-second whole brain FMRI and fast diffusion imaging. PLoS One. 2010; 5:e15710

45. Kannathal N, Puthusserypady SK, et al. Complex dynamics of epileptic EEG. Conf Proc IEEE Eng Med Biol Soc. 2004; 1: 604-–607.

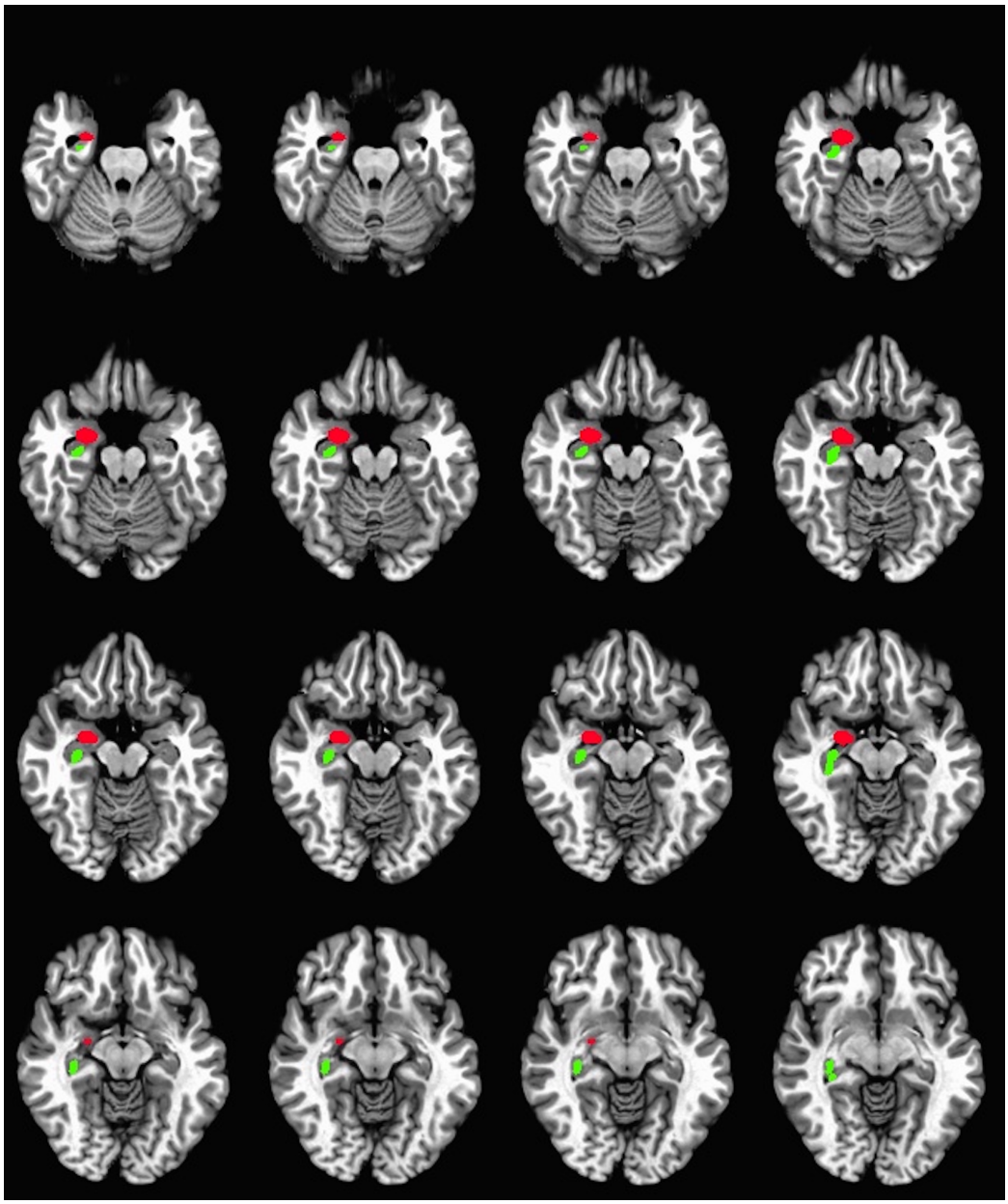

Fig 5. ROIs with $|Z| > 2.0$. Z-score map over grey matter mask was used to calculate the regions that significantly deviated (p=0.01) from the mean FD. This particular patient showed significant FD decreased in the right hippocampus (red) and the right amygdala (green)

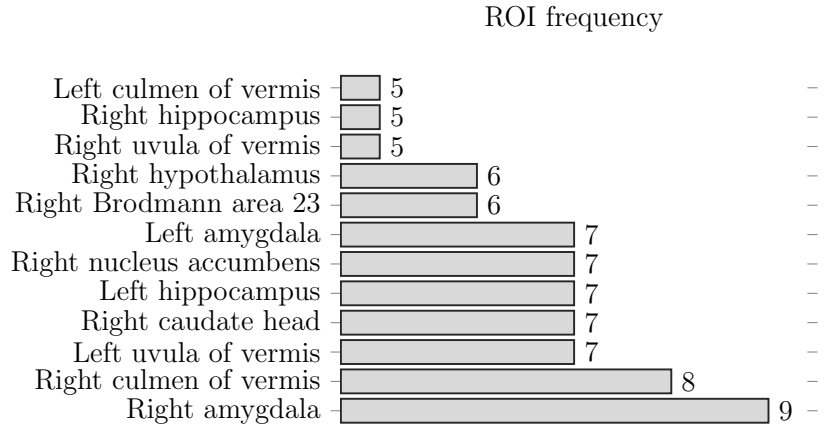

Fig 6. ROI frequency. Bar graph showing ROI frequency in mTBI. Regions where FD decreases significantly. i.e. 9 out of 15 patients showed decreased FD in the right amygdala while 5 out of 15 showed decreased FD in the right hippocampus

Chapter 5

Fractal Analysis of the rs-BOLD signal in Autism Spectrum Disorder (ASD) patients.

Regional Fractal Analysis of Brain Blood Oxygenation Level Dependent (BOLD) Signals from Children With Mild Traumatic Brain Injury (mTBI).
Olga Dona, Michael D. Noseworthy and Geoffrey Hall.

5.1 Context of the paper

Brain connectivity in autism spectrum disorders (ASD) has proven difficult to characterize due to the heterogeneous nature of the spectrum. Connectivity in the brain occurs in a complex, multilevel and multi-temporal manner, driving the fluctuations observed in local oxygen demand. These fluctuations can be characterized as fractals, as they auto-correlate at different time scales. In this study we propose a model-free complexity analysis based on the fractal dimension of the rs-BOLD signal, acquired with magnetic resonance imaging. The fractal dimension can be interpreted as measure of signal complexity and connectivity. Previous studies have suggested that reduction in signal complexity can be associated with disease. Therefore, we hypothesized that a detectable difference in rs-BOLD signal complexity could be observed between ASD patients and Controls.

Anatomical and functional data from fifty-five subjects with ASD (12.7 ± 2.4 y/o) and 55 age-matched (14.1 ± 3.1 y/o) healthy controls were accessed through the NITRC database and the ABIDE project. Subjects were scanned using a 3T GE Signa MRI and a 32-channel RF-coil. Axial FSPGR-3D images were used to prescribe rs-BOLD (TE/TR=30/2000ms) where 300 time points were acquired. Motion correction was performed on the functional data and anatomical and functional images were aligned and spatially warped to the N27 standard brain atlas. Fractal analysis, performed on a grey matter mask, was done by estimating the Hurst exponent in the frequency

domain using a power spectral density approach and refining the estimation in the time domain with de-trended fluctuation analysis and signal summation conversion methods.

Voxel-wise fractal dimension (FD) was calculated for every subject in the control group and in the ASD group to create ROI-based Z-scores for the ASD patients. Voxel-wise validation of FD normality across controls was confirmed, and non-Gaussian voxels were eliminated from subsequent analysis. To maintain a 95% confidence level, only regions where Z-score values were at least 2 standard deviations away from the mean (i.e. where $|Z| > 2.0$) were included in the analysis. We found that the main regions, where signal complexity significantly decreased among ASD patients, were the amygdala (p=0.001), the vermis (p=0.02), the basal ganglia (p=0.01) and the hippocampus (p=0.02). No regions reported significant increased in signal complexity in this study. Our findings were correlated with ADIR and ADOS assessment tools, reporting the highest correlation with the ADOS metrics. Brain connectivity is best modeled as a complex system. Therefore a measure of complexity as the fractal dimension of the fluctuations in the brain oxygen demand could provide important information about connectivity issues in ASD. Moreover, this technique can be used in the characterization of a single subject respect to controls without the need of group analysis, making it ideal for personalized diagnostic, thus providing unique patient specific assessment.

5.2 Declaration Statement

Olga M. Dona, as first author, acquired the data, performed the data analysis and interpretation of the results and drafted the article including tables and figures.

Contributions by Olga M. Dona warranted her name as first author.

Dr. Michael D. Noseworthy, as corresponding author, designed and conceptualized this project which is part of a his long trajectory on developing applications based on the fractal analysis in human brain signals. He performed the critical revision of the article and the final approval of the version to be published. Furthermore, Dr. Noseworthy provided constant guidance and advice through out the duration of this study and secured the required funds.

Dr. Geoffrey Hall actively collaborated in the interpretation of the results due to his vast experience studying ASD. Moreover, he exhaustively revised and edited the final version of this article

This paper has been submitted for publication to the journal Nature Scientific Reports on December 10^{th}, 2016 .

5.3 Paper

Temporal Fractal Analysis Identifies Brain Abnormalities in Autism Spectrum Disorder.

Olga Dona [1,2], Geoffrey Hall. [2,5] and Michael D. Noseworthy [1,2,3,4,*]

[1] McMaster School of Biomedical Engineering, McMaster University, Hamilton, Ontario, Canada.
[2] Imaging Research Centre, St. Josephs Healthcare, Hamilton, Ontario, Canada.
[3] Department of Electrical and Computer Engineering, McMaster University, Hamilton, Ontario, Canada.
[4] Department of Radiology, McMaster University, Hamilton, Ontario, Canada.
[5] Department of Psychology, Neuroscience & Behaviour, McMaster University, Hamilton, Ontario, Canada.
[*] Corresponding author: Michael D. Noseworthy.nosewor@mcmaster.ca

Brain connectivity occurs in a complex multi-level manner driving fluctuations in local brain oxygen demand. These fluctuations have been previously characterized as fractals, as they autocorrelate at different time scales. In this study, we performed fractal analysis of MRI resting state blood oxygenation level dependent (rs-BOLD) signals to study autism spectrum disorder (ASD). It has been suggested that reduction in signal complexity is associated with abnormality. Therefore, we hypothesized that a detectable regional difference in temporal rs-BOLD fractal dimension (FD) would be observed between ASD patients and healthy controls. We found regional signal complexity was significantly lower among ASD patients for the amygdala (p=0.001), vermis (p=0.02), basal ganglia (p=0.01) and hippocampus (p=0.02), all commonly reported as dysfunctional in ASD. This fast non-invasive approach can be used to assist in patient management and the monitoring of potential targeted therapies for ASD.

Introduction

Clinical and neurobiological heterogeneity in autism spectrum disorder (ASD) is a marked obstacle in trying to understand the underlining mechanisms of the disorder and a barrier in increasing treatment efficacy. Early intervention with behavioral therapies has consistently reported to improve the quality of life of ASD patients; therefore development of methods for early diagnosis that focus on patient specific abnormalities has been highly prioritized around the globe. Neuroimaging research has explored anatomical and functional disturbances in ASDs aiming at gaining insight into the pathophysiology of the disorder. However, giving the heterogeneous nature of ASD, a wide range of brain structures and brain networks have been identified as atypical by different studies. In terms of anatomic abnormalities, recent MRI studies have found overgrowth of the brain in early stages of the disorder and abnormal decline during later stages, specifically in adolescence.[1] The decline in adolescence is characterized by cortical atrophy,[2] frontal cortex volume reduction[3] and atrophy of the amygdala.[4] Additionally, diffusion tensor imaging (DTI) studies in ASD have shown reduced white matter integrity in corpus callosum,[5] anterior cingulate gyri, bilateral superior temporal sulcus and temporal lobes approaching the amygdala.[6] The abnormalities detected in these anatomical regions, combined with reduced structural connectivity, suggested changes in functional connectivity that could be of interest for diagnosis and assessment of the disorder.

Functional connectivity has been widely studied using either task-based or resting estate functional MRI techniques. However, reported results have been inconsistent or inconclusive. For instance, while some task based-fMRI studies have shown increased connectivity on ASD patients respect to controls[7–9] others have reported decreased or weaker connectivity.[10–14] Furthermore, rs-fMRI studies have reported results that range from broad reduced connectivity in the default mode network (DMN)[15] to reduced connectivity between the superior frontal gyrus and the posterior cingulate cortex (PCC) and stronger connectivity between right parahippocampal gyrus and the PCC.[16]

One of the flaws of the current methodologies to assess brain connectivity in ASD patients is that they heavily rely on group analysis. Large datasets of rs-fMRI are assessed using probabilistic independent component analysis (PICA) to find temporal synchrony among regions of

the brain. This determines the brain networks and the correlation coefficients, where the latter represents the connectivity strength within each network. This approach is generally unsuitable when drawing conclusions on such heterogeneous disorders and to assess the condition on a single patient basis. As a result, the aim of this work consists in proposing an alternative single-subject approach, using a model-free complexity analysis based on the fractal nature of the rs-BOLD signal acquired with magnetic resonance imaging.

The rs-BOLD signal is produced by temporal fluctuations of blood oxygen in the brain. At rest, this fluctuations are caused by complex neuronal connective functions, that demand an increase in local oxygen consumption. When the deoxyhaemoglobin to oxyhaemoglobin ratio decreases, the local magnetic field is perturbed due to changes in magnetic properties, which cause the MR signal to increase. Previous studies by Logothetis et al.[17,18] have shown that activation of apical dendrites in particular, is reflected in the BOLD signal. Greater spine densities in apical dendrites have been found in ASD,[19] suggesting connection changes specifically in the cerebral cortex. Furthermore, a recent study have identified ASD-linked mutations in synaptic genes that affect excitatory neuron dendrite development and synapse function in the cortex.[20] These alterations in the structural organization and functional connectivity in ASD could be reflected in rs-BOLD signal.

Studies on the brain rs-BOLD signal have shown that the signal contains spontaneous low frequency fluctuations (LFF)[21] that originate from physiological functions such as cerebral blood oxygenation and cerebral blood flow and volume as well as from instrument noise added during fMRI acquisition.[22–26] These LFF follow the inverse power law scaling in the frequency domain, which is a defined indication of fractality. Time signals are considered fractals when they are self-similar and auto-correlate across different time scales. The fractal dimension (FD) is considered a metric of signal complexity, which has been previously used as a descriptor of the neural activity based on hemodynamics and metabolic response.[24,27]

Fractal analysis of brain signals has been done in a range of pathologies that include epilepsy, Alzheimers disease and vascular dementia and acquired through different imaging modalities such as electroencephalography (EEG), magnetoencephalography (MEG) and single photon emission computed tomography (SPECT).[28–31] Additionally, recent studies have done fractal analysis, specifically on brain rs-BOLD signals, obtaining insightful information about connec-

tivity issues on Alzheimer Disease among others.[32,33]

In this study, we hypothesize that patients with ASD could show changes in the FD of the rs-BOLD signal and that theses changes would reflect underlying alterations of neural structural organization and functional connectivity. The viability of this method to asses individual patients could help to overcome the heterogeneity issues and could have important treatment implications.

Materials and Methods

Patients and normal controls

The data for this study was accessed through NITRC and the ABIDE-1 data-base.[34] Fifty-five ASD subjects (12.7 ± 2.4 y/o) participated in this study. Forty-five were diagnosed with Autistic Disorder, seven with Asperger's Disorder, one with PDD-NOS and two with ASD of undetermined subtype. Diagnosis was established with the Autism Diagnostic Observation Schedule (ADOS),[35] the Autism Diagnostic Interview Revised (ADI-R)[36] as well as clinical consensus. Fifty-five age-matched (14.1 ± 3.1 y/o) subjects were MRI scanned as typical controls. In order to avoid controls with borderline intelligence quotient (IQ), typical controls were required to score more than 85 on the IQ, less than 10 on the Social Communication Questionnaire[37] and less than 6 on the obsessive-compulsive sub-scale of the Spence Children's Anxiety scale (SCAS).[38] See *Table 1* for phenotypic information.

Data acquisition and pre-processing

Resting state Blood Oxygenation Level Dependence (rs-BOLD) fMRI and anatomical data were acquired on a 3T GE Signa scanner using a 32-channel RF-coil (General Electric Healthcare, Milwaukee, WI). The anatomical data were acquired following a 3-plane localizer and a calibration scan designed for parallel imaging using a 3D inversion recovery-prepped T1-weighted pulse sequence (fSPGR, axial acquisition, TE/TR/flip angle = 1.8/15.63/15deg, 256x256 matrix with 1.2 mm slice thickness with 26 cm FOV). Resting state functional BOLD data was acquired in 10 min using an echo planar imaging (EPI) sequence with FOV = 22cm, image matrix = 64x64; flip angle = 90deg; echo time (TE) = 30 ms; repetition time (TR) = 2000ms

(i.e, 0.5Hz temporal sampling frequency); slice thickness of 3mm; and 300 temporal points. At the beginning of every scan, 4 additional data points were acquired but automatically discarded to allow the system to reach steady state. The rs-BOLD data were corrected for motion artifacts using a time series general affine registration for 12 parameters (3dWarpDrive/AFNI). Posterior ROI analysis required the rs-BOLD data to be transformed into a standard space where statistical maps of anatomically defined brain regions have been defined. Skull stripped anatomical data were aligned to the TT_N27 Tailarach standard space then warped with the rs-BOLD data using a 12-point affine transformation to obtain our final dataset. The 240 regions of interest (ROIs) defined for this study were extracted from the TT_Daemon human brain atlas[39] provided with the AFNI package.[40]

Fractal Analysis

Because the rs-BOLD signal has been associated with post-synaptic potentials, which are mainly localized in grey matter as opposed to action potentials more common in the white matter; we calculated FD over a grey matter mask. Fractal dimension estimation was done by calculating a voxel-wise Hurst exponent (H) on the grey matter mask, following the methodology proposed by Eke et al.[26] For self-affine processes in an n-dimensional space, the Hurst exponent is related to the fractal dimension (FD) such as $FD + H = n + 1$, where $n = 1$ for a time domain signal. The rs-BOLD raw signal was initially normalized, end matched and bridge de-trended following Ekes procedure. The data was normalized by subtracting the mean from every data point while end matching and bridge detrending was achieved by subtracting from the data the line that connects the first and the last point and multiplying the data by a parabolic window Eq (1).

$$W(j) = 1 - \left(\frac{2j}{N+1} - 1\right), j = 1 \rightarrow N, \tag{1}$$

Where N is the number of time points.

The series were Fourier transformed to the frequency domain and the scaling exponent (beta) of the inverse power law Eq (2) calculated. Where A is the amplitude of the discrete Fourier transform (DFT) at frequency f; β is the spectral index and c is a constant. The spectral index

was calculated in a frequency range from 0.08 - 0.16 Hz where power-law scaling behavior was consistently observed across all voxels and subjects. A previous study[24] have suggested excluding low frequency regions below 0.02 Hz due to the presence of MRI system noise in that region.[22] The spectral index calculated from this frequency range was exclusively used for signal classification while the entire signal in the time-domain was used in the final estimation of the Hurst exponent.

Following the dichotomous model proposed by Mandelbrot and Van Ness[41] the signals were classified as fractional Brownian motion (fBm) for $\beta > 1$ and fractional Gaussian noise (fGn) for $\beta < 1$.

$$|A(f)^2| \propto cf^{-\beta}, \tag{2}$$

The Hurst exponent on fGn signals was calculated by using the dispersional analysis proposed by Bassingthwaighte,[42] which is based on the variability of the local averages of the signal over different time windows (τ) Eq (3). However, a scaled window variance analysis was used to calculate H on the fBM signals where the series, were divided in non-overlapping windows.

$$SD(\tau) = SD(\tau_0)\left(\frac{\tau}{\tau_0}\right)^H, \tag{3}$$

Signals where β was near 1 produced ambiguous results, therefore the classification method was refined using the signal summation conversion method (SSCM) described by.[26] It is important to mention here that fractal dimension estimation based on a dispersional analysis is quite robust with respect to uncorrelated noise and does not require preprocessing.[42] For instance, uncorrelated noise generated by motion artifacts will not affect the estimation of the fractal dimension.

Z-score Analysis

A voxel-based Z-scoring methodology and the Pearson Product Moment Correlation PPMC was used in the statistical analysis. Efficacy of the Z-score is based on the assumption of normality of the data. Therefore, the data was subjected to analyses of normality such as the Kolmogorov-Smirnov test,[43] Kurtosis and Skewness assessment, where voxels that didnt fit the model were

excluded from the analysis *Fig. 1*. Additionally, the voxels that contained data from less than 11 subjects in the control group were filtered in order to sustain a statistical power of 90% over the entire mask. This approach removed less than 3.0 $\%$ of the voxels in the mean mask for normal controls and it was deemed acceptable for its use in the Z-score methodology. This study was conceived as an exploratory study rather than a hypothesis driven design, therefore the overall false positive rate, accounting for multiple comparisons was controlled by selecting only regions that showed significant decrease in FD in a significant proportion of the patients. This approach is overly conservative, however, a Bonferroni correction was deemed not appropriate as we could not establish independence of the data and smoothing of the signal across voxels could significantly affect the true nature of the fractal behavior. PPMC was used to establish correlation between ROI based Z-score values and ADI-R and ADOS questionnaires. For the purpose of this study the strength of the correlation was classified as low for $0.1 < r < 0.3$, moderate for $0.3 < r < 0.5$ and high, for $0.5 < r < 1.0$.

Results

Fractal dimension and Z-scoring

To determine regions of the brain of ASD patients with increased or decreased signal complexity respect to a typical control group, we estimated the voxel-wise FD on every subject of both groups. Following the calculation of a mean FD and standard deviation per voxel in the control group, we proceeded to calculate the Z-score of every voxel in the ASD group respect to controls. Only Z-score values greater than two were considered statistically significant for a 0.95 confidence level. *Fig. 2* shows a montage of a typical FD-score map of a randomly selected ASD patient and *Fig. 3* shows the same montage for the average healthy control.

A mean Z-score value was calculated for each of the ROIs and the ten regions the deviated the most from the control group were extracted for each patient. The frequency each region repeats among the ASD subjects is shown in *Fig. 4*. The sample size needed to detect a difference between a Z-score value of 1 and 2 with a power of 0.90, considering a maximum standard deviation of 1.24, was 19; therefore we only included in the analysis, regions that repeated at least in 19 patients out of the total. *Table 2* shows mean Z-score, standard deviation and p-values

for the ROIs that followed this criteria. Positive Z-scores were minimal in every patient and in none of the ASD subjects, we found a FD value of at least one standard deviation above the mean. This indicates that there were no regions where signal complexity significantly increased respect to controls among the ASD patients.

Correlation between fractal dimension and symptom severity

To assess correlation between FD and measures of symptoms severity, we implemented a PPMC analysis. Severity of the symptoms was quantified using the scores from the ADI-R and ADOS assessment tools. Higher ADI-R and ADOS scores indicate that a patient has a greater number of items representing core deficits and greater severity of impairment. To eliminate the confounding from IQ differences between the groups, the data was IQ matched with IQ(ASD) = 103.1 $\pm$ 17.7 and IQ(controls) = 105.9 $\pm$ 10.38.

The ADI-R covers the three autism domains: difficulties in verbal and non-verbal communication, impairment in social interaction and restricted and repetitive behaviors. Each domain is coded in a scale from 0 (absence of the symptom) to 3 (present in extreme form). The total combines each of the three domains and a patient is diagnosed if the three domains are above cutoff. While ADI-R is based on parental report, a trained examiner, who exposes the patient to behavioral presses that allow for the observation of behaviors associated with ASD, performs the ADOS test. *Table 3* shows the correlation coefficients and p values between FD Z-score and three ADI-R measurements: ADI-R social interaction, ADI-R verbal communication and ADI-R restricted and repetitive behaviors on the selected regions of interest. Additionally, *Table 4* shows the correlation coefficients and p values between FD Z-score and four ADOS measurements: ADOS social interaction, ADOS restricted and repetitive behaviors, ADOS total and ADOS severity on the selected regions of interest

Low FD characterizes less complex signals, which has been previously associated with pathologies of the brain[33,44–46] . We hypothesized, that as the severity of the symptoms increase, FD should decrease respect to the mean for that ROI, therefore Z-score decreases (absolute value increases) and we expect negative correlation. Positive correlation means that although FD values are all bellow the mean for the selected ROIs, they increase (absolute value decreases) as symptoms severity increase.

Discussion

The present study explored the differences between ASD patients and controls in terms of signal complexity using the fractal analysis of the rs-BOLD signal. Brain connectivity is best described in a multilevel model that takes into account three distinctive levels of interaction: synaptic connections that link independent neurons, networks that connect neuronal populations and brain regions linked by fiber pathways. A measure of complexity of this model constitutes an ideal indicator of multilevel and multitemporal connectivity within different brain regions. Tentatively, a healthy brain is associated with more complex signals and high FD, while a diseased or dysfunctional brain is associated with less complex signals and low FD.[33,44–46] The capacity of the brain to perform real-time adaptation and processing of these connections is reflected in the local demand of glucose and oxygen consumption, which drives the brain metabolic fluctuation observed in the rs-BOLD signal.

Overall, we found reduced signal complexity in the ASD subjects with respect to controls. Out of 250 regions, 14 regions showed significantly low FD in at least 19 subjects simultaneously (see *Fig. 4*). On average these regions had Z-scores values of -2.55 ± 0.25, or 2.55 standard deviations below the mean for that specific region. Positive Z-scores or regions where FD increased respect to controls were minimal in every patient and in none of the ASD subjects we found a FD value of at least one standard deviation above the mean. This indicates that there were no regions where signal complexity significantly increased respect to controls among the ASD patients.

In twenty-nine out of fifty ASD patients, the left amygdala and the left nucleus accumbens were among the regions with lower Z-score values, and the left nucleus accumbens reported the lowest values among all the studied ROIs. Abnormal function of the amygdala is considered a strong neurobiological marker in ASD and it is associated with deficits of social perception, affiliation and anxiety.[12,47,48] Our study showed decreased FD in the amygdala ($Z - score = -2.8 \pm 0.78$) with respect to controls. However, no significant negative correlation was found between the Z-score in the amygdala and any of the metrics from the ADI-R or ADOS. Positive low correlation was detected for ADI-R social and ADOS (RRB), which means that as the severity of the symptoms increase in these areas the Z score increases and FD values or signal

complexity increases. The role of the amygdala in ASD is still under scrutiny. While some authors report that diminished amygdala function correlates with deficits in social intelligence, perception and motivation, on patients with ASD[47,49] others have reported increased amygdala activity during the perception and experience of emotion, and fear.[50,51] It has been established that anxiety disorders occur simultaneously with with social impairment in ASD,[52] creating a confounding situation in terms of determining the role of the amygdala in ASD.

The nucleus accumbens and the caudate head are functional components of the basal ganglia. These two regions showed significantly reduced fractal dimension and thus reduced signal complexity, reporting Z-scores of ($Z - score = -2.68 \pm 1.22$) and ($Z - score = -2.67 \pm 0.59$) respectively. We found significant low correlation between the caudate head and ADI-RRB (r = -0.11), ADOS_Social (r = -0.27), ADOS_RRB (r = -0.18), ADOS_TOTAL (r = -0.19) and ADOS_Severity (r = -0.13), implying that signal complexity in the region decreases as symptoms severity increases. The basal ganglia is known to be involved in voluntary movement and social behavior. Previous animal studies have shown that deletion of the SAPAP3 gene in mice leads to defective neuronal communication in the basal ganglia and repetitive behaviors implicated in obsessive compulsive disorders and ASD.[53] Furthermore, structural abnormalities in the basal ganglia have been correlated to behavioral features of ASD[54] and deep brain stimulation (DBS), targeting the frontocortical-basal ganglia circuitry, have been used in the treatment of low functioning ASD patients.[55] Analysis of the fractal dimension in the basal ganglia could become a diagnostic marker to assess individual patients in order to determine whether this patient could benefit from a targeted treatment as DBS.

Several regions of the cerebellum in the ASD cohort showed significant reduced FD, specifically in the vermis (Table 2). These results mildly correlate with the ADIRRB and ADOSRRB metrics, hence, when severity of the symptoms increase in those domains, the FD and signal complexity decreases (See Tables 3 and 4). Reduced complexity in this region was expected as the cerebellum is the most consistent region of neural abnormality in autism. Postmortem studies in individuals diagnosed with autism revealed reduced number of Purkinje neurons[56,57] while in-vivo MRI studies have found that cerebellar gray matter volume was reduced relative to normal in ASD patients. The cerebellar vermis, which is a predominately a gray matter region, is also frequently reported as atrophied.[58] Impaired cerebellar dysfunction, if detected

in an early stage, could benefit from interventional approaches that can help the patients develop compensatory strategies. Analysis of the FD relative to controls could add important information in the process of deciding whether a specific patients could benefits from these interventions.

We acknowledge two main limitations of this study. First, most of the ASD patients included in this study received psychotropic medication. Since the use of medication is extraordinarily high in ASD, excluding subjects under medication would potentially lead to an unrepresentative sample size. We did not explore how the use of different classes of medications affected signal complexity in our regions of interest, which could be confounding the results. Secondly, the rs-BOLD signal was acquired at a relatively low sampling frequency (0.5 Hz). Accuracy of the fractal analysis is based on the ability to capture true dynamics of the processes being studied which could be achieved with higher sampling frequencies and by increasing the sampling time. Our sampling frequency was technically limited by the EPI acquisition as it limits the number of slices that can be acquired on a single shot. To cover the human brain at a resolution of 3mm per slice we were required to read around 30 slices on a single shot, which limited the minimum TR to 1.7 s (0.58 Hz). Additionally, we took into account the RF pulses and the safety limits required for human studies. We would recommend for future studies newer acquisition techniques such as multi-band EPI as they are able to achieve full brain sampling rates up to 2.5 Hz.

This study shows how the fractal dimension analysis of the fluctuations in the brain oxygen demand appears to provide additional patient-specific brain focal information that can be used to assess and possibly monitor ASD patients. Previous functional imaging approaches have focused exclusively on characterization of brain networks through group-based statistics. This approach, while providing important information of the disorder as a whole, failed to succeed in providing single patient assessment. A measure of complexity as FD could provide a method to assess brain connectivity in ASD patients. In this study, we were able to find regions in the brain with reported decreased signal complexity using the FD methodology. These regions have been previously reported as dysfunctional for ASD patients and correlated with behavioral assessments. The method we have proposed is able to provide additional information of ASD in a non-invasive and fast manner and could hopefully help in deciding whether a patient could

benefit from targeted treatments and interventional techniques.

References

1. Courchesne, E. *et al.* Unusual brain growth patterns in early life in patients with autistic disorder: An MRI study. *Neurology* **57**, 245–254 (2001). URL `http://www.neurology.org/content/57/2/245.full`. DOI 10.1212/WNL.57.2.245.

2. Hadjikhani, N., Joseph, R. M., Snyder, J. & Tager-Flusberg, H. Anatomical differences in the mirror neuron system and social cognition network in autism. *Cerebral Cortex* **16**, 1276–1282 (2006). DOI 10.1093/cercor/bhj069.

3. Kosaka, H. *et al.* Smaller insula and inferior frontal volumes in young adults with pervasive developmental disorders. *NeuroImage* **50**, 1357–1363 (2010). DOI 10.1016/j.neuroimage.2010.01.085.

4. Aylward, E. H. *et al.* MRI volumes of amygdala and hippocampus in non-mentally retarded autistic adolescents and adults. *Neurology* **53**, 2145–2150 (1999).

5. Alexander, A. L. *et al.* Diffusion tensor imaging of the corpus callosum in Autism. *NeuroImage* **34**, 61–73 (2007). DOI 10.1016/j.neuroimage.2006.08.032.

6. Barnea-Goraly, N. *et al.* White matter structure in autism: Preliminary evidence from diffusion tensor imaging. *Biological Psychiatry* **55**, 323–326 (2004). DOI 10.1016/j.biopsych.2003.10.022.

7. Mizuno, A., Villalobos, M. E., Davies, M. M., Dahl, B. C. & Muller, R.-A. Partially enhanced thalamocortical functional connectivity in autism. *Brain research* **1104**, 160–174 (2006). DOI 10.1016/j.brainres.2006.05.064.

8. Noonan, S. K., Haist, F. & Muller, R.-A. Aberrant functional connectivity in autism: evidence from low-frequency BOLD signal fluctuations. *Brain research* **1262**, 48–63 (2009). DOI 10.1016/j.brainres.2008.12.076.

9. Turner, K. C., Frost, L., Linsenbardt, D., McIlroy, J. R. & Muller, R.-A. Atypically diffuse functional connectivity between caudate nuclei and cerebral cortex in autism. *Behavioral and brain functions : BBF* **2**, 34 (2006). DOI 10.1186/1744-9081-2-34.

10. Just, M. A., Cherkassky, V. L., Keller, T. A., Kana, R. K. & Minshew, N. J. Functional and anatomical cortical underconnectivity in autism: evidence from an FMRI study of an executive function task and corpus callosum morphometry. *Cerebral cortex (New York, N.Y. : 1991)* **17**, 951–961 (2007). DOI 10.1093/cercor/bhl006.

11. Kana, R. K., Keller, T. A., Cherkassky, V. L., Minshew, N. J. & Just, M. A. Sentence comprehension in autism: thinking in pictures with decreased functional connectivity. *Brain : a journal of neurology* **129**, 2484–2493 (2006). DOI 10.1093/brain/awl164.

12. Kleinhans, N. M. *et al.* Abnormal functional connectivity in autism spectrum disorders during face processing. *Brain : a journal of neurology* **131**, 1000–1012 (2008). DOI 10.1093/brain/awm334.

13. Welchew, D. E. *et al.* Functional disconnectivity of the medial temporal lobe in Asperger's syndrome. *Biological psychiatry* **57**, 991–998 (2005). DOI 10.1016/j.biopsych.2005.01.028.

14. Wicker, B. *et al.* Abnormal cerebral effective connectivity during explicit emotional processing in adults with autism spectrum disorder. *Social cognitive and affective neuroscience* **3**, 135–143 (2008). DOI 10.1093/scan/nsn007.

15. Cherkassky, V. L., Kana, R. K., Keller, T. A. & Just, M. A. Functional connectivity in a baseline resting-state network in autism. *Neuroreport* **17**, 1687–1690 (2006). DOI 10.1097/01.wnr.0000239956.45448.4c.

16. Monk, C. S. *et al.* Abnormalities of intrinsic functional connectivity in autism spectrum disorders,. *NeuroImage* **47**, 764–772 (2009). URL `http://dx.doi.org/10.1016/j.neuroimage.2009.04.069`. DOI 10.1016/j.neuroimage.2009.04.069.

17. Logothetis, N. K. The neural basis of the blood-oxygen-level-dependent functional magnetic resonance imaging signal. *Philosophical transactions of the Royal Society of London. Series B, Biological sciences* **357**, 1003–1037 (2002). DOI 10.1098/rstb.2002.1114.

18. Logothetis, N. K. MR imaging in the non-human primate: studies of function and of dynamic connectivity. *Current opinion in neurobiology* **13**, 630–642 (2003).

19. Hutsler, J. J. & Zhang, H. Increased dendritic spine densities on cortical projection neurons in autism spectrum disorders. *Brain research* **1309**, 83–94 (2010). DOI 10.1016/j.brainres.2009.09.120.

20. Kwan, V. *et al.* DIXDC1 Phosphorylation and Control of Dendritic Morphology Are Impaired by Rare Genetic Variants. *Cell Reports* **17**, 1892–1904 (2016). URL `http://dx.doi.org/10.1016/j.celrep.2016.10.047`. DOI 10.1016/j.celrep.2016.10.047.

21. Fox, M. D. & Raichle, M. E. Spontaneous fluctuations in brain activity observed with functional magnetic resonance imaging. *Nature reviews. Neuroscience* **8**, 700–711 (2007). DOI 10.1038/nrn2201.

22. Zarahn, E., Aguirre, G. K. & D'Esposito, M. Empirical analyses of BOLD fMRI statistics. I. Spatially unsmoothed data collected under null-hypothesis conditions. *NeuroImage* **5**, 179–197 (1997).

23. El Boustani, S. *et al.* Network-state modulation of power-law frequency-scaling in visual cortical neurons. *PLoS computational biology* **5**, e1000519 (2009). DOI 10.1371/journal.pcbi.1000519.

24. Herman, P., Sanganahalli, B. G., Hyder, F. & Eke, A. Fractal analysis of spontaneous fluctuations of the BOLD signal in rat brain. *NeuroImage* **58**, 1060–1069 (2011). DOI 10.1016/j.neuroimage.2011.06.082.

25. Eke, A. *et al.* Physiological time series: distinguishing fractal noises from motions. *Pflugers Archiv : European journal of physiology* **439**, 403–415 (2000).

26. Eke, A., Herman, P., Kocsis, L. & Kozak, L. R. Fractal characterization of complexity in temporal physiological signals. *Physiological measurement* **23**, R1–38 (2002).

27. Bullmore, E. *et al.* Generic aspects of complexity in brain imaging data and other biological systems. *NeuroImage* **47**, 1125–1134 (2009). DOI 10.1016/j.neuroimage.2009.05.032.

28. Li, X. *et al.* Fractal spectral analysis of pre-epileptic seizures in terms of criticality. *Journal of neural engineering* **2**, 11–16 (2005). DOI 10.1088/1741-2560/2/2/002.

29. Kannathal, N., Puthusserypady, S. K. & Choo Min, L. Complex dynamics of epileptic EEG. *Conference proceedings : ... Annual International Conference of the IEEE Engineering in Medicine and Biology Society. IEEE Engineering in Medicine and Biology Society. Annual Conference* **1**, 604–607 (2004). DOI 10.1109/IEMBS.2004.1403230.

30. Yoshikawa, T. *et al.* Quantification of the heterogeneity of cerebral blood flow in vascular dementia. *Journal of neurology* **250**, 194–200 (2003). DOI 10.1007/s00415-003-0972-9.

31. Gomez, C., Mediavilla, A., Hornero, R., Abasolo, D. & Fernandez, A. Use of the Higuchi's fractal dimension for the analysis of MEG recordings from Alzheimer's disease patients. *Medical engineering & physics* **31**, 306–313 (2009). DOI 10.1016/j.medengphy.2008.06.010.

32. Maxim, V. *et al.* Fractional Gaussian noise, functional MRI and Alzheimer's disease. *NeuroImage* **25**, 141–158 (2005). DOI 10.1016/j.neuroimage.2004.10.044.

33. Warsi, M. A., Molloy, W. & Noseworthy, M. D. Correlating brain blood oxygenation level dependent (BOLD) fractal dimension mapping with magnetic resonance spectroscopy (MRS) in Alzheimer's disease. *Magma (New York, N.Y.)* **25**, 335–344 (2012). DOI 10.1007/s10334-012-0312-0.

34. Di Martino, A. *et al.* The autism brain imaging data exchange: towards a large-scale evaluation of the intrinsic brain architecture in autism. *Mol Psychiatry* **19**, 659–667 (2014). URL `http://dx.doi.org/10.1038/mp.2013.78 http://10.1038/mp.2013.78`.

35. Lord, C. *et al.* The autism diagnostic observation schedule-generic: a standard measure of social and communication deficits associated with the spectrum of autism. *Journal of autism and developmental disorders* **30**, 205–223 (2000).

36. Lord, C., Rutter, M. & Le Couteur, A. Autism Diagnostic Interview-Revised: a revised version of a diagnostic interview for caregivers of individuals with possible pervasive developmental disorders. *Journal of autism and developmental disorders* **24**, 659–685 (1994).

37. Rutter, M., Bailey, A., Lord, C. *The Social Communication Questionnaire - Manual.* (Western Psychological Services, Los Angeles, CA, 2003).

38. Spence, S. H. Structure of anxiety symptoms among children: a confirmatory factor-analytic study. *Journal of abnormal psychology* **106**, 280–297 (1997).

39. Eickhoff, S., Stephan, H., KE.and Mohlberg, Grefkes, C., Fink, G. & Amunts, K., K.and Zilles. A new SPM toolbox for combining probabilistic cytoarchitectonic maps and functional imaging data. *NeuroImage* **25**, 1325–1335 (2005).

40. Cox, R. W. AFNI: software for analysis and visualization of functional magnetic resonance neuroimages. *Computers and biomedical research, an international journal* **29**, 162–173 (1996).

41. Mandelbrot, J. W. V. & B., B. Fractional Brownian Motions, Fractional Noises and Applications. *SIAM Rev.* **10**, 422–437 (1967). DOI 10.1137/1010093.

42. Bassingthwaighte, J. B. & Raymond, G. M. Evaluation of the dispersional analysis method for fractal time series. *Annals of biomedical engineering* **23**, 491–505 (1995).

43. Smirnov, N. Table for Estimating the Goodness of Fit of Empirical Distributions. *The Annals of Mathematical Statistics* **19**, 279–281 (1948). URL `http://projecteuclid.org/euclid.aoms/1177730256`. DOI 10.1214/aoms/1177730256.

44. Weber, A. M., Soreni, N. & Noseworthy, M. D. A preliminary study on the effects of acute ethanol ingestion on default mode network and temporal fractal properties of the brain. *Magma (New York, N.Y.)* **27**, 291–301 (2014). DOI 10.1007/s10334-013-0420-5.

45. Smits, F. M. *et al.* Electroencephalographic Fractal Dimension in Healthy Ageing and Alzheimer's Disease. *PloS one* **11**, e0149587 (2016). DOI 10.1371/journal.pone.0149587.

46. Goldberger, A. L. *et al.* Fractal dynamics in physiology: alterations with disease and aging. *Proceedings of the National Academy of Sciences of the United States of America* **99 Suppl 1**, 2466–2472 (2002). DOI 10.1073/pnas.012579499.

47. Pelphrey, K. A., Shultz, S., Hudac, C. M. & Vander Wyk, B. C. Research Review: Constraining heterogeneity: the social brain and its development in autism spectrum disorder. *Journal of Child Psychology and Psychiatry* **52**, 631–644 (2011). URL `http://dx.doi.org/10.1111/j.1469-7610.2010.02349.x`. DOI 10.1111/j.1469-7610.2010.02349.x.

48. Herrington, J. D., Miller, J. S., Pandey, J. & Schultz, R. T. Anxiety and social deficits have distinct relationships with amygdala function in autism spectrum disorder. *Social cognitive and affective neuroscience* **11**, 907–914 (2016). DOI 10.1093/scan/nsw015.

49. Chevallier, C., Kohls, G., Troiani, V., Brodkin, E. S. & Schultz, R. T. The social motivation theory of autism. *Trends in Cognitive Sciences* **16**, 231–239 (2012). URL `http://www.sciencedirect.com/science/article/pii/S1364661312000526`. DOI http://dx.doi.org/10.1016/j.tics.2012.02.007.

50. Phelps, E. A. & LeDoux, J. E. Contributions of the Amygdala to Emotion Processing: From Animal Models to Human Behavior. *Neuron* **48**, 175–187 (2005). URL `http://www.sciencedirect.com/science/article/pii/S0896627305008238`. DOI http://dx.doi.org/10.1016/j.neuron.2005.09.025.

51. Wilensky, A. E., Schafe, G. E., Kristensen, M. P. & LeDoux, J. E. Rethinking the fear circuit: the central nucleus of the amygdala is required for the acquisition, consolidation, and expression of Pavlovian fear conditioning. *The Journal of neuroscience : the official journal*

of the Society for Neuroscience **26**, 12387–12396 (2006). DOI 10.1523/JNEUROSCI.4316-06.2006.

52. van Steensel, F. J. A., Bögels, S. M. & Perrin, S. Anxiety Disorders in Children and Adolescents with Autistic Spectrum Disorders: A Meta-Analysis (2011).

53. Welch, J. M. Cortico-striatal synaptic defects and OCD-like behaviors in SAPAP3 mutant mice (2007).

54. Qiu, A., Adler, M., Crocetti, D., Miller, M. I. & Mostofsky, S. H. Basal ganglia shapes predict social, communication, and motor dysfunctions in boys with autism spectrum disorder. *Journal of the American Academy of Child and Adolescent Psychiatry* **49**, 539–51, 551.e1–4 (2010). DOI 10.1016/j.jaac.2010.02.012.

55. Sinha, S., McGovern, R. A. & Sheth, S. A. Deep brain stimulation for severe autism: from pathophysiology to procedure. *Neurosurgical focus* **38**, E3 (2015). DOI 10.3171/2015.3.FOCUS1548.

56. Bailey, A. *et al.* A clinicopathological study of autism. *Brain : a journal of neurology* **121 (Pt 5)**, 889–905 (1998).

57. Vargas, D. L., Nascimbene, C., Krishnan, C., Zimmerman, A. W. & Pardo, C. A. Neuroglial activation and neuroinflammation in the brain of patients with autism. *Annals of neurology* **57**, 67–81 (2005). DOI 10.1002/ana.20315.

58. Carper, R. A. & Courchesne, E. Inverse correlation between frontal lobe and cerebellum sizes in children with autism. *Brain : a journal of neurology* **123 (Pt 4)**, 836–844 (2000).

Author Contributions

O.D, as first author, acquired the data, performed the data analysis and interpretation of the results and drafted the article including tables and figures. Contributions by Olga M. Dona warranted her name as first author. M.D.N, as corresponding author, designed and conceptualized this project which is part of a long trajectory on developing applications based on the

fractal analysis in human brain signals. He performed the critical revision of the article and the final approval of the version to be published. Furthermore, M.D.N provided constant guidance and advice through out the duration of this study and secured the required funds. G.H actively collaborated in the interpretation of the results due to his vast experience studying ASD. Moreover, he exhaustively revised and edited the final version of this article. All authors agreed to be accountable for all aspects of the work in ensuring that questions related to the accuracy or integrity of any part of the work were appropriately investigated and resolved.

Additional Information

Competing financial interests

The authors declare that the research was conducted in the absence of any commercial or financial relationships that could be construed as a potential conflict of interest.

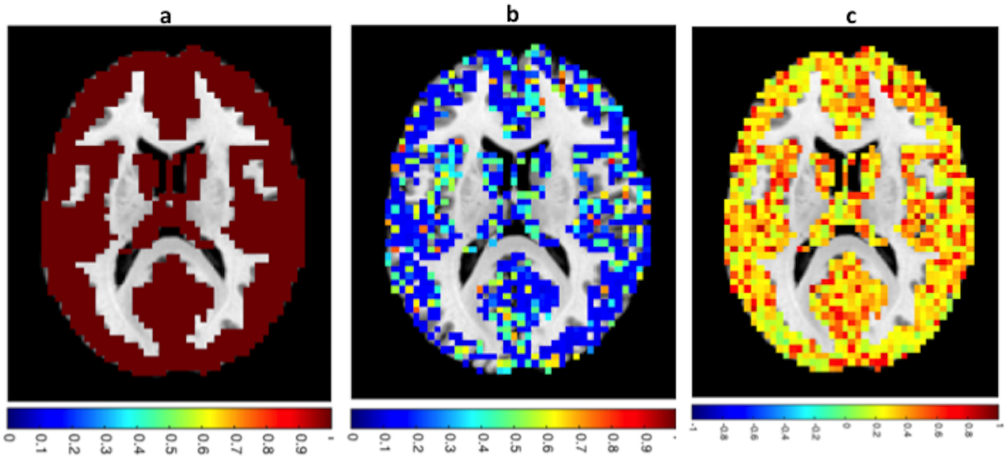

Fig. 1. Analysis of normality. (a) Kolmogorov Smirnov normality test. h=1 indicates rejection of the null hypothesis at a 5% significance level. (b) Kurtosis map. Voxels where $k \neq 3.0 \pm 0.5$ were removed from analysis. The map was centered at k=3. (c) Skewness map. Skewness measures asymmetry of the distribution. Positive skew(sk) indicates more data points above the mean while negative skew indicates more data points below the mean. Voxels where $sk \neq 0.0 \pm 0.5$ were removed from the analysis and the sk map was normalized.

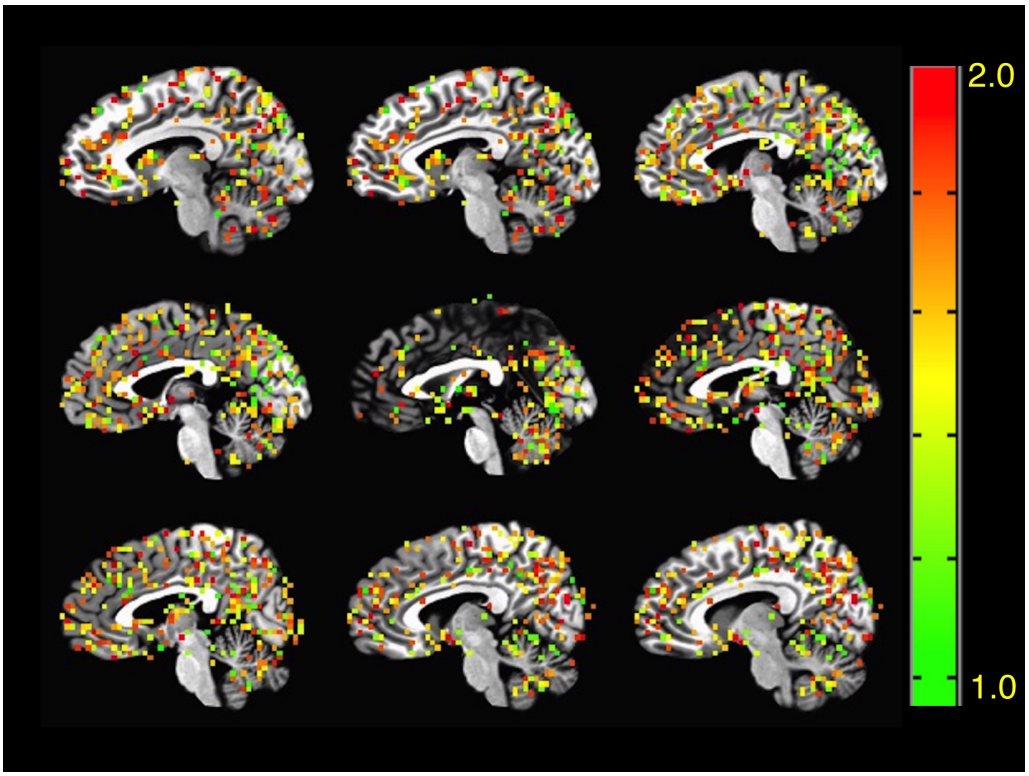

Fig. 2. FD map of ASD. FD map over a gray matter mask of a randomly selected ASD patient showing regions with decreased FD and signal complexity

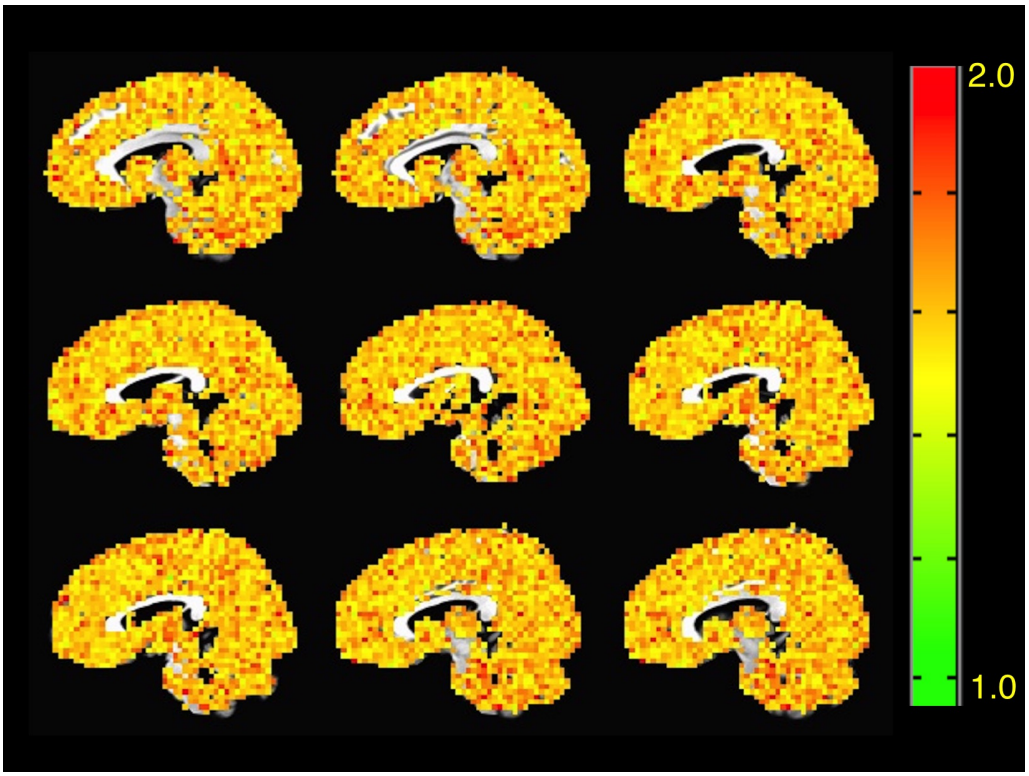

Fig. 3. FD map of Controls. Mean FD map calculated from the voxel-wise mean FD value for healthy controls. Grey matter mask was calculated from a probability atlas[39]

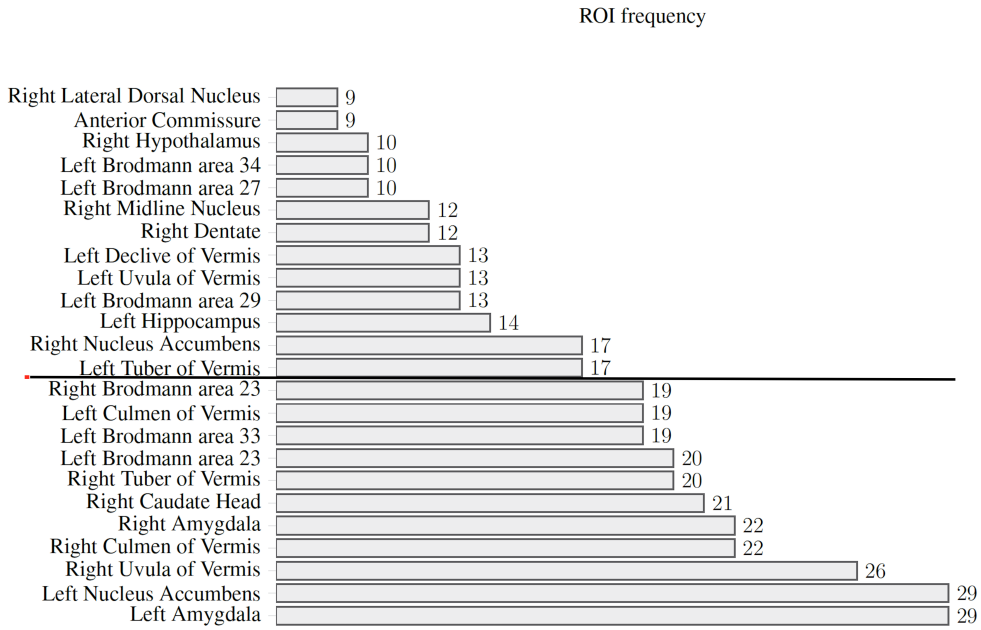

Fig. 4. ROI frequency. Bar graph showing frequency of regions where FD decreases significantly. Statistically significant regions below the bold line are indicated.

Table 1. Phenotypic Data.

	ASD subjects		**Typical Controls**	
	Mean	STD	Mean	STD
Age(y)	12.7	2.4	14.1	3.1
IQ	103.1	17.7	105.9	10.4
Male to Female ratio	46:9		38:17	
Right to Left handedness ratio	41:6		44:8	
ADI-R total	41.6	8.7		
ADOS severity	6.5	2.2		

Table 2. Mean Z-score(μ), standard deviation(σ) and p-values for ROIs where FD values deviated greatest from healthy controls

ROIs	μ	σ	**p**
Left Amygdala	-2.88	0.73	0.00
Left Brodmann area 23	-2.66	0.60	0.01
Left Brodmann area 33	-2.17	1.34	0.03
Left Culmen of Vermis	-2.70	1.09	0.01
Left Hippocampus	-2.32	0.85	0.02
Left Nucleus Accumbens	-2.94	1.43	0.00
Left Tuber of Vermis	-2.22	1.11	0.03
Right Amygdala	-2.72	0.83	0.01
Right Brodmann area 23	-2.64	0.57	0.01
Right Caudate Head	-2.67	0.59	0.01
Right Culmen of Vermis	-2.43	1.35	0.02
Right Nucleus Accumbens	-2.42	1.01	0.02
Right Tuber of Vermis	-2.26	1.26	0.02
Right Uvula of Vermis	-2.65	1.20	0.01

Table 3. Pearson correlation coefficients and p-values for ADI-R compared against regional rs-BOLD Z-score

ROIs	**ADI_SOCIAL**		**ADI_VERBAL**		**ADI_RRB**		**ADI_TOTAL**	
	r	p	r	p	r	p	r	p
Left Amygdala	0.07	0.62	0.14	0.30	-0.02	0.91	0.10	0.48
Left Brodmann area 23	0.30	0.03	0.17	0.21	-0.04	0.78	0.23	0.09
Left Brodmann area 33	0.20	0.15	-0.11	0.42	-0.10	0.50	0.04	0.80
Left Culmen of Vermis	0.11	0.42	0.02	0.88	-0.10	0.46	0.04	0.75
Left Hippocampu s	0.07	0.59	-0.04	0.76	-0.11	0.44	-0.01	0.96
Left Nucleus Accumbens	-0.02	0.87	-0.03	0.81	0.07	0.61	-0.01	0.95
Left Tuber of Vermis	0.03	0.85	0.02	0.90	-0.22	0.11	-0.04	0.79
Right Amygdala	0.25	0.07	0.31	0.02	-0.03	0.83	0.27	0.05
Right Brodmann area 23	0.13	0.36	0.15	0.28	0.12	0.38	0.17	0.22
Right Caudate Head	0.12	0.40	0.03	0.83	-0.11	0.44	0.05	0.72
Right Culmen of Vermis	0.03	0.85	0.06	0.69	-0.16	0.26	0.00	0.98
Right Nucleus Accumbens	0.09	0.50	0.15	0.28	0.24	0.09	0.18	0.19
Right Tuber of Vermis	0.07	0.61	0.06	0.66	-0.10	0.48	0.04	0.77
Right Uvula of Vermis	0.30	0.03	0.13	0.35	-0.02	0.88	0.22	0.11

Table 4. Pearson correlation coefficients and p-values for ADOS compared against regional rs-BOLD Z-score

ROIs	**ADOS_SOC**		**ADOS_RRB**		**ADOS_TOT**		**ADOS_SEV**	
	r	p	r	p	r	p	r	p
Left Amygdala	0.04	0.80	0.18	0.26	0.02	0.86	0.05	0.76
Left Brodmann area 23	0.09	0.57	-0.04	0.78	0.01	0.94	0.06	0.67
Left Brodmann area 33	-0.02	0.92	-0.06	0.72	-0.07	0.63	-0.05	0.74
Left Culmen of Vermis	0.01	0.94	0.09	0.58	0.02	0.87	0.06	0.66
Left Hippocampus	-0.15	0.33	0.01	0.95	-0.09	0.52	-0.03	0.81
Left Nucleus Accumbens	-0.05	0.76	-0.07	0.64	-0.04	0.80	0.01	0.96
Left Tuber of Vermis	-0.10	0.54	-0.20	0.21	-0.15	0.29	-0.12	0.40
Right Amygdala	0.11	0.49	0.20	0.21	0.03	0.81	0.07	0.65
Right Brodmann area 23	0.17	0.29	0.16	0.31	0.12	0.43	0.15	0.31
Right Caudate Head	-0.27	0.08	-0.18	0.26	-0.19	0.19	-0.13	0.38
Right Culmen of Vermis	-0.14	0.37	-0.19	0.22	-0.17	0.25	-0.15	0.31
Right Nucleus Accumbens	-0.04	0.81	0.10	0.52	-0.07	0.65	-0.04	0.76
Right Tuber of Vermis	-0.07	0.67	0.07	0.65	-0.04	0.76	0.01	0.92
Right Uvula of Vermis	-0.08	0.60	-0.19	0.22	-0.18	0.22	-0.12	0.41

Chapter 6

Fractal Analysis of the brain rs-BOLD signal in cancer patients experiencing chemotherapy-related cognitive impairment.

Fractal Analysis of the brain rs-BOLD signal in cancer patients experiencing chemotherapy-related cognitive impairment.
Olga Dona, Michel Doughty, Geoffrey Hall, Raimond Wong and Michael D. Noseworthy.

6.1 Context of the paper

Chemotherapy-related cognitive impairment, also known as chemo-brain or chemo-fog, is a long lasting and disturbing side effect of chemotherapy. The rapidly increasing number of patients who have survived cancer, yet now live with the side effects of treatment, has lead to an increase of chemo-brain related studies. However, there is yet to be a definitive answer describing the etiology of chemo-brain, the affected brain regions and how to manage the symptoms.

The purpose of this study was to assess the viability of using a complexity analysis of the rs-BOLD signal in combination with DTI to detect brain abnormalities in chemo-brain patients. Five patients were scanned using a GE Discovery MR750 3T MRI and 32-channel RF-coil. Axial FSPGR-3D images were used to prescribe rs-BOLD (TE/TR=35/2000ms) and DTI (60 directions, TR/TE = 8800/87ms). Complexity analysis, performed on gray matter, was done by estimating the voxel-wise Hurst exponent using de-trended fluctuation analysis and signal summation conversion methods. Voxel-wise analysis of the DTI data was performed obtaining FA, MD, AD and RD. All the results were normalized with a large database of healthy controls using a Z-score analysis. Although no significant differences were found on the fractal dimension of the rs BOLD signal when compared to controls, we were able to detect significant ($p<0.05$) changes in FA specifically in the the corpus callosum, inferior fronto occipital fasciculus and right inferior longitudinal fasciculus. These regions also

correlated with neuropsychological scores of visuospacial constructional ability and visuospacial memory.

This study demonstrates that white matter and gray matter integrity can be explored on patients experiencing chemo-brain with a single subject approach based on FD and DTI. The combination of these techniques provides a deeper, multifocal understanding of chemo-brain and will hopefully lead to design of improved drugs and treatments to prevent or lessen the cognitive collateral effects.

6.2 Declaration Statement

Olga M. Dona, as first author, acquired the data, performed the data analysis and interpretation of the results and drafted the article including tables and figures. Contributions by Olga M. Dona warranted her name as first author.

Mitchel Doughty as a co-author performed the data analysis of the DTI section and drafted the respective figures and tables. He participated in proofreading the article.

Dr. Michael D. Noseworthy, as corresponding author, designed and conceptualized this project which is part of a his long trajectory on developing applications based on the fractal analysis in human brain signals. He performed the critical revision of the article and the final approval of the version to be published. Furthermore, Dr. Noseworthy provided constant guidance and advice through out the duration of this study and secured the required funds.

Dr. Geoffrey Hall actively collaborated in the interpretation of the results due to his vast experience studying neurological disorders. He provided guidance with application and interpretation of the neuropsychological testings. Moreover, he

exhaustively revised and edited the final version of this article.

Dr. Raimond Wong recruited the patients for this study and participated in the conception and design of this work. Additionally, Dr. Wong participated in the critical revision of the article and the final approval of the version to be published.

This paper was submitted for publication to the journal Clinical Cancer Research (AACR) on February 8th, 2017 .

6.3 Paper

Patient-Specific Brain Changes Caused by Chemotherapy: Using Resting State Blood Oxygenation Level Dependent (rsBOLD) Signal and Diffusion Tensor Imaging (DTI)

Olga Dona [1,2], Mitchell Doughty [1,2], Geoffrey B. Hall. [2,5], Raimond Wong [6], and Michael D. Noseworthy [1,2,3,4,*]

[1] McMaster School of Biomedical Engineering, McMaster University, Hamilton, ON, Canada.
[2] Imaging Research Centre, St. Josephs Healthcare, Hamilton, ON, Canada.
[3] Department of Electrical and Computer Engineering, McMaster University, Hamilton, ON, Canada.
[4] Department of Radiology, McMaster University, Hamilton, ON, Canada.
[5] Department of Psychology, Neuroscience & Behaviour, McMaster University, Hamilton, ON, Canada.
[6] Department of Medicine, Division of Oncology, McMaster University, Hamilton, ON, Canada.

[*] Corresponding Author: Dr. Michael D. Noseworthy, Ph.D., P.Eng.
Email:nosewor@mcmaster.ca
Mailing address: McMaster University
Engineering Technology Building, ETB-406.
1280 Main St. West, Hamilton, Ontario. Canada L8S 4K1
Phone: +1 (905) 525-9140 ext. 23727

Abstract

Chemotherapy-related cognitive impairment (chemobrain), is a lasting and disturbing side effect of chemotherapy. However, the aetiology of chemobrain and how we can identify affected brain regions on a patient specific basis, has so far been elusive. Due to patient genotypic and metabolic heterogeneity, and the many different chemotherapy treatment regimes, it is difficult if not impossible to predict who will exhibit chemobrain and what regional brain areas may become affected. Here, we explore a novel approach, using MRI resting state BOLD (rs-BOLD) and DTI, to map out abnormal brain gray and white matter, respectively, in a single patient. This personalized assessment of chemotherapy-induced brain change can provide physicians clear knowledge of location and severity of brain alterations as they appear during and following cancer treatment. This information can then be used to better design chemotherapy regimes that minimally affect the brain and provide a way to monitor brain recovery, on a patient-specific basis, following treatment.

Introduction

Innovations in cancer treatment as well as screening the population for certain types of cancers have lead to an increase in survival rate. The Canadian Cancer Statistic Advisory Committee reported that people diagnosed with cancer today have a better relative survival rate than people diagnosed a decade ago (*1*). Yet, cancer survivors experience temporary, or even permanent side effects due to their therapies.

Chemotherapy is known to be one of the most aggressive treatments for cancer. Although efficacious, chemotherapy causes many side effects including nausea, vomiting, anemia, peripheral neuropathy and chemo-brain among others. While many of these symptoms resolve within months of treatment, chemo-brain can persists for years and is considered one of the main impediments for a return to normal life. Chemo-brain is the common name assigned to chemotherapy related cognitive impairment experienced by cancer patients. Recent work has found that the occurrence rate of chemo-brain for breast cancer patients who underwent chemotherapy is about 33% (*2, 3*). The symptoms associated with this condition are: memory lapses, concentration problems, disorganized thinking and slower mental processing. The duration of symptoms is very difficult to predict. While for most patients chemo-brain symptoms subside after the last dose of chemotherapy (*4–6*), deRuiter et al. and Kopplemans et al. have found evidence of cognitive impairment in patients more than two decades after completing therapy (*7, 8*).

Chemo-brain has proved to be very difficult to diagnose due to a variety of confounding factors that are also associated with cognitive impairment. Patients undergoing chemotherapy are usually under psychological distress which can impact their cognitive performance. Furthermore, patients may be affected by medications prescribed to attenuate side effects of chemotherapy, such as anti-nauseates and anti-inflammatories. In cases in which estrogen or progesterone

receptors are detected in the tumor, hormone therapy can be prescribed which may also impact on cognition (*9*). MRI techniques in combination with performance-based neuropsychological testing have been previously used to assess structural and functional changes in the brain following chemo-therapy exposure (*10–16*). However, reported findings have been inconsistent or inconclusive. For instance, in a study by Zunini et al. a prospective functional MRI (fMRI) verbal recall task was conducted in chemotherapy patients and healthy controls. The focus of the study was on breast cancer patients and the evaluation was done before and after chemotherapy. Chemotherapy patients showed less activation, than controls, specifically in the left middle temporal gyrus, orbitofrontal cortex, insula and temporal pole (*11*). On the other hand, Silverman et al. conducted a similar functional study using ^{15}O and ^{18}F positron emission tomography (PET) producing differing results. They found increased activation in the prefrontal cortex and cerebellum using a working memory task in chemotherapy treated patients while untreated patients showed the greatest activation in parietal and occipital cortex (*14*).

The major limitation with task-based fMRI is the ability of the subject to adequately and consistently perform or respond to the task. Furthermore activation requires appropriate control tasks that may be difficult to determine as they need to cause similar patterns of activation across all subjects. Because of these difficulties, assessment of brain connectivity has shifted towards the use of resting state networks, based on the resting state blood oxygenation level dependent (rsBOLD) signal. These networks are known to be consistent across healthy subjects and do not rely on subject capacity to perform. However, a limitation of rsBOLD assessment of brain connectivity in chemobrain patients is the reliance upon group analysis comparisons, which is generally unsuitable when drawing conclusions on a presumed heterogeneous disorder.

As a result, the aim of this work was to propose an alternative single-subject approach, using model-free complexity analysis based on the fractal nature of the MRI rsBOLD signal. The fractal dimension (FD) is considered a metric of signal complexity, and has previously been

used as a descriptor of neural activity based on hemodynamics and metabolic response (*17, 18*).

Because the rsBOLD signal has been associated with post-synaptic potentials, localized mainly in gray matter, diffusion tensor imaging (DTI) was also included in this study to assess the white matter micro-structural integrity. A number of studies examining the structural changes in the brain of patients treated with chemotherapy have been published. For example, Deprez et al. (*13*) studied chemotherapy induced structural changes in cerebral white matter using DTI techniques combined with cognitive assessment. They showed decreased fractional anisotropy (FA) and increased mean diffusivity (MD) in the frontal and temporal tracts of chemotherapy patients. A further DTI study by De Ruiter et al. (*12*) also showed decreased white matter integrity in high dose chemotherapy breast cancer survivors.

In our current work, we show how Z-scoring of both grey matter fractal rsBOLD, and white matter structural integrity (from DTI), can identify specific abnormal brain regions in individual chemobrain patients.

Materials and Methods

Patients and controls.

Five subjects (60.6 $\pm$ 14.8 y/o) experiencing chemo-brain symptoms were recruited for this study. The study was approved by our Institutional Research Ethics Board, (Hamilton Integrated Research Ethic Board (HIREB)) and all patients gave written informed consent. The study was conducted according to the principles expressed in the Declaration of Helsinki. Healthy control data were acquired throughout the NITRC data base directly from the Human Connectome Project (180 subjects, $21.2 \pm 1.9yo$) (*19*), (19 subjects, $36.4 \pm 9.2yo$) and The Alzheimer's Disease Neuroimaging Initiative (ADNI)(32 subjects, $73.7 \pm 6.5yo$) (*20*). Although the data was not age matched, patients above 70 years old were only matched with healthy controls from the ADNI data base due to normal aging brain atrophy occurring at higher rates after this

age (*21, 22*).

Data acquisition

Five patients were scanned using a GE MR750 Discovery 3T MRI scanner with a 32-channel RF receiver coil (General Electric Healthcare, Milwaukee, WI). Following a routine 3-plane localizer and calibration scan for parallel imaging, a 3D inversion recovery-prepped T1-weighted anatomical data set was acquired (fSPGR, axial acquisition, TE/TR/flip angle = 4.25/11.36/12°, 256x256 matrix with 1mm slice thickness with 25.6cm FOV, 1mm isotropic acquisition). Resting state functional BOLD data was acquired using an echo planar imaging (EPI) sequence with FOV = 22cm, image matrix = 64x64; flip angle = 90°; echo time (TE) = 35ms; repetition time (TR) = 2000ms (i.e, 0.5Hz temporal sampling frequency); slice thickness of 3mm; and 180 temporal points. At the beginning of every scan, 4 additional data points were acquired but automatically discarded (allowing the system to reach steady state), making the final scan time 6 minutes and 8 seconds. Axial Diffusion Tensor Imaging (DTI) data was acquired using a dual echo EPI sequence. Imaging parameters were as follows: 60 non-coplanar directions, TE/TR = 87/8800 ms, b = 1000 s/mm2, 122x122 matrix, 70 slices, 2.0 mm slice thickness, 244 mm FOV, ASSET = 2.

Anatomical, functional and diffusion data for healthy control subjects were downloaded from the NITRC database, the Human Connectome Project and the ADNI database respectively. Two cohorts of healthy subjects (N=180 (21.2 ± 1.9yo) and N=19 (36.4 ± 9.2yo)) downloaded from the Human Connectome project were acquired with the following parameters: a T1-weighted sagittal three-dimensional magnetization-prepared rapid gradient echo (MPRAGE) sequence was acquired, covering the entire brain: 128 slices, TR = 2530 ms, TE = 3.39 ms, slice thickness = 1.33 mm, flip angle = $7\mathrm{deg}$, inversion time = 1100 ms, FOV = 256 x 256 mm, and in-plane resolution = 256 x 192. The rsBOLD images were obtained using an

echo-planar imaging sequence with the following parameters: 33 axial slices, thickness/gap = 3/0.6 mm, in-plane resolution = 64 x 64, TR = 2000 ms, TE = 30 ms, flip angle = $90\mathrm{deg}$, FOV = 200 x 200 mm. Diffusion tensor images were acquired by using a single-shot Echo-Planar Imaging-based sequence (coverage of the whole brain, 2.0 mm slice thickness with no inter-slice gap, 70 axial slices, TR = 8800 ms, TE = 87 ms, 64 diffusion directions. Additionally, one cohort of healthy subjects (N=36 (73.7 ± 6.5yo)) was downloaded from the ADNI database with the following parameters: A T1-weighted sagittal three-dimensional SPGR sequence was acquired, covering the entire brain: 200 slices, TR = 2530 ms, TE = min full , slice thickness = 1.2 mm, flip angle = $11\mathrm{deg}$, inversion time = 400 ms, FOV = 256 x 256 mm. The rsBOLD images were obtained using an echo-planar imaging sequence with the following parameters: 48 axial slices, thickness/gap = 3.3 mm, in-plane resolution = 64 x 64, TR = 2925 ms, TE = 30 ms, flip angle = $90\mathrm{deg}$, FOV = 200 x 200 mm. Diffusion tensor images were acquired by using a single-shot Echo-Planar Imaging-based sequence (coverage of the whole brain, 2.7 mm slice thickness with no inter-slice gap, 70 axial slices, TR = 12300 ms, TE = minimum, 64 diffusion directions.

In addition to imaging, patients were administered the following neuropsychological tests: Hopkins Verbal Learning Test Revised (HVLT-R) (*23*), Rey Complex Figure Test and Recognition Trial (RCFT) (*24*), Digit Span - Wechsler adult intelligence scales (WAIS-III) (*25*), Cognitive Failures Questionnaire (*26*) and the Edinburgh Handedness Inventory (*27*). See Table 1 for phenotypic data of the chemobrain patients.

Data pre-processing

Motion correction was performed on all resting state data, using a 6 point affine transformation, with the AFNI tool `3DVolreg`. Images were spatially registered to the first volume of the rsBOLD data. Then anatomical and motion corrected rsBOLD data were aligned and spatially

warped using a 12-point affine transformation to the TT_N27 atlas using AFNI (*28*). DTI data was corrected for eddy current and head motion using FMRIB's Diffusion Toolbox (FDT). Next, the skull and other non-brain tissues were removed using the Brain Extraction Tool (BET) from FSL (*29*).

Fractal Analysis

FD was calculated over a grey matter mask. Fractal dimension estimation was done by calculating a voxel-wise Hurst exponent (H) on the gray matter mask, following the methodology proposed by Eke et al. (*30*). For self-affine processes with n-dimensions, the Hurst exponent is related to the fractal dimension (FD) such as $FD + H = n + 1$, where $n = 1$ for a time domain signal. The rs-BOLD raw signal was initially normalized, end matched and bridge de-trended following Ekes procedure. The data was normalized by subtracting the mean from every data point while end matching and bridge detrending was achieved by subtracting from the data the line that connects the first and the last point, and multiplying the data by a parabolic window Eq (1).

$$W(j) = 1 - \left(\frac{2j}{N+1} - 1\right), j = 1 \rightarrow N, \tag{1}$$

Where N is the number of time points.

The series were Fourier transformed to the frequency domain and the scaling exponent (beta) of the inverse power law Eq (2) calculated. Where A is the amplitude of the discrete Fourier transform (DFT) at frequency f; β is the spectral index and c is a constant. The spectral index was calculated in a frequency range from 0.08 - 0.16 Hz where power-law scaling behavior was consistently observed across all voxels and subjects . A previous study (*17*) suggested excluding low frequency regions below 0.02 Hz due to the presence of MRI system noise in that spectral region (*31*). The spectral index calculated from this frequency range was exclusively used for

signal classification while the entire signal in the time-domain was used in the final estimation of the Hurst exponent.

Following the dichotomous model proposed by Mandelbrot and Van Ness (*32*) the signals were classified as fractional Brownian motion (fBm) for $\beta > 1$ and fractional Gaussian noise (fGn) for $\beta < 1$.

$$|A(f)^2| \propto cf^{-\beta}, \tag{2}$$

The Hurst exponent on fGn signals was calculated using dispersional analysis, proposed by Bassingthwaighte (*33*), which is based on the variability of the local averages of the signal over different time windows (τ) Eq (3). However, a scaled window variance analysis was used to calculate H on the fBM signals where the series, were divided in non-overlapping windows.

$$SD(\tau) = SD(\tau_0)\left(\frac{\tau}{\tau_0}\right)^H, \tag{3}$$

Signals where β was near 1 produced ambiguous results, therefore the classification method was refined using the signal summation conversion method (SSCM) described by Eke (*30*). It is important to mention here that fractal dimension estimation based on a dispersional analysis is quite robust with respect to correlated noise and does not require preprocessing (*33*). For instance, uncorrelated noise generated by motion artifacts will not affect the estimation of the fractal dimension.

Diffusion Tensor Imaging

In order to perform a whole-brain, voxel wise analysis of the DTI data, the FMRIB Diffusion Toolbox (FDT) programs were used. Through FDT, diffusion tensors were reconstructed by fitting a tensor model to the raw diffusion data, resulting in images of FA, MD, AD, and RD. Then a common registration target was created and using a Z-score methodology, each subject's aligned images (FA, MD, axial diffusivity (AD) and radial diffusivity (RD)) were projected onto

this common target. Voxel wise statistics were performed in addition to region of interest (ROI) analysis of 20 individual structures according to the JHU DTI-based white-matter atlas.

Z-score and Normalization

A voxel-based Z-scoring methodology was used for the statistical analysis of both fractal rs-BOLD and DTI analysis. The Z-score was calculated as the number of standard deviations (σ) a data point is above ($Z > 0$) or below the mean ($Z < 0$). The Z-score of the voxel-wise fractal dimension was calculated as: $Z_{FD} = (x - \mu)/\sigma$. Where x is the localized voxel rs-BOLD FD and μ and σ are the voxel mean and standard deviation of that same voxel, from the control group, respectively. Similarly, Z-scores of the voxel-wise FA, MD, RD and AD were calculated as: $Z_{FA} = (x_1 - \mu_1)/\sigma_1$. Where x_1 is the localized voxel FA and μ_1 and σ_1 are the voxel mean and standard deviation of that same voxel from the control group, respectively. Voxel-wise validation of normality was performed on the control group data (i.e. voxel-wise skewness and kurtosis was investigated) and voxels that deviated from the univariate normal distribution, were subsequently removed from the final Z-score map. This study was conceived as an exploratory study rather than a hypothesis driven design, therefore the overall false positive rate, accounting for multiple comparisons was controlled by selecting only regions of interests where significant decrease in mean FD was observed. This approach was considered overly conservative, however, a Bonferroni correction was deemed not appropriate as we could not establish independence of the data and smoothing of the signal across voxels could significantly affect the true nature of the fractal behavior.

Regions of interest (ROIs)

The FD Z-score maps from patients were co-registered to the TT_Daemon (*34*) human brain atlas and the mean FD Z-score was was calculated for each of the 240 regions included in

the atlas. In contrast, FA Z-score maps on WM regions were co-registered to the Johns Hopkins University and International Consortium of Brain Mapping atlases of human white matter anatomy (*35*).

Results

FD analysis

To determine regions of the brain of chemobrain patients with increased or decreased signal complexity respect to a typical control group, we estimated the voxel-wise FD on every subject of both groups and calculated the Z-score of every voxel in the chemobrain group respect to controls. The mean Z-score value was obtained per ROI, however, only Z-score values greater than two were considered statistically significant for a 0.95 confidence level and therefore included in the analysis. Figure 1 shows the FD maps of the five patients, mean FD map for controls below 70 years old and controls above 70 years old. After doing a Z-score normalization with the healthy control maps, we found no significant difference in any of the ROIS, except the posterior commissure in Patient 3 (Z=-2.11,p=0.017). The posterior commissure is a white matter structure completely surrounded by gray matter. We suspect that this result was caused by a misregistration of the gray matter map and what we are actually detecting is the culmen of vermis. Reduced FD compared to controls suggests decreased in signal complexity and therefore a decreased local neural activity somewhere around that region for this patient in particular.

Mean FD for in gray matter was calculated for patients and controls respectively. We performed a Crawford-Howell t-test commonly used between single cases and normative groups of controls for each patient independently, the results are presented in Table 2. We found no significant difference between the mean FD in each subject and the healthy control groups

DTI analysis

Voxel-wise FA, MD, AD and RD Z-score maps were calculated for the patients on the 20 white matter tract labels previously selected as ROIs. The regions that significantly deviated from the respective control group mean were extracted. Table 3 shows the Z-score of FA, MD, AD and RD calculated based on control mean values. Figure 2 shows the z scored FA maps for patients 1($< 70yo$) and 2($< 70yo$), offering visual insight into the observed differences. Two healthy control groups were used, one for patients below 70 years old and another group for patients above 70 years old. All patients, independently of age, showed significantly reduced FA in the corpus callosum, inferior fronto occipital fasciculus and right inferior longitudinal fasciculus. Additionally, patients above 70 years old showed significantly reduced FA in the bilateral uncinate fasciculus and in the superior longitudinal fasciculus temporal. FA is a scalar metric that represents the degree of anisotropy in the diffusion tensor and ranges between 0 and 1. A FA value of zero indicates completely isotropic diffusion (spherical shaped ellipsoid) and a FA value of one indicates completely anisotropic diffusion (cigar shaped ellipsoid). Healthy white matter tracts are expected to follow the anisotropic diffusion model. Therefore, a decrease in FA indicates a potential decrease in structural connectivity within that tract.

Each patient showed additional regions that significantly deviated from controls however of particular interest was Patient 4 who showed a marked increased diffusivity in several ROIs. MD, AD and RD are three distinct metrics that provide information about diffusivity in the brain. MD offers information about the size of the diffusion ellipsoid, rather than its shape, as is quantified with FA measures. MD is an inverse measure of membrane density, and is expected to increase with damage to tissue due to increased free diffusion. AD is a measure of the principal (largest) eigenvalue of the diffusion tensor, and is sensitive to axonal diameter and integrity, as well as myelination. RD offers more insight into myelin pathology and it is sensitive to changes in axonal packing, myelination/demyelination, as well as axonal degeneration (*36–38*).

Correlation analysis of neuropsychological scores with FA values

Significant correlations between FA values and neuro-psychological test scores were found in the the corpus callosum (CC), inferior fronto occipital fasciculus (IFOF) and right inferior longitudinal fasciculus (ILF)(Table 4 and Figure 3).

FA correlated significantly with the Cognitive Failure questionnaire in the IFOF, in which a strong positive correlation was demonstrated. FA was negatively correlated with Rey Complex Copy Trial in the left CC and the Rey Complex Recognition Trial showed a strong positive correlation in the right CC, right IFOF and right ILF.

Discussion

The neurotoxicity of chemotherapy drugs has, for many years, been a source of debate among researchers and clinicians. While neurotoxic effects of these drugs have been demonstrated when delivered directly to the central nervous system (CNS) (*39*), the effects they cause in the brain when administered orally or intravenously are not yet well understood. In the case of non-CNS cancer, it was previously believed that chemotherapy agents did not penetrate the blood brain barrier (BBB). Endothelial cells in the BBB restrict the diffusion of large or hydrophilic molecules into the cerebrospinal fluid (CSF), while permitting the diffusion (or transport) of small hydrophobic molecules and hormones. Nevertheless, there is enough evidence to think that in fact chemotherapy cross the BBB (*40*). Several studies, intending to find an association between chemotherapy and cognitive dysfunction, have been conducted on breast cancer patients in the last 10 years. Wefel et al. (*40*) have summarized the results of at least 80 studies, concluding there is already enough evidence to support the connection between chemotherapy drugs and chemotherapy-induced cognitive dysfunction. Despite evidence of cognitive changes associated with chemotherapy in breast cancer patients, the pathophysiology of these changes

stills unknown. MRI techniques in combination with performance-based neuropsychological testing have been previously used to assess structural and functional changes in the brain following CTD exposure (*10–15, 41*). However, all the studies to date show significant variability in results. The main reason for this is the lack of a standardized acquisition protocol and subsequent analysis. Studies that rely on group based statistics face the challenge of finding enough patients with the same type of cancer and under the same treatment. Additionally, co-morbidity is usually encountered in cancer patients which adds another level of complexity in the analysis of chemobrain. As the medical field moves towards personalized medicine, the need to develop diagnostic techniques based on a single subject approach becomes indispensable. In this study we proposed a combination of a FD analysis for the gray matter and a DTI analysis for the white matter tracts as alternative methods that could be used for a single subject analysis approach.

Previous analysis of rs BOLD signals using complexity analysis, based on fractals, has been done to assess early onset Alzheimer's disease (AD) (*42, 43*). These studies have shown that decreased FD is consistent with AD severity. A more recent study in our laboratory have shown regions in the brain with decreased FD in mild traumatic brain injury patients that correlates with neurological symptoms (*44*). Although no significant changes were found in the FD of the rs BOLD signal of the studied chemo brain patients, the analysis of the FD in the rs BOLD signal provides additional patient-specific brain information that can be used to assess the gray matter in brain disorders. In the case of the chemo brain subjects, changes in gray matter are either below our detection limit or non existent.

The main limitation of the FD analysis arises from our technical capacity of sampling the signal at higher frequencies. Ideally, accuracy of FD depends on the ability to capture the true dynamics of the rs BOLD signal. The sampling frequency should be one order of magnitude higher than the highest frequency of the hemodynamic response to neuronal activation. The BOLD responses have a temporal width on the order of 4 –6 s (*45*), therefore the signal needs

to be sampled at 0.125 Hz. In order to acquire the rs-BOLD signal for the entire brain in a reasonable time for the patients, we were only able to sample at a frequency of 0.5 Hz which significantly limited the scope of our study. The minimum TR (frequency = 1/TR) is limited by the number of slices being acquired on a single shot. To cover the human brain at a resolution of 3mm per slice we were required to read around 30 slices on a single shot, which limited the minimum TR to 1.7 s (0.58 Hz).

Previous studies have done DTI analysis to assess white matter integrity in patients experiencing chemo-brain (*12, 13*) . They have found significant FA reduction in the inferior longitudinal fasciculus and inferior fronto-occipital fasciculus among other regions which is consistent with our findings.

This study shows that integrity of the white matter tracts, evaluated with DTI measures, specifically FA, is significantly lower in chemo-brain patients when compared with healthy controls. Three regions (CC, IFOF, ILF) were identified as common among all patients independently of age while three additional regions (bilateral uncinate fasciculus and the superior longitudinal fasciculus temporal) were exclusively detected on older patients.

ILF and IFOF are long association tracts that structurally connect frontal, parietal, and temporal association cortices, involved in the execution of complex cognitive tasks (*46*). Decreased FA in these tracts has been associated with mild cognitive impairment (*47*), cognitive deficits in mild traumatic brain injury (*48*) and reduced cognitive processing speed in healthy subjects (*49*). We found a strong correlation between FA in these regions and the Rey Complex recognition Trial, which is a measure of visuospatial memory and a strong correlation between IFOF and the cognitive failure questionnaire. Additionally, we found decreased FA in the bilateral CC of the chemo-brain patients when compared to controls. The role of CC is the integration and coordination of information between the two cerebral hemispheres. It is involved in learning, memory, thinking, three-dimensional visual ability, executive functions, as well as visual reac-

tion time (*50*). In this study, FA in the CC showed strong correlation with the Rey Complex copy trial (visuospatial constructional ability) and the recognition trial(visuospatial memory).

Although significant differences in white matter integrity were detected in all the studied chemo-brain patients when compared to untreated healthy controls, we cannot completely assume that these differences, and their associate cognitive disturbances, are exclusively attributed to the chemotherapy treatment. One way to overcome this limitation in future studies could be acquiring baseline data before the treatment begins. The results of this baseline acquisition could help in the exclusion of confounding factors such as stress, hormonal therapies and co-morbidity.

In summary, this study demonstrates that white and gray matter integrity can be explored in patients experiencing the effects of chemotherapy-related cognitive impairment through a single subject approach. This alternative method will hopefully shed further light on the etiology of chemo-brain, and provide the means for development of a standardized approach for assessing chemo-brain, enhancing patient care through targeted treatments and personalized interventional techniques.

Acknowledgements

Data were provided in part by the Human Connectome Project, WU-Minn Consortium (Principal Investigators: David Van Essen and Kamil Ugurbil; 1U54MH091657) funded by the 16 NIH Institutes and Centers that support the NIH Blueprint for Neuroscience Research; and by the McDonnell Center for Systems Neuroscience at Washington University. This research was supported by a Cancer Care Ontario grant (CINO-2014) and private funds donated by Mr. Dunsmore.

References and Notes

1. Marrett, L. D. *et al.* Cancer in canada in 2008. *Canadian Medical Association Journal* **179**, 1163–1170 (2008).

2. Collins, B., MacKenzie, J., Tasca, G. A., Scherling, C. & Smith, A. Cognitive effects of chemotherapy in breast cancer patients: a dose-response study. *Psycho-oncology* **22**, 1517–1527 (2013). DOI 10.1002/pon.3163.

3. Stewart, A. *et al.* The cognitive effects of adjuvant chemotherapy in early stage breast cancer: a prospective study. *Psycho-oncology* **17**, 122–130 (2008). DOI 10.1002/pon.1210.

4. Jansen, C. E., Dodd, M. J., Miaskowski, C. A., Dowling, G. A. & Kramer, J. Preliminary results of a longitudinal study of changes in cognitive function in breast cancer patients undergoing chemotherapy with doxorubicin and cyclophosphamide. *Psycho-oncology* **17**, 1189–1195 (2008). DOI 10.1002/pon.1342.

5. Ahles, T. A. *et al.* Longitudinal assessment of cognitive changes associated with adjuvant treatment for breast cancer: impact of age and cognitive reserve. *Journal of clinical oncology : official journal of the American Society of Clinical Oncology* **28**, 4434–4440 (2010). DOI 10.1200/JCO.2009.27.0827.

6. Weis, J., Poppelreuter, M. & Bartsch, H. Cognitive deficits as long-term side-effects of adjuvant therapy in breast cancer patients:subjectivecomplaints and objectiveneuropsychological test results. *Psycho-Oncology* **18**, 775–782 (2009).

7. de Ruiter, M. B. *et al.* Cerebral hyporesponsiveness and cognitive impairment 10 years after chemotherapy for breast cancer. *Human brain mapping* **32**, 1206–1219 (2011). DOI 10.1002/hbm.21102.

8. Koppelmans, V. *et al.* Neuropsychological performance in survivors of breast cancer more than 20 years after adjuvant chemotherapy. *Journal of clinical oncology : official journal of the American Society of Clinical Oncology* **30**, 1080–1086 (2012). DOI 10.1200/JCO.2011.37.0189.

9. O'Farrell, E., MacKenzie, J. & Collins, B. Clearing the air: a review of our current understanding of "chemo fog". *Current oncology reports* **15**, 260–269 (2013). DOI 10.1007/s11912-013-0307-7.

10. Brown, M. S. *et al.* MR and proton spectroscopy of white matter disease induced by high-dose chemotherapy with bone marrow transplant in advanced breast carcinoma. *AJNR. American journal of neuroradiology* **16**, 2013–2020 (1995).

11. Lopez Zunini, R. A. *et al.* Differences in verbal memory retrieval in breast cancer chemotherapy patients compared to healthy controls: a prospective fMRI study. *Brain imaging and behavior* **7**, 460–477 (2013). DOI 10.1007/s11682-012-9213-0.

12. de Ruiter, M. B. *et al.* Late effects of high-dose adjuvant chemotherapy on white and gray matter in breast cancer survivors: converging results from multimodal magnetic resonance imaging. *Human brain mapping* **33**, 2971–2983 (2012). DOI 10.1002/hbm.21422.

13. Deprez, S. *et al.* Longitudinal assessment of chemotherapy-induced structural changes in cerebral white matter and its correlation with impaired cognitive functioning. *Journal of clinical oncology : official journal of the American Society of Clinical Oncology* **30**, 274–281 (2012). DOI 10.1200/JCO.2011.36.8571.

14. Silverman, D. H. *et al.* Altered frontocortical, cerebellar, and basal ganglia activity in adjuvant-treated breast cancer survivors 5–10 years after chemotherapy. *Breast cancer research and treatment* **103**, 303–311 (2007).

15. Inagaki, M. *et al.* Smaller regional volumes of brain gray and white matter demonstrated in breast cancer survivors exposed to adjuvant chemotherapy. *Cancer* **109**, 146–156 (2007). DOI 10.1002/cncr.22368.

16. McDonald, B. C., Conroy, S. K., Ahles, T. A., West, J. D. & Saykin, A. J. Gray matter reduction associated with systemic chemotherapy for breast cancer: a prospective MRI study. *Breast cancer research and treatment* **123**, 819–828 (2010). DOI 10.1007/s10549-010-1088-4.

17. Herman, P., Sanganahalli, B. G., Hyder, F. & Eke, A. Fractal analysis of spontaneous fluctuations of the BOLD signal in rat brain. *NeuroImage* **58**, 1060–1069 (2011). DOI 10.1016/j.neuroimage.2011.06.082.

18. Bullmore, E. *et al.* Generic aspects of complexity in brain imaging data and other biological systems. *NeuroImage* **47**, 1125–1134 (2009). DOI 10.1016/j.neuroimage.2009.05.032.

19. Van Essen, D. C. *et al.* The wu-minn human connectome project: an overview. *Neuroimage* **80**, 62–79 (2013).

20. Mueller, S. G. *et al.* Ways toward an early diagnosis in alzheimers disease: the alzheimers disease neuroimaging initiative (adni). *Alzheimer's & Dementia* **1**, 55–66 (2005).

21. Peters, R. Ageing and the brain (2006).

22. Scahill, R. I. *et al.* A longitudinal study of brain volume changes in normal aging using serial registered magnetic resonance imaging. *Archives of neurology* **60**, 989–994 (2003). DOI 10.1001/archneur.60.7.989.

23. Benedict, R. H. B. & Brandt, J. Hopkins Verbal Learning Test-Revised (HVLT-R): Professional Manual. *Lutz: Psychological Assessment Resources* (2001).

24. Meyers, J. E. & Meyers, K. R. *Rey Complex Figure Test and recognition trial professional manual* (Psychological Assessment Resources, 1995).

25. Wechsler, D. Wechsler Adult Intelligence ScaleFourth Edition (WAISIV) (2014).

26. Broadbent, D. E., Cooper, P. F., FitzGerald, P. & Parkes, K. R. The Cognitive Failures Questionnaire (CFQ) and its correlates. *The British journal of clinical psychology* **21 (Pt 1)**, 1–16 (1982).

27. Oldfield, R. C. The assessment and analysis of handedness: the Edinburgh inventory. *Neuropsychologia* **9**, 97–113 (1971).

28. Cox, R. W. AFNI: software for analysis and visualization of functional magnetic resonance neuroimages. *Computers and biomedical research, an international journal* **29**, 162–173 (1996).

29. Woolrich, M. W. *et al.* Bayesian analysis of neuroimaging data in fsl. *Neuroimage* **45**, S173–S186 (2009).

30. Eke, A., Herman, P., Kocsis, L. & Kozak, L. R. Fractal characterization of complexity in temporal physiological signals. *Physiological measurement* **23**, R1–38 (2002).

31. Zarahn, E., Aguirre, G. K. & D'Esposito, M. Empirical analyses of BOLD fMRI statistics. I. Spatially unsmoothed data collected under null-hypothesis conditions. *NeuroImage* **5**, 179–197 (1997).

32. Mandelbrot, J. W. V. & B., B. Fractional Brownian Motions, Fractional Noises and Applications. *SIAM Rev.* **10**, 422–437 (1967). DOI 10.1137/1010093.

33. Bassingthwaighte, J. B. & Raymond, G. M. Evaluation of the dispersional analysis method for fractal time series. *Annals of biomedical engineering* **23**, 491–505 (1995).

34. Eickhoff, S., Stephan, H., KE.and Mohlberg, Grefkes, C., Fink, G. & Amunts, K., K.and Zilles. A new SPM toolbox for combining probabilistic cytoarchitectonic maps and functional imaging data. *NeuroImage* **25**, 1325–1335 (2005).

35. Wakana, S., Jiang, H., Nagae-Poetscher, L. M., van Zijl, P. C. M. & Mori, S. Fiber tract-based atlas of human white matter anatomy. *Radiology* **230**, 77–87 (2004). DOI 10.1148/radiol.2301021640.

36. Shenton, M. E. *et al.* A review of magnetic resonance imaging and diffusion tensor imaging findings in mild traumatic brain injury. *Brain imaging and behavior* **6**, 137–192 (2012). DOI 10.1007/s11682-012-9156-5.

37. Roosendaal, S. D. *et al.* Regional DTI differences in multiple sclerosis patients. *NeuroImage* **44**, 1397–1403 (2009). DOI 10.1016/j.neuroimage.2008.10.026.

38. Song, S.-K. *et al.* Demyelination increases radial diffusivity in corpus callosum of mouse brain. *NeuroImage* **26**, 132–140 (2005). DOI 10.1016/j.neuroimage.2005.01.028.

39. Rutkowski, S. *et al.* Treatment of early childhood medulloblastoma by postoperative chemotherapy alone. *The New England journal of medicine* **352**, 978–986 (2005). DOI 10.1056/NEJMoa042176.

40. Wefel, J. S. & Schagen, S. B. Chemotherapy-related cognitive dysfunction. *Current neurology and neuroscience reports* **12**, 267–275 (2012). DOI 10.1007/s11910-012-0264-9.

41. McDonald, B. C., Conroy, S. K., Ahles, T. A., West, J. D. & Saykin, A. J. Gray matter reduction associated with systemic chemotherapy for breast cancer: a prospective MRI study. *Breast cancer research and treatment* **123**, 819–828 (2010). DOI 10.1007/s10549-010-1088-4.

42. Maxim, V. *et al.* Fractional Gaussian noise, functional MRI and Alzheimer's disease. *NeuroImage* **25**, 141–158 (2005). DOI 10.1016/j.neuroimage.2004.10.044.

43. Warsi, M. A., Molloy, W. & Noseworthy, M. D. Correlating brain blood oxygenation level dependent (BOLD) fractal dimension mapping with magnetic resonance spectroscopy (MRS) in Alzheimer's disease. *Magma (New York, N.Y.)* **25**, 335–344 (2012). DOI 10.1007/s10334-012-0312-0.

44. Dona, O., Noseworthy, M., DeMatteo, C. & Connolly, J. Fractal Analysis of Brain Blood Oxygenation Level Dependent (BOLD) Signals from Children with Mild Traumatic Brain Injury (mTBI). *PLoS ONE* **12**, e0169647 (2017). DOI 10.1371/journal.pone.0169647.

45. Bandettini, P. A., Wong, E. C., Hinks, R. S., Tikofsky, R. S. & Hyde, J. S. Time course epi of human brain function during task activation. *Magnetic resonance in medicine* **25**, 390–397 (1992).

46. Schmahmann, J. D., Smith, E. E., Eichler, F. S. & Filley, C. M. Cerebral white matter. *Annals of the New York Academy of Sciences* **1142**, 266–309 (2008).

47. Cho, H. *et al.* Abnormal integrity of corticocortical tracts in mild cognitive impairment: a diffusion tensor imaging study. *Journal of Korean medical science* **23**, 477–483 (2008).

48. Niogi, S. *et al.* Extent of microstructural white matter injury in postconcussive syndrome correlates with impaired cognitive reaction time: a 3t diffusion tensor imaging study of mild traumatic brain injury. *American Journal of Neuroradiology* **29**, 967–973 (2008).

49. Turken, U. *et al.* Cognitive processing speed and the structure of white matter pathways: convergent evidence from normal variation and lesion studies. *Neuroimage* **42**, 1032–1044 (2008).

50. Caillé, S., Sauerwein, H. C., Schiavetto, A., Villemure, J.-G. & Lassonde, M. Sensory and motor interhemispheric integration after section of different portions of the anterior corpus callosum in nonepileptic patients. *Neurosurgery* **57**, 50–59 (2005).

Author Contributions

Olga M. Dona, as first author, acquired the data, performed the data analysis and interpretation of the results and drafted the article including tables and figures. Contributions by Olga M. Dona warranted her name as first author. Mitchel Doughty as a co-author performed the data analysis of the DTI section and drafted the respective figures and tables. He participated in proofreading the article. Dr. Michael D. Noseworthy, as corresponding author, designed and conceptualized this project which is part of a his long trajectory on developing applications based on the fractal analysis in human brain signals. He performed the critical revision of the article and the final approval of the version to be published. Furthermore, Dr. Noseworthy provided constant guidance and advice through out the duration of this study and secured the required funds. Dr. Geoffrey Hall actively collaborated in the interpretation of the results due to his vast experience studying neurological disorders. He provided guidance with application and interpretation of the neuropsychological testings. Moreover, he exhaustively revised and edited the final version of this article.Dr. Raimond Wong recruited the patients for this study and participated in the conception and design of this work. Additionally, Dr. Wong participated in the critical revision of the article and the final approval of the version to be published. All authors agreed to be accountable for all aspects of the work in ensuring that questions related to the accuracy or integrity of any part of the work were appropriately investigated and resolved.

Additional Information

Competing financial interests

The authors declare that the research was conducted in the absence of any commercial or financial relationships that could be construed as a potential conflict of interest.

Tables

Table 1: Phenotypic Data.

	Patient 1	**Patient 2**	**Patient 3**	**Patient 4**	**Patient 5**
Age(y)	46	43	70	74	70
Sex	M	F	F	M	M
Handessness	L	R	R	R	R
Cognitive Failure	51	57	40	36	38
Digit Span Scaled	12	9	8	8	14
HVL Learning index	6	2	3	0	4
HVL Retention %	88	100	100	100	100
HVL delayed discrimination index	8	7	11	9	10
Rey Copy	34	33	33	36	36
Rey Immediate Recall	21	21	17	19	18.5
Rey Delayed Recall	20.5	21	15	21	17.5
Rey Recognition Trial	20	22	20	18	22

Table 2: Mean gray matter FD for chemo-brain patients and controls. Patients 1 and 2 are below 70 years old and patients 3, 4 and 5 above 70 years old. T-test was performed with corresponding control group based on age.

Subjects	**Mean(FD)**	**std(FD)**	**t**	**p**
Patient 1	1.64	0.23	0.68	0.49
Patient 2	1.66	0.22	1.30	0.19
Patient 3	1.62	0.24	0.11	0.91
Patient 4	1.59	0.25	-0.12	0.90
Patient 5	1.62	0.24	0.11	0.91
Controls < 70	1.62	0.03		
Controls ≥ 70	1.61	0.12		

Table 3: Z score values for FA, MD, AD and RD in the the ROIs. Highlighted in red are $Zscores < 2$ ($p < 0.05$), which represents the number of standard deviation this value is below the mean. Highlighted in green are $Zscores > 2$ ($p < 0.05$), which represents the number of standard deviations this value is above the mean.

ROI		<70		>70			ROI		<70		>70		
		Pat 1	Pat 2	Pat 3	Pat 4	Pat 5			Pat 1	Pat 2	Pat 3	Pat 4	Pat 5
Anterior Thalamic L	FA	-2.14	-1.96	-1.52	-1.76	-1.61	Forceps Minor	FA	-1.18	-1.19	-1.42	-1.71	-1.55
	MD	-0.56	-0.58	-0.46	1.89	0.15		MD	-0.33	0.21	-0.24	1.19	0.21
	AD	-0.11	-0.18	-0.08	2.27	0.60		AD	0.37	0.93	0.26	1.82	0.75
	RD	0.12	0.05	0.13	2.43	0.76		RD	0.77	1.26	0.51	2.02	1.01
Anterior Thalamic R	FA	-2.06	-1.97	-1.36	-1.43	-1.37	Inferior Fronto Occipital Fasciculus L	FA	-2.06	-1.86	-2.27	-2.68	-2.48
	MD	-0.60	-0.39	-0.56	-0.23	-0.33		MD	-0.55	-0.59	-1.02	2.31	-0.11
	AD	-0.20	0.01	-0.23	0.08	-0.02		AD	1.13	0.96	-0.19	3.64	0.97
	RD	0.13	0.26	-0.05	0.24	0.19		RD	2.09	1.78	0.33	4.14	1.45
Cingulum Cingulate Gyrus L	FA	-1.94	-2.14	-1.40	-2.45	-1.91	Inferior Fronto Occipital Fasciculus R	FA	-2.21	-2.11	-2.42	-2.63	-2.27
	MD	-0.92	0.23	-0.85	9.40	-0.21		MD	-0.60	-0.91	-0.84	0.25	-0.32
	AD	0.83	2.59	0.28	15.94	1.97		AD	1.10	0.64	-0.02	1.25	0.48
	RD	1.22	2.77	0.85	13.21	2.31		RD	1.95	1.56	0.46	1.76	0.91
Cingulum Cingulate Gyrus R	FA	-2.34	-2.68	-1.34	-2.52	-2.11	Inferior Longitudinal Fasciculus L	FA	-1.92	-1.75	-1.81	-2.14	-1.88
	MD	-0.68	0.03	-1.38	8.25	-0.13		MD	-0.24	-0.66	-0.82	0.93	0.12
	AD	1.06	2.49	-0.46	10.15	1.04		AD	1.04	0.57	-0.10	1.58	0.94
	RD	1.66	2.61	0.14	9.22	1.66		RD	1.30	0.98	0.28	1.84	1.15
Corpus Callosum L	FA	-2.17	-2.01	-2.04	-2.69	-2.27	Inferior Longitudinal Fasciculus R	FA	-2.38	-2.24	-2.45	-2.57	-2.23
	MD	-0.05	0.41	-0.90	2.58	-0.48		MD	-0.96	-1.13	-1.11	-0.25	-0.52
	AD	0.99	1.49	-0.20	3.79	0.26		AD	0.54	0.37	-0.10	0.87	0.38
	RD	1.26	1.60	0.29	4.38	0.74		RD	1.32	1.11	0.44	1.40	0.87
Corpus Callosum R	FA	-2.15	-2.03	-2.45	-2.65	-2.17	Sup. Long. Fasciculus Temporal Part L	FA	-1.94	-1.91	-2.20	-1.97	-2.07
	MD	0.04	1.01	-0.25	1.76	0.33		MD	-1.21	-1.24	-1.04	2.89	-0.01
	AD	0.80	1.88	0.35	2.33	0.83		AD	0.71	0.68	0.74	4.15	1.63
	RD	1.45	2.60	0.55	2.56	1.15		RD	1.12	1.09	1.37	4.01	2.08
Corticospinal Tract L	FA	-1.10	-1.10	-1.36	-1.88	-1.43	Sup. Long. Fasciculus Temporal Part R	FA	-1.97	-1.89	-2.54	-2.34	-2.29
	MD	-0.33	0.11	-0.32	1.86	-0.74		MD	-1.56	-1.66	-0.62	2.10	-0.68
	AD	0.27	0.70	0.26	2.47	-0.16		AD	0.50	0.37	1.22	3.92	0.88
	RD	0.67	1.07	0.49	2.64	0.18		RD	0.96	0.97	1.88	4.18	1.50
Forceps Major	FA	-1.67	-1.79	-1.45	-1.90	-1.61	Uncinate Fasciculus L	FA	-1.91	-1.84	-2.59	-2.64	-2.79
	MD	-0.61	0.50	-0.75	0.40	-0.39		MD	-0.72	-0.57	-1.07	1.50	0.03
	AD	0.41	2.09	-0.18	1.38	0.25		AD	0.05	0.17	-0.06	2.12	1.20
	RD	0.78	2.31	0.20	1.88	0.63		RD	0.34	0.43	0.38	2.33	1.44
							Uncinate Fasciculus R	FA	-1.56	-1.55	-2.20	-2.52	-2.31
								MD	-0.83	-0.56	-1.19	0.21	-0.81
								AD	-0.25	0.01	-0.28	0.93	-0.03
								RD	0.14	0.38	0.14	1.18	0.32

Table 4: Correlation coefficients and p-values of Neuropsychological scores with normalized (Z-score) FA values in the corpus callosum (CC), inferior fronto occipital fasciculus (IFOF) and right inferior longitudinal fasciculus (ILF). Values with higher than 90% confidence are highlighted in red..

	Z(FA)_CC L		Z(FA)_CC R		Z(FA)_IFOF R		Z(FA)_ILF R	
	r	p	r	p	r	p	r	p
Cognitive_Failure	0.64	0.24	0.77	0.12	0.82	0.08	0.51	0.37
Digit Span Total	0.17	0.78	0.64	0.23	0.57	0.3	0.6	0.28
HVL Learning Index	0.52	0.35	0.6	0.28	0.61	0.28	0.45	0.44
HVL Retention	-0.13	0.82	-0.31	0.61	-0.32	0.59	0.02	0.97
HVL Delayed Disc. index	-0.09	0.88	-0.54	0.35	-0.53	0.36	-0.29	0.62
Rey Copy	-0.83	0.07	-0.37	0.53	-0.49	0.39	-0.18	0.76
Rey Immediate Recall	0.11	0.85	0.6	0.27	0.59	0.29	0.34	0.57
Rey Delayed Recall	-0.37	0.53	0.17	0.78	0.13	0.83	-0.02	0.96
Rey Recognition Trial	0.7	0.18	0.87	0.05	0.85	0.06	0.98	0.003

Figures

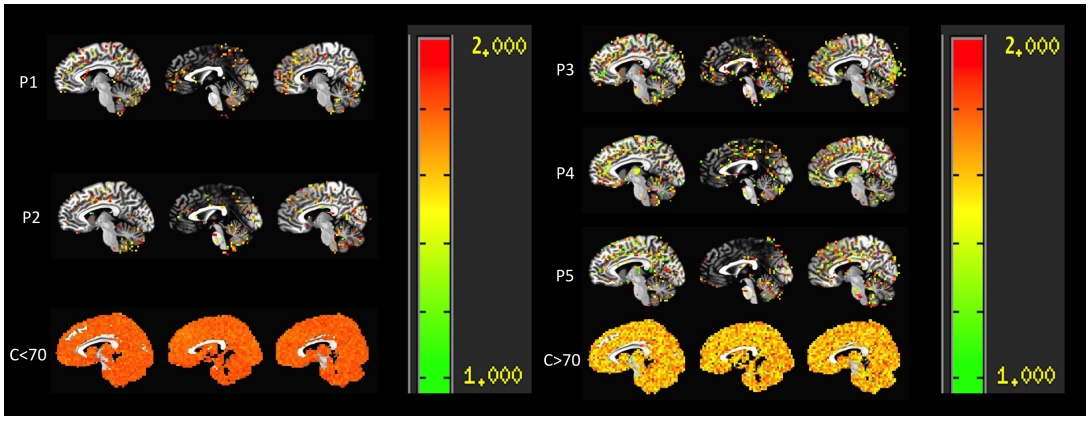

(a) (b)

Figure 1: FD analysis. (a) FD maps for patients younger than 70 y compared to healthy controls ($C < 70$). (b) FD maps for patients older than 70 y compared to healthy controls ($C > 70$). The gray matter mask for the mean FD in healthy controls was calculated using a probability distribution atlas while the gray matter for patients was done using a segmentation tool from fsl (fast).

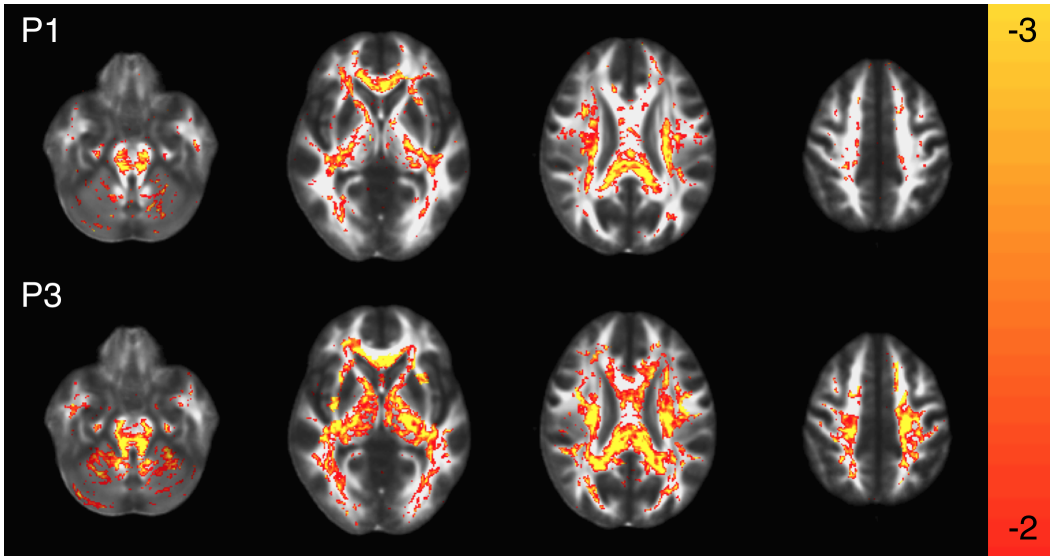

Figure 2: DTI Analysis. DTI results of patients 1 (P1) and 3 (P3) shown on a standard 1mm MNI FA overlay. The top image is of chemo-brain patient 1 ($<$ 70 yo). Red-yellow areas indicate regions along white matter tracts in the chemo-brain patient where FA is significantly lower than the HCP control population (Z-score < -2). Similar to the top image, the FA result for patient 3 ($\geq$ 70 yo) is shown overlain into standard space. Again, red-yellow regions indicate areas in the chemo-brain patient where FA is significantly lower than the ADNI controls (Z-score < -2). The colour-bar shown on the right side of the figure gives a visual representation of the significance of the deficits between these chemo-brain patients, and controls. Red areas indicate a Z-score of -2 ($p < 0.05$), ranging up to yellow regions which indicate a Z-score of -3 ($p < 0.01$).

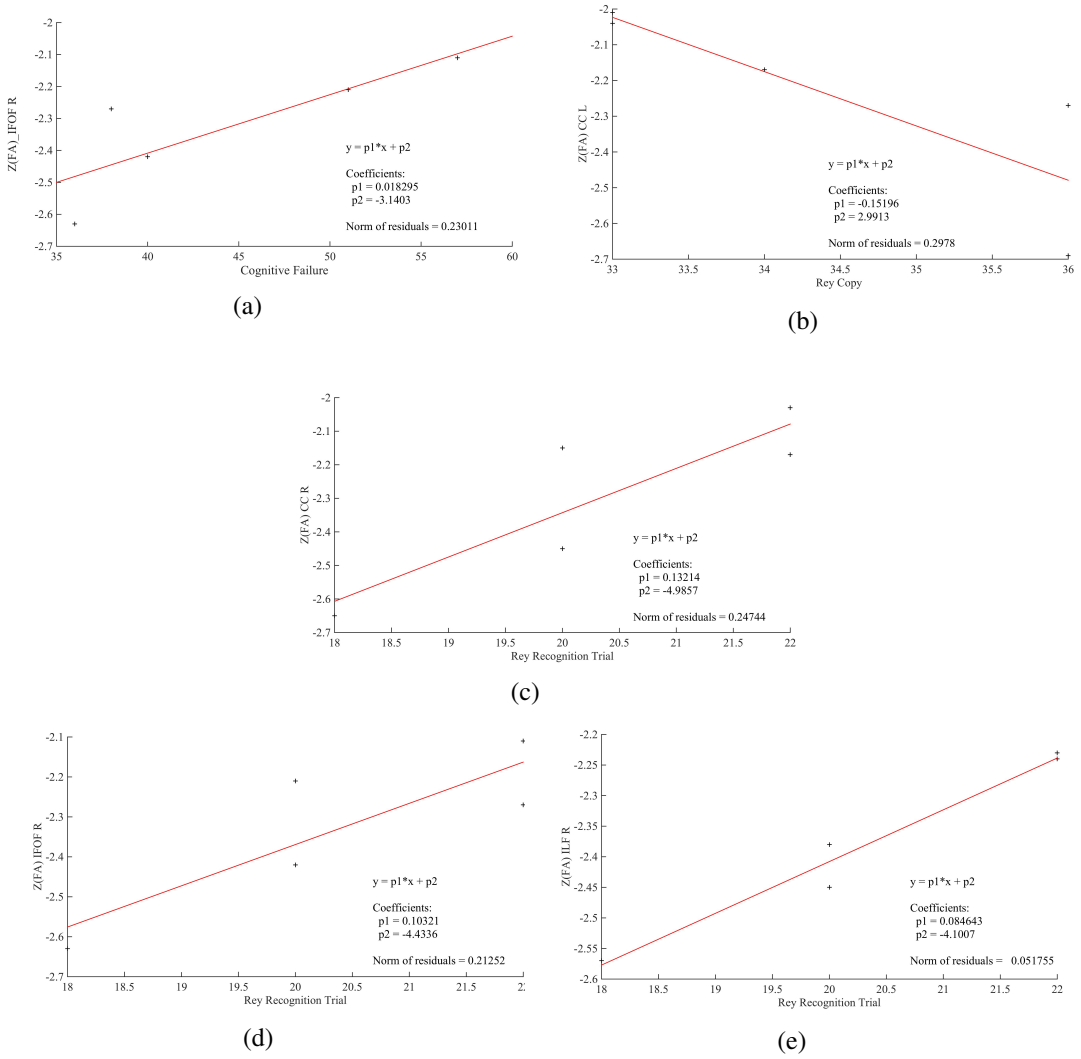

Figure 3: Scatter plot of significantly correlated neuropsychological scores and normalized FA values. (a) Cognitive failure correlated with IFOF. (b) Rey copy trail positively correlated with left CC. (c) Rey complex recognition trial negatively correlated with right CC. (d) Rey complex recognition trial positively correlated with right IFOF. (e) Rey complex recognition trial positively correlated with right ILF.

Chapter 7

Preliminary Study on Chronic Fatigue Syndrome

Case Report: Voxel-wise DTI and Fractal Analysis in a Chronic Fatigue Syndrome Patient .

Olga Dona, Mitchell Doughty, Peter Powles, Heather McNeely and Michael D. Noseworthy.

7.1 Context of the paper

Chronic fatigue syndrome (CSF) is a disorder characterized by extreme fatigue that cannot be attributed to a specific physical activity or to any underlying medical condition. Previous imaging techniques have been unable to identify anatomical or functional markers of this disease.

The purpose of this study was to explore the viability of using a complexity analysis of the rs-BOLD signal in combination with DTI to detect brain abnormalities in a single patient with a diagnostic of CSF. The patient was scanned twice in a three month period using a GE Discovery MR750 3T MRI and 32-channel RF-coil. Axial FSPGR-3D images were used to prescribe rs-BOLD (TE/TR=35/2000ms) and DTI (60 directions, TR/TE = 8800/87ms). Complexity analysis, was done by estimating the voxel-wise Hurst exponent using de-trended fluctuation analysis and signal summation conversion methods. Voxel-wise analysis of the DTI data was performed obtaining FA, MD, AD and RD measures. All the results were normalized with a database healthy controls using a Z-score methodology.

No significant differences were found on the global fractal dimension of the rs-BOLD signal when compared to controls in both trials. However, we found significant ($p<0.05$) decrease of the rs-BOlD fractal dimension in the cerebellar vermis on trial 2. In terms of structural connectivity, we detected significant ($p<0.05$) changes in

MD specifically in the bilateral cingulum cingulate gyrus for trial 1. The cerebellar vermis and the cingulate gyrus have been previously reported as dysfunctional by other studies .

This study demonstrates that white matter and gray matter integrity can be assessed on patients experiencing CFS using a single subject approach based on the FD of the rs-BOLD signal and DTI analysis. The combination of these techniques provides a non invasive alternative in the study of CFS and will hopefully lead to improved and targeted therapies for patients experiencing this condition.

7.2 Declaration Statement

Olga M. Dona, as first author, performed the data analysis and interpretation of the results and drafted the article including tables and figures. Contributions by Olga M. Dona warranted her name as first author.

Mitchell Doughty, as second author, acquired the data, performed the DTI data analysis and interpretation of the DTI results and collaborated in drafting the article including tables and figures.

Dr. Powles and Dr. McNeely recruited the participant for this study and provided guidance in the interpretation of the results.

Dr. Michael D. Noseworthy, as corresponding author, designed and conceptualized this project which is part of a his long trajectory on developing applications based on the fractal analysis and diffusion tensor imaging in human brain signals. He performed the critical revision of the article and the final approval of the version to be published. Furthermore, Dr. Noseworthy provided constant guidance and advice through out the duration of this study and secured the required funds.

This paper will be submitted for publication to the journal JMC Case Reports on March 10^{th}, 2017 .

7.3 Paper

Case Report: Voxel-wise DTI and Fractal Analysis in a Chronic Fatigue Syndrome Patient

Olga Dona [1,2], Mitchell Doughty [1,2], Peter Powles [5] , Heather McNeely [6] and Michael D. Noseworthy [1,2,3,4,*]

[1] McMaster School of Biomedical Engineering, McMaster University, Hamilton, ON, Canada.
[2] Imaging Research Centre, St. Josephs Healthcare, Hamilton, ON, Canada.
[3] Department of Electrical and Computer Engineering, McMaster University, Hamilton, ON, Canada.
[4] Department of Radiology, McMaster University, Hamilton, ON, Canada.
[5] Department of Medicine, Division of Respirology, McMaster University, Hamilton, ON, Canada.
[6] Department of Psychiatry and Behavioral Neurosciences, McMaster University, Hamilton, ON, Canada.

[*] Michael D. Noseworthy. email:nosewor@mcmaster.ca

1 Abstract

Abstract : Chronic fatigue syndrome (CSF) is a disorder characterized by extreme fatigue that cannot be attributed to a specific physical activity or to any underlying medical condition. Previous imaging techniques have been unable to identify anatomical or functional markers of this disease **Purpose**. The purpose of this study was to explore the viability of using a complexity analysis of the rs-BOLD signal in combination with DTI to detect brain abnormalities in a single patient with a diagnostic of CSF. **Materials and Methods**. The patient was scanned twice in a three month period using a GE Discovery MR750 3T MRI and 32-channel RF-coil. Axial FSPGR-3D images were used to prescribe rs-BOLD (TE/TR=35/2000ms) and DTI (60 directions, TR/TE = 8800/87ms). Complexity analysis, was done by estimating the voxel-wise Hurst exponent using de-trended fluctuation analysis and signal summation conversion

methods. Voxel-wise analysis of the DTI data was performed obtaining FA, MD, AD and RD measures. All the results were normalized with a database healthy controls using a Z-score methodology. **Results** No significant differences were found on the global fractal dimension of the rs-BOLD signal when compared to controls in both trials. However, we found significant ($p<0.05$) decrease of the rs-BOlD fractal dimension in the cerebellar vermis on trial 2. In terms of structural connectivity, we detected significant ($p<0.05$) changes in MD specifically in the bilateral cingulum cingulate gyrus for trial 1. The cerebellar vermis and the cingulate gyrus have been previously reported as dysfunctional by other studies . **Conclusions** This study demonstrates that white matter and gray matter integrity can be assessed on patients experiencing CFS using a single subject approach based on the FD of the rs-BOLD signal and DTI analysis. The combination of these techniques provides a non invasive alternative in the study of CFS and will hopefully lead to improved and targeted therapies for patients experiencing this condition.

Keywords: Chronic fatigue syndrome, Fractal Analysis, DTI, Z-score, BOLD fMRI.

2 Introduction

Chronic fatigue syndrome (CFS) is a particular case of myalgic encephalomyelitis, where clear inflammation of the brain or spinal cord cannot be detected. Patients diagnosed with CFS experience marked fatigue and weakness in the absence of a relatively proportional physical activity. A variety of other symptoms usually accompany this disease such as muscle pain, headaches, impaired memory and concentration and mental fog (*1*). The psychopathology of CFS is not fully understood and the causes have been attributed either to an abnormal immune system and brain function in response to an infection or virus or to genetic and environmental factors. Brain imaging, specifically MRI, have been previously used to study CFS. However, the results have been inconclusive or inconsistent. A study conducted by Puri et al. (*2*) applied a voxel based

morphometry approach to calculate regional gray and white matter volumetric changes in CSF, reporting significant neuroanatomical changes in CFS when compared to controls. However, a different study by Perrin et al. (*3*) reported that no cerebral abnormality was observed in a longitudinal MRI study of CFS. In terms of structural and functional connectivity, a study by Zeineh et al. (*4*) found a significant decrease in the fractional anisotropy of the right arcuate fasciculus which is involved with short term memory. Additionally, a functional study by Wortinger et al. (*5*) hypothesized that the hypersensitivity experienced by CFS patients could be attributed to an aberrant neurobiological stress response, which is controlled by brain networks involving autonomic, endocrine, and immune adjustments. In this study, they found a significant decrease in the Salience Network functional connectivity to the right posterior insula compared to healthy controls. Reduced connectivity of this network has been highly related to the fatigue symptoms that patients experience. The objective of this case study report consisted in exploring the structural connectivity and neuronal activity of a single patient by normalizing the analysis with a Z-score approach. Structural connectivity was assessed using 60 direction Diffusion Tensor Imaging (DTI) to calculate different measures of the diffusion tensor, mainly: fractional anisotropy (FA), mean diffusivity (MD), axial diffusivity (AD) and radial diffusivity (RD). Neuronal activity was investigated by analyzing the fractal dimension (FD) of the rs-BOLD signal.

3 Case Report

A 53 year old female patient came to our department in the Image Research Center at St. Joseph Health Care, Hamilton, Ontario with a diagnosis of chronic fatigue syndrom (CFS). The patient had reported neuro-psychological symptoms such as reduced concentration, headaches, sleeping disorder and impaired short term memory along with the symptoms of fatigue and extreme exhaustion. Traditional brain MRI scanning did not reveal clear abnormalities in this patient.

Subsequently, we decided to implement an experimental imaging protocol to assess functional and structural brain connectivity and its correlation with the clinical symptoms.

4 Methods

The patient was scanned twice in a three month period using a GE MR750 Discovery 3T MRI scanner, and a 32-channel RF receiver coil (General Electric Healthcare, Milwaukee, WI). Anatomical images were acquired using a 3-plane localizer and calibration scan for parallel imaging followed by a 3D inversion recovery-prepped T1-weighted (fSPGR, axial acquisition, TE/TR/flip angle = 4.25/11.36/12°, 256x256 matrix with 1mm slice thickness with 25.6cm FOV, 1mm isotropic acquisition). To assess the functional connectivity, a resting state functional BOLD data was acquired using an echo planar imaging (EPI) sequence with FOV = 22cm, image matrix = 64x64; flip angle = 90°; echo time (TE) = 35ms; repetition time (TR) = 2000ms (i.e, 0.5Hz temporal sampling frequency); slice thickness of 3mm; and 180 temporal points.

Axial Diffusion Tensor Imaging (DTI) data was acquired using a dual echo EPI sequence. Imaging parameters were as follows: 60 non-coplanar directions, TE/TR = 87/8800 ms, b = 1000 s/mm2, 122x122 matrix, 70 slices, 2.0 mm slice thickness, 244 mm FOV, ASSET = 2.

4.1 Pre-processing

Motion correction was performed on the rs-BOLD data, using a 6 point affine transformation, with the AFNI tool `3DVolreg`. Images were spatially registered to the first volume of the rs-BOLD data. Then anatomical and motion corrected rs-BOLD data were aligned and spatially warped using a 12-point affine transformation to the TT_N27 atlas using AFNI (*6*). DTI data was corrected for eddy current and head motion using FMRIB's Diffusion Toolbox (FDT). Next, the skull and other non-brain tissue were removed using Brain Extraction Tool (BET) from FSL

(*7*).

4.2 Fractal Analysis

Fractal analysis of the rs-BOLD signal, was done by calculating the Hurst exponent according to the procedure described by Eke et al. (*8*), using Matlab (v.8.3.0, The Mathworks, Natick MA). The Hurst exponent is related to the fractal dimension (FD) as $H = 2 - FD$, and is a measure of the correlation or anti-correlation of the signal. Studies on human and animal brain have shown that the rs-BOLD signal contains spontaneous low frequency fluctuations (LFF) (*9*) that originate from physiological functions such as cerebral blood oxygenation and cerebral blood flow and volume as well as from some instrument noise added during fMRI acquisition (*8, 10–13*). These LFF follow the inverse power law scaling in the frequency domain, which is a defined indication of fractal behavior. Time signals are considered fractals when they are self-similar and auto-correlate across different time scales. The fractal dimension (FD) is considered a metric of signal complexity, which has been previously used as a descriptor of the neural activity based on hemodynamics and metabolic response (*12, 14*). Increased FD is a sign of higher signal complexity which implies high neural activity and functionality while decreased FD is associated with decreased neural activity and disease (*15–18*).

4.3 Diffusion Tensor Imaging

In order to perform a whole-brain, voxelwise analysis of the DTI data, the FMRIB Diffusion Toolbox (FDT) and Tract-Based Spatial Statistics (TBSS) programs were used. Through FDT, diffusion tensors were reconstructed by fitting a tensor model to the raw diffusion data, this resulting in images of FA, MD, AD, and RD. From here, a common registration target was created and using TBSS, each subjects aligned image (FA, MD, AD and RD) was projected onto this common target. Voxel wise statistics were performed in addition to region of inter-

est (ROI) analysis of 20 individual structures according to the JHU DTI-based white-matter atlas. Group differences in DTI measures were probed through permutation testing methods (FSL randomise). The design of a simple linear model placing patients and controls in different subcategories, and subsequent application of Threshold-Free Cluster Enhancement (TFCE) provided the basis for observing group differences in structural integrity between the CFS patient and healthy controls.

FA is a scalar metric that represents the degree of anisotropy in the diffusion tensor and ranges between 0 and 1. A FA value of zero indicates completely isotropic diffusion (spherical shaped ellipsoid) and a FA value of one indicates completely anisotropic diffusion (cigar shaped ellipsoid). Healthy white matter tracts are expected to follow the anisotropic diffusion model. Therefore, a decrease in FA indicates a potential decrease in structural connectivity within that tract. MD offers information about the size of the diffusion ellipsoid, rather than its shape, as is quantified with FA measures. MD is an inverse measure of membrane density, and is expected to increase with damage to tissue due to increased free diffusion. AD is a measure of the principal (largest) eigenvalue of the diffusion tensor, and is sensitive to axonal diameter and integrity, as well as myelination. The final measure recorded was RD, which aims to offer more insight into myelin pathology. RD is sensitive to changes in axonal packing, myelination/demyelination, as well as axonal degeneration (*19–21*).

4.4 Z-scoring

A voxel-based Z-scoring methodology was used for the statistical analysis of fractal and DTI analysis respectively. Anatomical, functional and diffusion data for healthy control subjects were downloaded from the NITRC database and the Human Connectome Project. The data for the 180 healthy subjects (21.2 ± 1.9 yo) were acquired with similar acquisition protocols as the CFS patient and the following parameters : 1)Anatomical: A T1-weighted sagittal three-

dimensional magnetization-prepared rapid gradient echo (MPRAGE) sequence was acquired, covering the entire brain: 128 slices, TR = 2530 ms, TE = 3.39 ms, slice thickness = 1.33 mm, flip angle = $7\mathrm{deg}$, inversion time = 1100 ms, FOV = 256 x 256 mm, and in-plane resolution = 256 x 192. 2) Functional: The rs- BOLD images were obtained using an echo-planar imaging sequence with the following parameters: 33 axial slices, thickness/gap = 3/0.6 mm, in-plane resolution = 64 x 64, TR = 2000 ms, TE = 30 ms, flip angle = $90\mathrm{deg}$, FOV = 200 x 200 mm.

The control data used for DTI analysis consisted of 19 healthy, adult subjects (36.4 ± 9.2 y.o). The following acquisition parameters were used in the recording of this database: spin-echo Echo-Planar Imaging-based sequence (coverage of the whole brain), 1.5 mm slice thickness with no inter-slice gap, b = 1000 s/mm2, 140x140 matrix, 96 axial slices, TR/TE = 8800/57 ms, 64 diffusion directions and 210 mm FOV.

The Z-score was calculated as the number of standard deviations (σ) a data point is above ($Z > 0$) or below the mean ($Z < 0$). The Z-score of the voxel-wise fractal dimension was calculated as: $Z_{FD} = (x - \mu)/\sigma$. Where x is the localized voxel rs-BOLD FD and μ and σ are the voxel mean and standard deviation of that same voxel from the control group respectively. Similarly, The Z-score of the voxel-wise FA, MD, RD and AD was calculated as: $Z_{FA,MD,RD,AD} = (x_1 - \mu_1)/\sigma_1$. Where x_1 is the localized voxel FA, MD, RD, AD respectively and μ_1 and σ_1 are the voxel mean and standard deviation of that same voxel from the control group respectively. Voxel-wise validation of normality was performed on the control group data (i.e. voxel-wise skewness and kurtosis was investigated) and voxels that deviated from the univariate normal distribution, were subsequently removed from the final Z-score map.

4.5 Regions of Interest(ROIs)

The FD Z-score maps from patients were co-registered to the TT_Daemon (*22*) human brain atlas and the mean FD Z-score was was calculated for each of the 240 regions included in

the atlas. In contrast, FA Z-score maps on WM regions were co-registered to the John Hopkins University and International Consortium of Brain Mapping (JHUICBM) atlases of human white matter anatomy (*23*).

5 Preliminary Results

5.1 Global Fractal Dimension

Voxel-wise FD values (Figure 1)were calculated for each voxel in the brain of the patient and averaged for the gray matter. The rs-BOLD signal has been associated with post-synaptic potentials, which are mainly localized in gray matter as opposed to action potentials more common in the white matter. Similarly, mean FD in the gray matter was calculated for the healthy controls. The mean gray matter FD for the CFS patient was 1.58 ± 0.25 while the mean gray matter FD for controls was 1.62 ± 0.04. We performed a Crawford-Howell t-test commonly used between single cases and normative groups of controls. We found t and p values of -0.75 and 0.45 respectively which implies there is not significant difference between these two values.

5.2 FD Z-score and ROI analysis

A voxel-wise FD Z-score map was calculated for the patient on the 240 defined regions. Ten regions that deviated the most from the control group mean were extracted. Table1 and Table2 show mean Z-score, and p values calculated for those regions of interest that deviated greatest from control mean values. To achieve a p value of 0.95 the Z score must be above 1.96. Therefore the only region where FD significantly decreased in this patient was the posterior commisure and this only occurred on Trial 2 (3 months re-scanning)(Table2). rs-BOLD signal complexity in the posterior commisure significantly decreased in Trial two. The posterior comissure is a white matter structure completely surrounded by gray matter. We suspect that this result was caused by a misregistration of the gray matter map and that the region we are

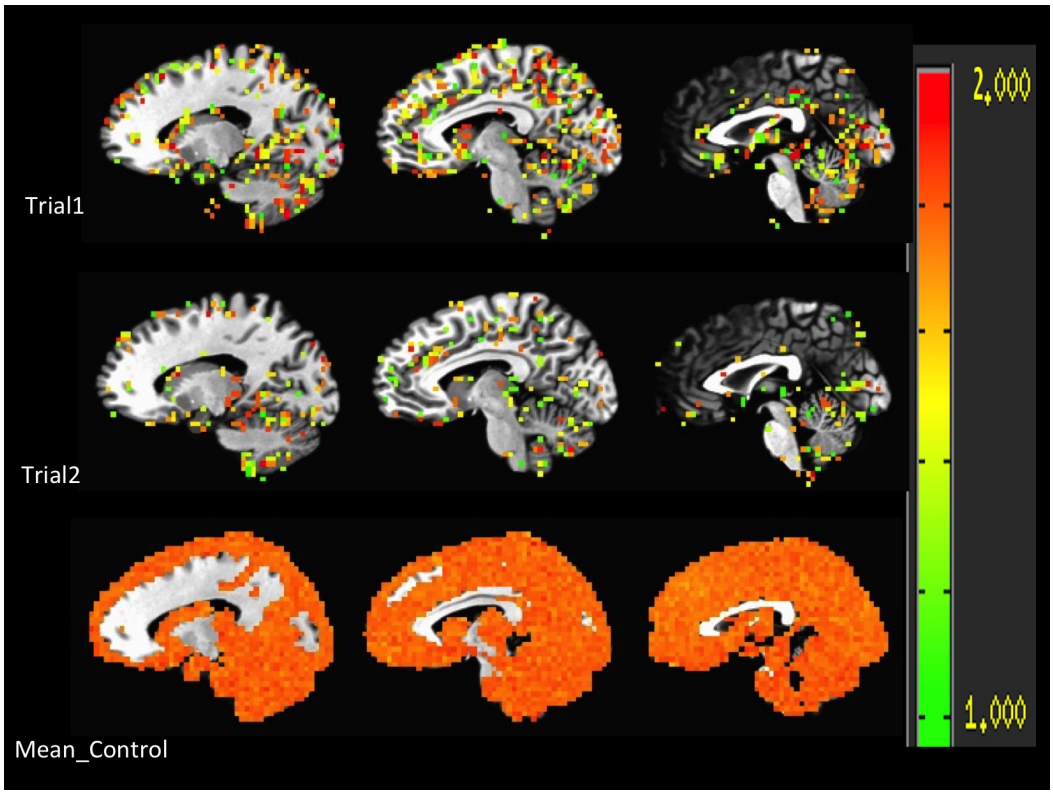

Figure 1: FD maps for Trial 1 and Trial 2 compared to healthy controls. The gray matter mask for the mean FD in healthy controls was done using a probability distribution atlas while the gray matter for patients was done using a segmentation tool from fsl (fast)

actually detecting is the culmen of vermis. Reduced FD in this region translates into reduction in local neural activity.

5.3 DTI Z-score and ROI analysis

Voxel-wise FA, MD, AD and RD Z-score maps were calculated for the patient on the 48 white matter tract labels from the JHUICBM atlas. Table 3 shows mean Z-score, and p values calculated for those regions on both trials. Although no significant differences between the patient and healthy controls were found in Trial 2, we found a statistically significant increase in MD

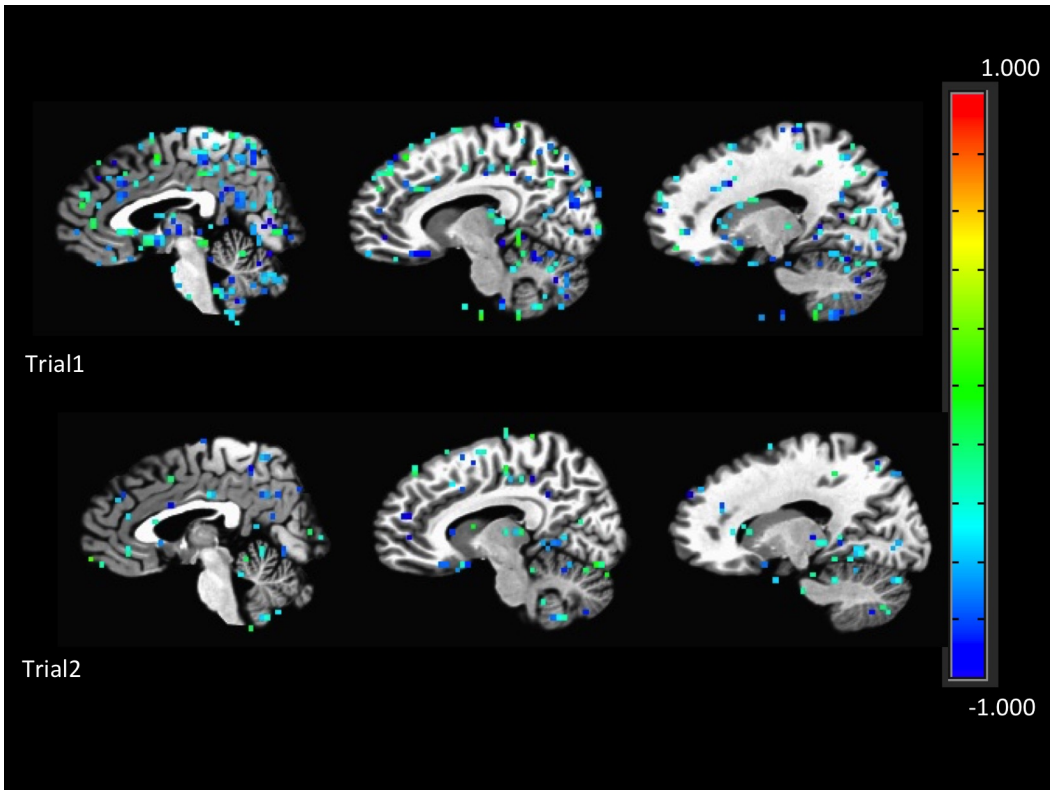

Figure 2: Z-score maps for Trial 1 and Trail 2 over gray matter mask was used to calculate the regions that significantly deviated $(p < 0.05)$ from the mean FD. Scale was normalized(1,-1)

in the bilateral cingulum cingulate gyrus on Trail 1. MD is sensitive to axonal diameter and integrity, as well as myelination *(20, 21)*. Increased MD in the cingulum cingulate Gyrus of the CFS patient when compared to healthy controls, could suggest increased axonal diameter and axonal demyelination, which could also be reflective of localized swelling.

6 Discussion

In this case report study of a CFS patient, we did not find significant differences in global neuronal activity based on the fractal analysis of the BOLD signal. We evaluated FD for the whole brain gray matter as well as for 240 regions of interests and we only found a significant

Table 1: **Trial 1. Mean Z-score and p-value for ROI FD values that deviated greatest from healthy controls.**

ROIs	**Z − Score**	p
Right Caudate	-0.78	0.43
Left Hippocampus	-0.78	0.43
Left Brodmann area 34	-0.79	0.43
Right Brodmann area 36	-0.86	0.39
Left Brodmann area 36	-0.88	0.38
Right Caudate Head	-0.90	0.37
Left Amygdala	-0.92	0.36
Right Hippocampus	-0.95	0.34
Left Brodmann area 27	-0.97	0.33
Left Uvula of Vermis	-1.08	0.28

Table 2: **Trial 2. Mean Z-score and p-value for ROI FD values that deviated greatest from healthy controls.**

ROIs	**Z − Score**	p
Right Caudate	-0.17	0.87
Left Uvula of Vermis	-0.18	0.86
Right Uvula of Vermis	-0.19	0.85
Right Declive of Vermis	-0.25	0.80
Right Brodmann area 28	-0.28	0.78
Right Caudate Head	-0.33	0.74
Left Lateral Dorsal Nucleus	-0.34	0.73
Right Lateral Dorsal Nucleus	-0.39	0.69
Right Cerebellar Lingual	-0.40	0.68
Posterior Commissure	**-2.31**	**0.02**

difference (p¡0.05) in the posterior commissure (cerebellar vermis) on Trial 2. The cerebellar vermis is a region of the cerebellum and lesions on this region are commonly associated to clinical depression (*24, 25*). A recent study by Roelcke et al. (*26*) used 18F-Positron Emission Tomography (PET) to study fatigue in Multiple Sclerosis(MS) patients. Patients who suffer poliomyelitis or MS commonly experience weakness and fatigue (*27, 28*). MS patients showing fatigue symptoms showed elevated glucose metabolism in the anterior cingulate and the cerebellar vermis compared to non fatigue MS patients. The authors concluded that abnormal

Table 3: Mean Z-score and p-values for ROI DTI values in Trial 1 and Trial 2. Statistically significant values are highlighted in red

ROI		Trial 1		Trial 2		ROI		Trial 1		Trial 2	
		Z-score	p	Z-score	p			Z-score	p	Z-score	p
Anterior Thalamic L	FA	0.09	0.47	-0.09	0.54	Inferior Fronto Occipital Fasciculus L	FA	0.08	0.47	-0.17	0.57
	MD	-0.16	0.56	0.08	0.47		MD	0.87	0.19	0.47	0.32
	AD	-0.24	0.59	0.01	0.50		AD	0.91	0.18	0.78	0.22
	RD	-0.24	0.59	-0.03	0.51		RD	0.60	0.27	0.68	0.25
Anterior Thalamic R	FA	-0.15	0.56	-0.01	0.50	Inferior Fronto Occipital Fasciculus R	FA	-0.07	0.53	-0.05	0.52
	MD	0.09	0.46	0.17	0.43		MD	0.63	0.27	0.37	0.35
	AD	0.05	0.48	0.13	0.45		AD	0.60	0.28	0.40	0.34
	RD	0.04	0.48	0.10	0.46		RD	0.43	0.33	0.34	0.37
Cingulum Cingulate Gyrus L	FA	0.17	0.43	-0.04	0.52	Inferior Longitudinal Fasciculus L	FA	-0.14	0.56	-0.26	0.60
	MD	2.30	0.01	1.53	0.06		MD	0.63	0.26	0.47	0.32
	AD	1.12	0.13	1.10	0.14		AD	0.51	0.31	0.49	0.31
	RD	0.47	0.32	0.65	0.26		RD	0.35	0.36	0.35	0.36
Cingulum Cingulate Gyrus R	FA	-0.35	0.64	-0.30	0.62	Inferior Longitudinal Fasciculus R	FA	-0.16	0.56	-0.18	0.57
	MD	1.71	0.04	1.35	0.09		MD	0.96	0.17	0.69	0.24
	AD	1.43	0.08	1.60	0.05		AD	0.76	0.22	0.72	0.24
	RD	0.73	0.23	0.98	0.16		RD	0.54	0.30	0.57	0.29
Corpus Callosum L	FA	-0.39	0.65	-0.64	0.74	Superior Longitudinal Fasciculus L	FA	-0.12	0.55	-0.32	0.63
	MD	0.70	0.24	0.06	0.48		MD	0.55	0.29	0.44	0.33
	AD	0.80	0.21	0.39	0.35		AD	0.14	0.44	0.35	0.36
	RD	0.49	0.31	0.26	0.40		RD	0.03	0.49	0.26	0.40
Corpus Callosum R	FA	0.09	0.46	0.02	0.49	Superior Longitudinal Fasciculus R	FA	-0.27	0.61	-0.36	0.64
	MD	0.89	0.19	0.36	0.36		MD	0.69	0.24	0.70	0.24
	AD	0.66	0.25	0.27	0.39		AD	0.34	0.37	0.49	0.31
	RD	0.73	0.23	0.41	0.34		RD	0.26	0.40	0.42	0.34
Corticospinal Tract L	FA	0.17	0.43	0.18	0.43	Sup. Long. Fasciculus Temporal Part L	FA	0.09	0.47	-0.16	0.56
	MD	0.92	0.18	0.84	0.20		MD	0.74	0.23	0.30	0.38
	AD	0.78	0.22	0.69	0.25		AD	0.03	0.49	0.18	0.43
	RD	0.71	0.24	0.64	0.26		RD	-0.20	0.58	0.03	0.49
Corticospinal Tract R	FA	0.16	0.44	0.18	0.43	Sup. Long. Fasciculus Temporal Part R	FA	-0.27	0.61	-0.37	0.64
	MD	1.15	0.13	1.22	0.11		MD	0.51	0.30	0.78	0.22
	AD	1.05	0.15	1.21	0.11		AD	0.22	0.41	0.69	0.24
	RD	0.91	0.18	1.08	0.14		RD	0.14	0.44	0.50	0.31
Forceps Major	FA	0.21	0.42	0.27	0.40	Uncinate Fasciculus L	FA	0.03	0.49	-0.19	0.57
	MD	1.11	0.13	0.21	0.42		MD	0.77	0.22	1.02	0.15
	AD	0.70	0.24	-0.07	0.53		AD	0.61	0.27	0.94	0.17
	RD	0.19	0.42	-0.28	0.61		RD	0.44	0.33	0.69	0.25
Forceps Minor	FA	-0.10	0.54	-0.33	0.63	Uncinate Fasciculus R	FA	-0.03	0.51	-0.17	0.57
	MD	1.04	0.15	1.16	0.12		MD	0.66	0.25	1.00	0.16
	AD	0.95	0.17	1.29	0.10		AD	0.49	0.31	0.97	0.17
	RD	0.84	0.20	1.21	0.11		RD	0.46	0.32	0.90	0.18

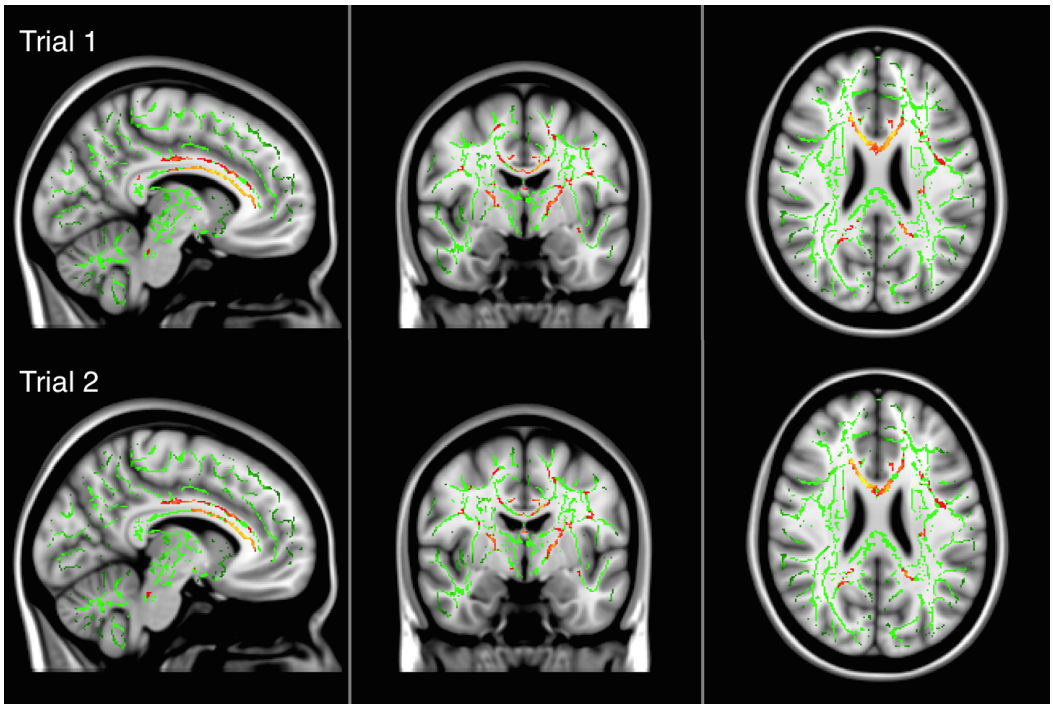

Figure 3: DTI TBSS results shown on a standard MNI 1mm anatomical overlay. The green underlay is the mean FA skeleton across the two CFS patient trials and healthy controls. Red-yellow shading indicates regions where the CFS patient had significantly higher measures of MD than the control populous ($p < 0.05$). Brighter areas indicate more significant correlation. Results for both trials are shown. Fewer regions of significant difference are observed in the trial 2 image in deep brain structures.

cerebral activity in the basal ganglia and prefrontal regions can be associated with fatigue in persons with MS. Additionally, another study by Cook et al. (*29*) used task-based fMRI to explore the relationship between fatigue and functional brain activity in CFS patients. They found that reports of fatigue after task performance correlated positively with brain activity in the cerebellar vermis among other regions. The absence of other regions were FD significantly decreased in the gray suggested that the the symptoms experienced by this patient could potentially be related to changes mainly occurring in the white matter. In this study, structural connectivity in the white matter was evaluated in 48 white matter tracts of the brain. We found significantly in-

creased MD in the bilateral cingulum cingulate gyrus tract (p¡0.05) which suggests local axonal demyelination, and localized swelling.

Previous studies have shown a connection between the cingulate gyrus and CFS. For instance, a study by Yamamoto et al. (*30*) assessed involvement of serotonergic neurotransmitters in CFS using 11C-PET . They found that the density of serotonergic neurotransmitters (5-HTTs) in the CFS brain, was significantly reduced in the anterior cingulate compared healthy controls. A similar study by Siessmeier et al. (*31*) evaluated glucose metabolism with 18F-PET in CFS patients compared to controls. The study showed hypometabolism bilaterally in the cingulate gyrus on CFS patients. Additionally , a study by Lutz et al. (*32*) explored the microstructural changes of patients with fibromyalgia using DTI. Fibromyalgia is closely related to chronic fatigue syndrome, however pain is more predominant than in chronic fatigue syndrome. This study reported increased FA in the cingulate gyrus and positive correlation was found with fatigue symptoms.

7 Conclusions

This preliminary study study shows how the fractal dimension analysis in combination with a DTI analysis can to provide additional patient-specific information respect to brain functional and structural connectivity. Fatigue symptoms experienced by CFS patients appears to be related to abnormalities in the white matter tracts possibly arising from inflammatory processes that caused demyelination of the axons. This was reflected by the FA decrease detected on the bilateral cingulum cingulate gyrus. Since no significant difference was found in the fractal analysis of the rs-BOLD signal, we could say that this patient could benefit the most from therapies that target inflammation of the white matter. This new methodology we have proposed combining the analysis of functional and anatomical connectivity is able to provide additional information for CFS patients in a non-invasive and fast manner and could hopefully help in

deciding whether a patient could benefit from specific White matter targeted treatments and interventional techniques.

References and Notes

1. N. Afari, D. Buchwald, *American Journal of Psychiatry* **160**, 221 (2003).
2. B. K. Puri, *et al.*, *The British journal of radiology* **85**, e270 (2012).
3. R. Perrin, K. Embleton, V. W. Pentreath, A. Jackson, *The British journal of radiology* **83**, 419 (2010).
4. M. M. Zeineh, *et al.*, *Radiology* **274**, 517 (2015).
5. L. A. Wortinger, *et al.*, *PloS one* **11**, e0159351 (2016).
6. R. W. Cox, *Computers and biomedical research, an international journal* **29**, 162 (1996).
7. M. W. Woolrich, *et al.*, *NeuroImage* **45**, S173 (2009).
8. A. Eke, *et al.*, *Pflugers Archiv : European journal of physiology* **439**, 403 (2000).
9. M. D. Fox, M. E. Raichle, *Nature reviews. Neuroscience* **8**, 700 (2007).
10. E. Zarahn, G. K. Aguirre, M. D'Esposito, *NeuroImage* **5**, 179 (1997).
11. S. El Boustani, *et al.*, *PLoS computational biology* **5**, e1000519 (2009).
12. P. Herman, B. G. Sanganahalli, F. Hyder, A. Eke, *NeuroImage* **58**, 1060 (2011).
13. A. Eke, P. Herman, L. Kocsis, L. R. Kozak, *Physiological measurement* **23**, R1 (2002).
14. E. Bullmore, *et al.*, *NeuroImage* **47**, 1125 (2009).

15. M. Warsi, A. Weber, M. Noseworthy, *Visualization, Image Processing and Computation in Biomedicine* **2** (2013).

16. V. Maxim, *et al.*, *NeuroImage* **25**, 141 (2005).

17. O. Dona, M. Noseworthy, C. DeMatteo, J. Connolly, *PLoS ONE* **12**, e0169647 (2017).

18. A. M. Weber, N. Soreni, M. D. Noseworthy, *Magma (New York, N.Y.)* **27**, 291 (2014).

19. M. E. Shenton, *et al.*, *Brain imaging and behavior* **6**, 137 (2012).

20. S. D. Roosendaal, *et al.*, *NeuroImage* **44**, 1397 (2009).

21. S.-K. Song, *et al.*, *NeuroImage* **26**, 132 (2005).

22. Z. K. Eickhoff S, Stephan KE, Mohlberg H, Grefkes C, Fink GR, Amunts K, *NeuroImage* **25**, 1325 (2005).

23. S. Wakana, H. Jiang, L. M. Nagae-Poetscher, P. C. M. van Zijl, S. Mori, *Radiology* **230**, 77 (2004).

24. J. A. Sweeney, M. H. Strojwas, J. J. Mann, M. E. Thase, *Biological psychiatry* **43**, 584 (1998).

25. J. D. Schmahmann, *The Journal of neuropsychiatry and clinical neurosciences* **16**, 367 (2004).

26. U. Roelcke, *et al.*, *Neurology* **48**, 1566 (1997).

27. R. L. Bruno, R. Sapolsky, J. R. Zimmerman, N. M. Frick, *Annals of the New York Academy of Sciences* **753**, 257 (1995).

28. D. S. Reich, *et al.*, *AJNR. American journal of neuroradiology* **29**, 333 (2008).

29. D. B. Cook, P. J. OConnor, G. Lange, J. Steffener, *NeuroImage* **36**, 108 (2007).

30. S. Yamamoto, *et al.*, *Neuroreport* **15**, 2571 (2004).

31. T. Siessmeier, *et al.*, *Journal of Neurology, Neurosurgery & Psychiatry* **74**, 922 (2003).

32. J. Lutz, *et al.*, *Arthritis & Rheumatism* **58**, 3960 (2008).

Chapter 8

Conclusions and Future Directions

8.1 General remarks

A complexity analysis based on the fractal dimension of the brain rs-BOLD signal appears to provide additional information regarding neural activity that can be used to assess and possibly monitor a spectrum of brain disorders. Brain connectivity is best described as a multilevel model that takes into account three distinctive levels of interaction: synaptic connections that link independent neurons, networks that connect local neuronal populations and broader brain regions linked by fiber pathways. A measure of complexity of this model constitutes an ideal indicator of multilevel and multitemporal connectivity within different brain regions. Tentatively, a healthy brain is associated with more complex signals and high FD, while a diseased or dysfunctional brain is associated with less complex signals and low FD. The capacity of the brain to perform real-time adaptation and processing based on these connections is reflected in the local demand of glucose and oxygen consumption, which drives the brain metabolic fluctuation observed in the rs-BOLD signal and its fractal dimension.

Estimation of the fractal dimension, when normalized for a large control group, can be used in the study of individual patients. As it is independent of group statistics, the FD methodology is applicable when heterogeneous brain disorders are being investigated. In this study, applicability of the FD methodology was explored in mTBI, ASD, CFS and chemo-brain and significant differences in FD between diseased and healthy control were encountered with higher prevalence among the mTBI and ASD groups.

8.2 Main findings

The fractal dimension maps produced for mTBI showed that overall, gray matter rs-BOLD FD in mTBI patients decreased compared to controls. This reduction in temporal complexity of the rs-BOLD leading us to our hypothesis that patients with mTBI experience a decrease in brain connectivity and that this could be observed with the FD approach. Z-score and subsequent regional ROI analysis revealed a group of brain regions where FD values were observed to deviate the greatest from mean values, as calculated from a population of healthy controls. The regions that showed significant decreased in signal complexity were the amygdala, the cerebellar vermis, caudate nucleus, nucleus accumbens and hippopotamus. All of these regions have been previously reported as dysfunctional for mTBI in animal studies, DTI and SWI human studies. These regions also functionally correlate with symptoms of memory loss, concentration and sleep impairment experienced by mTBI patients. No significant correlation was found between regional FD and the PCSS score. The PCSS does not characterize symptoms associated with unique brain regions. Still, PCSS is the most common test used clinically to characterize mTBI. This study highlighted the

issues related with the use of a self-reported metric while trying to characterize a complex phenomenon. Neuropsychological tests specifically designed to measure a psychological function related to a particular brain structure or pathway would be of greater interest for future studies.

When applying fractal analysis to ASD, we found reduced signal complexity in the ASD patients compared to controls. Out of 250 regions, 14 regions showed significantly low FD in 19 of the 50 studied subjects. Positive Z-scores or regions where FD increased compared to controls were minimal in every patient and in none of the ASD subjects we found a FD value of at least one standard deviation above the mean. This indicated that there were no regions where signal complexity significantly increased with respect to controls among the ASD patients. The regions that showed significant decrease in signal complexity in ASD respect to controls were the amygdala, nucleus accumbens, cerebellar vermis and caudate head. These regions have been previously reported as dysfunctional in ASD and have been correlated to behavioral features of the patients. Additionally, the FD in the cerebellar vermis correlated with the ADI and ADOS restricted repetitive behavior metrics, hence, when severity of the symptoms increased in those domains, the FD and signal complexity decreased.

Regarding the study on chemo-brain patients, no significant changes were found in the FD of the rs-BOLD signal compared to healthy controls. In this case, FD changes in gray matter were either below our detection limit or non existent. However, this study showed that integrity of the white matter tracts, evaluated with DTI measures (e.g.FA), was significantly lower in chemo-brain patients when compared with healthy controls. Three regions (corpus callosum, inferior fronto-occipital fasciculus and right inferior longitudinal fasciculus) were identified as common among all patients independently

of age while three more regions were exclusively detected on older (above 70 years old) patients (bilateral uncinate fasciculus and superior longitudinal fasciculus temporal). Decreased FA in the corpus callosum, inferior fronto-occipital fasciculus and right inferior longitudinal fasciculus correlated with the Rey Complex copy trial and the recognition trial which measure visuospatial memory and visuospatial constructional ability. Furthermore, a strong correlation was found between the cognitive failure questionnaire and reduced FA in the inferior fronto-occipital fasciculus.

With reference to the study on CFS, we did not find significant differences in global neuronal activity based on the fractal analysis of the BOLD signal. We evaluated FD for the whole brain gray matter as well as for 240 regions of interests and we only found a significant difference in the cerebellar vermis on Trial 2 (three months after first scan). The absence of other regions where FD significantly decreased in the gray matter suggested that the the symptoms experienced by this patient could potentially be related to changes mainly occurring in the white matter. Structural connectivity in the white matter was evaluated in 48 white matter tracts of the brain and it was found that mean difussivity significantly increased in the bilateral cingulum cingulate gyrus tract which suggested local axonal demyelination, and localized swelling.

8.3 Limitations

The main limitation of the FD analysis arises from the low sampling frequency that can be achieved when measuring the rs-BOLD signal. The effectiveness of the fractal analysis is based on the ability of the signal to capture the true dynamics of the processes being studied. Ideally the sampling frequency should be one order of magnitude higher than the highest frequency of the hemodynamic response to

neuronal activation. For example, the BOLD responses are delayed by $1-2$ s and have a temporal width on the order of 46 s, therefore we need to be able to sample the signal at 1.25 Hz. In order to acquire the rs-BOLD signal for the entire brain in a reasonable time for the patients we were only able to sample at a frequency of 0.5 Hz which significantly limited the scope of our study. New techniques such as multi-band EPI can perhaps be ideal to overcome this issue as they are able to achieve full brain sampling rates up to 2.5 Hz.

8.4 Contribution and future directions

To the best of our knowledge, we believe that fractal analyses of rs-BOLD signal have not been applied previously in the study of mTBI, ASD, chemo-brain or CFS. Furthermore, a Z-score methodology has not been previously used to normalize the FD to a large healthy control dataset. Although fractal analysis of brain signals has been done in Alzheimer's disease and vascular dementia and acquired through different imaging modalities such as EEG, MEG and SPECT, few studies have performed fractal analysis specifically on brain rs-BOLD signals. This work is a continuation of previous studies performed at the Imaging Research Centre where FD was explored as a viable technique to assess complexity of the rs-BOLD signal in AD and in brain alcohol intoxication.

In this study, we complemented the fractal analysis of the rs-BOLD signal with DTI to obtain information of the white matter integrity. In the future, we would like to explore the viability of a fractal analysis directly on the white matter. The two main reasons why white matter is excluded from fMRI BOLD studies are that first, the BOLD signal depends on cerebral blood flow and volume, which are lower

in white matter than gray matter. Second, the BOLD signal has been associated with post-synaptic potentials, which are more common in gray matter as opposed to action potentials which are more predominant in white matter. Regardless of these two reasons, which are not a direct evidence against measuring BOLD signal in white matter, many studies frequently report activation in white matter, predominately in the corpus callosum.

Additionally, we would like to combine in future studies the highly spatially-resolved MRI BOLD signal with highly temporally-resolved signals as EEG and NIR. This will enable FD measurements to more precisely capture the dynamics of the processes that occur at lower scales of fractals.

8.5 Concluding statement

Fractals, a quantitative measure of complexity, have enabled a new perspective in studying the human brain. Brain connectivity is best described as a complex system due to the many levels of interactions that take place among independent neurons, neuronal populations and brain regions. Including fractals in the analysis of the brain signals may be critical for understanding neuronal behavior in response to different perturbations that occur at different time scales. It is our hope that this method sparks new interest in the scientific community and that future applications can lead to better diagnosis and monitoring of neurological conditions and ultimately their cure.

Appendix A

Summary of publications, journals, conference proceedings and Code

A.1 Journal articles

1. (2017). Temporal Fractal Analysis Identifies Brain Abnormalities in Autism Spectrum Disorder. Nature Scientific Reports. First Listed Author Submitted, AAAS, Refereed?: Yes, Open Access?: Yes

2. (2016). Fractal Analysis of Brain Blood Oxygenation Level Dependent (BOLD) Signals from Children With mild Traumatic Brain Injury. PLOS-ONE. First Listed Author Published, PLOSONE, Refereed?: Yes, Open Access?: Yes Number of Contributors: 4

3. (2016). A Comprehensive Review on MR Imaging of Alzheimer's Disease. Critical Reviews in Biomedical Engineering. First Listed Author Published, Bagel House, Refereed?: Yes Number of Contributors: 3

4. (2017). Fractal analysis of the blood oxygenation level dependent (BOLD) signal

and DTI analysis of white matter micro-structure in cancer patients experiencing chemotherapy-related cognitive impairment. First Listed Author Submitted, Clinical Cancer Research AACR, Refereed?: Yes Number of Contributors: 5

5. (2017). Case Report: Voxel-wise DTI and Fractal Analysis in a Chronic Fatigue Syndrome Patient. First Listed Author Submission pending, TBD, Refereed?: Yes Number of Contributors: 5

A.2 Conference proceedings

1. Fractal Analysis of the rs-BOLD signal in mTBI patients. ESMRMB, Vienna, Austria, Conference Date: 2016/9 Abstract First Listed Author Refereed?: Yes

2. Fractal Analysis of the brain blood oxygenation level dependent (BOLD) signal of mild traumatic brain injury (mTBI) patients. . COMP-OCPM ASM, Saint John's, Canada, Conference Date: 2016/7 Abstract First Listed Author Refereed?: Yes

3. Fractal Analysis of the brain blood oxygenation level dependent (BOLD) signal of mild traumatic brain injury (mTBI) patients. Conference Date: 2016/2 Abstract First Listed Author Refereed?: Yes

4. Fractal analysis of the brain blood oxygenation level dependent (BOLD) signal in the left putamen of mild traumatic brain injury (mTBI) patients. ISMRM-2016, Toronto, Canada (4047), Conference Date: 2015/5 Abstract First Listed Author Refereed?: Yes

A.3 Matlab code for Hurst, FD and Z-score methods

A.3.1 Hurst exponent

```
function [H, RSquare] = HurstOlga(rawBOLD, TR)
% This function will analyze an ROI timecourse and output the appropriate
% Hurst exponent according to the procedure of Eke et al. (Eur J Physiol
% (2000) 439:403?415)
% Olga Dona (2016/02/20), Saurabh Shaw(2015), Mohamed A. Warsi(2012), Alex
Weber(2012), Alya Elzybaak(2011), Evan McNabb(2013), Michael Noseworthy.


% Initialziation:
Hurst = NaN;
Hurst_SSC_fGN_Dispersion = NaN;
Hurst_SSC_fBM_SWV = NaN;
H = NaN;
abort = false;
% Common parameters:
fs = 1/TR;   % Sampling frequency
n = length(rawBOLD);  % Number of timepoints

% Normalizing the time series:
m1 = mean(rawBOLD);
rawBOLD_sub = rawBOLD - m1;

% Multiply each new value by parabolic window
N = length(rawBOLD_sub);
W = zeros(N, 1);
for j = 1:N
   W(j) = 1 - (2*j/(N+1)-1).^2;    % parabolic window
end
signal_pw = rawBOLD_sub.*W;

% Matching the ends:
y11 = signal_pw(1); y21 = signal_pw(end);
slope1 = (y21-y11)/(N-1);
y_int1 = y21 - slope1*N;
line = 1:N;
E1 = slope1 * line + y_int1;

% Bridge detrend:
signal_em1 = signal_pw - E1';
range = ceil((N+1) / 2);
freq = [fs * (0 : range-1) / N]';

% plot log (power) vs. log(frequency) --> make sure this is linear over a
% 2-decade range otherwise signal can't be analyzed using fractals

fftSignal1 = fft(signal_em1,N);
```

```
fftSignal1 = fftSignal1(1:range);  % 1st half of fft since it's symmetric
PSD1 = (abs(fftSignal1).^2)/N;

if rem(N,2)
   PSD1(2:end)=PSD1(2:end)*2;
else
   PSD1(2:end-1)=PSD1(2:end-1)*2;
end
[min_value1, min_index1] = min(abs(freq - 0.08));
[min_value2, min_index2] = min(abs(freq - 0.16));
 PSDpart = PSD1(min_index1 : min_index2);  % fit only low frequencies for the fit (0.08
Hz - 0.16 Hz). This is to exculde random white noise at higher frequencies and magnet
noise below 0.02 Hz
 freqpart = freq(min_index1 : min_index2);

logPSD = log10(PSDpart);
logfreq = log10(freqpart);

% Removing all the Inf values:
nu = ~isinf(logPSD) & ~isinf(logfreq);
logPSD_c = logPSD(nu);
logfreq_c = logfreq(nu);

if (~isempty(logPSD_c) && ~isempty(logfreq_c))
   fit_opts = fitoptions('Method', 'LinearLeastSquares', 'Robust', 'off');
   [fits_result, fit_goodness] = fit(logfreq_c, logPSD_c, 'poly1', fit_opts);

   % Beta is the negative of the slope of the fitted line:
   Beta = -1 * fits_result(1);
   RSquare_Beta = fit_goodness.rsquare;
else
   % Voxel lies outside the brain, disregard it.
   abort = true;
   Beta = 0;
   Hurst = NaN;
   Hurst_SSC_fGN_Dispersion = NaN;
   Hurst_SSC_fBM_SWV = NaN;
   return
end

% Analysis if signal is fractional Gaussian Noise (fGn)
if((Beta > -1 && Beta < 0.38) && ~abort)

   Hurst_PSD_fGn = (Beta + 1) / 2;   %This method of calculating H (from slope of line)
is not as accurate (according to Eke) as doing the dispersional analysis, so use H from
dispersional analysis
```

```
    % Dispersional analysis to get H for fGn signals:
    maxBins = nextpow2(length(rawBOLD)) - 1;
    signal_2 = rawBOLD(1 : 2^maxBins);

    DISP = zeros(maxBins, 1);
    tau = zeros(maxBins, 1);

    for i = 1 : maxBins
       m = 2^i;
       signal_binned = reshape(signal_2, [m, (length(signal_2)/m)]);

       mean_binned = mean(signal_binned);
       DISP(i) = std(mean_binned);
       tau(i) = m;
       if(DISP(i) == 0)
          DISP(i) = 0.0001;
       end
    end

    logDISP = log10(DISP(3:7));
    logtau = log10(tau(3:7));

    fit_opts = fitoptions('Method', 'LinearLeastSquares', 'Robust', 'off');
    [fits_result, fit_goodness] = fit(logtau, logDISP, 'poly1', fit_opts);

    Hurst_fGn_Dispersion = fits_result.p1 + 1;
    RSquare = fit_goodness.rsquare;
    H = Hurst_PSD_fGn;

 % Analysis if signal is fractional Brownian motion (fBm)
 elseif((Beta > 1.04 && Beta < 3) && ~abort)

    Hurst_PSD_fBm = (Beta - 1) / 2;

    %Bridge detrended SWV to get H for fBm signals
    %Recall: signal_em1 is the original bridge detrended data
    maxBins = nextpow2(length(rawBOLD)) - 1;
    signal_2 = signal_em1(1 : 2^maxBins);

    SWV = zeros(maxBins, 1);
    tau = zeros(maxBins, 1);

    for i = 1 : maxBins
       m = 2^i;
       signal_binned = reshape(signal_2, [m, (length(signal_2)/m)]);
```

```
    std_binned = std(signal_binned);
    SWV(i) = mean(std_binned);
    tau(i) = m;
  end

  logSWV = log10(SWV(3:7));
  logtau = log10(tau(3:7));

  fit_opts = fitoptions('Method', 'LinearLeastSquares', 'Robust', 'off');
  [fits_result, fit_goodness] = fit(logtau, logSWV, 'poly1', fit_opts);

  Hurst_fBm_SWV = fits_result.p1;
  RSquare = fit_goodness.rsquare;
  H = Hurst_PSD_fBm;
% Signal summation conversion for signals that fall in the non-classifiable region
elseif((Beta >= 0.38 && Beta <= 1.04) && ~abort)

  Y = zeros(size(rawBOLD));

  for j = 1:length(Y)
    temp = 0;

    for i = 1:j
      temp = temp + rawBOLD(i);
    end

    Y(j) = temp;
  end


  % Run SWV to get Hurst exponent:
  maxBins = nextpow2(length(rawBOLD)) - 1;
  signal_2 = signal_em1(1 : 2^maxBins);

  SWV = zeros(maxBins, 1);
  tau = zeros(maxBins, 1);

  for i = 1 : maxBins
    m = 2^i;
    signal_binned = reshape(signal_2, [m, (length(signal_2)/m)]);

    std_binned = std(signal_binned);
    SWV(i) = mean(std_binned);
    tau(i) = m;
  end
```

```
logSWV = log10(SWV(3:7));
logtau = log10(tau(3:7));

fit_opts = fitoptions('Method', 'LinearLeastSquares', 'Robust', 'off');
[fits_result, fit_goodness] = fit(logtau, logSWV, 'poly1', fit_opts);

Hurst= fits_result.p1;
Stats_RSquare = fit_goodness.rsquare;

if(Hurst < 0.8)
   % The signal is an fGn signal, so can do dispersion analysis on it
   % to get final Hurst

   maxBins = nextpow2(length(rawBOLD)) - 1;
   signal_2 = rawBOLD(1 : 2^maxBins);

   DISP = zeros(maxBins, 1);
   tau = zeros(maxBins, 1);

   for i = 1 : maxBins
      m = 2^i;
      signal_binned = reshape(signal_2, [m, (length(signal_2)/m)]);

      mean_binned = mean(signal_binned);
      DISP(i) = std(mean_binned);
      tau(i) = m;
      if(DISP(i) == 0)
         DISP(i) = 0.0001;
      end
   end

   logDISP = log10(DISP(3:7));
   logtau = log10(tau(3:7));

   fit_opts = fitoptions('Method', 'LinearLeastSquares', 'Robust', 'off');
   [fits_result, fit_goodness] = fit(logtau, logDISP, 'poly1', fit_opts);

   Hurst_SSC_fGN_Dispersion = fits_result.p1 + 1;
   RSquare = fit_goodness.rsquare;
   H = Hurst_SSC_fGN_Dispersion;
elseif(Hurst > 1)
   %The signal is an fBm signal, so can do SWV analysis on it to get
   %final Hurst

   maxBins = nextpow2(length(rawBOLD)) - 1;
```

```
        signal_3 = signal_em1(1 : 2^maxBins);

        SWV1 = zeros(maxBins, 1);
        tau1 = zeros(maxBins, 1);

        for v = 1 : maxBins
            mm = 2^v;
            signal_bin = reshape(signal_3, [mm, (length(signal_3)/mm)]);

            std_bin = std(signal_bin);
            SWV1(i) = mean(std_bin);
            tau1(i) = mm;
        end

        logSWV1 = log10(SWV1(3:7));
        logtau1 = log10(tau1(3:7));

        fit_opts = fitoptions('Method', 'LinearLeastSquares', 'Robust', 'off');
        [fits_result, fit_goodness] = fit(logtau1, logSWV1, 'poly1', fit_opts);

        Hurst_SSC_fBM_SWV= fits_result.p1;
        RSquare = fit_goodness.rsquare;
        H = Hurst_SSC_fBM_SWV;
    else
        % If H is not less than 0.8 or larger than 1, then it can't be
        % classified
        H = NaN;
    end
end
```

A.3.2 FD

```
%matlabpool close
matlabpool open

% Parameters:
TR = 2.0; % TR = 2600ms was used

% Load Data
%anatomical = load_nii('1399_anat_ns.nii');
functional = load_nii('363func_ALIGNED.nii');
[N1,N2,N3,NT] = size(functional.img);

% Fractal Dimension per voxel
Hurst = zeros(N1,N2,N3);
Hurst_fGN = zeros(N1,N2,N3);
Hurst_fBM = zeros(N1,N2,N3);
FD = zeros(N1,N2,N3);
FDstd = FD;
method = 'fgm';
parfor i = 1:N1
   tic
   for j = 1:N2
      for k = 1:N3
          if sum(abs(squeeze(functional.img(i,j,k,:))))>0
             [FD{i,j,k} FD2{i,j,k}] = fractaldim(squeeze(functional.img(i,j,k,:)),0,3);
          end
         rawBOLD = double(squeeze(functional.img(i,j,k,:)));
         [Hurst(i,j,k),Hurst_fGN(i,j,k),Hurst_fBM(i,j,k)] = HurstOlga(rawBOLD,TR);

      end
   end
   fprintf('Loop [%g/%g]... %g s\n',i,N1,toc);
end
FD(isnan(FD)) = 0;
FD(FD==0) = 1/2;

Hurst(isnan(Hurst)) = 0;
Hurst(Hurst==0) = 1/2;
```

A.3.3 Z-score

```
clear;
%setenv('PATH', [getenv('PATH'), ':/Users/omdona/abin'])
Deceased_numbers = {'5558','5771','5904'}%
%Controls =
{'0050327','0050328','0050329','0050330','0050331','0050332','0050333','0050334','0050
335','0050336','0050337','0050338','0050339','0050340','0050341','0050342','0050343','00
50344','0050346','0050347','0050348','0050349','0050350','0050351','0050352','0050353','
0050354','0050355','0050356','0050357','0050358','0050359','0050360','0050361','005036
2','0050363','0050364','0050365','0050367','0050368','0050369','0050370','0050371','0050
372','0050373','0050374','0050375','0050376','0050377','0050378','0050379','0050380','00
50381'};%Controls
nExams = length(Deceased_numbers);



current_dir = pwd;
cd(sprintf('Controls_old'));
count = 1;
Controls = {};
dir_list = dir();
num_dir = size(dir_list, 1);
for i = 1 : num_dir

    % Grab the current directory listing
    listing = dir_list(i);
    if(listing.isdir == 1)
        if(~(strcmp(listing.name, '.') || strcmp(listing.name, '..')))
            Controls{count} = listing.name;
            count = count + 1;
        end
    end
end
cd(current_dir)
%% Z-score

for subj = 1:nExams

    Hurst = load(['Patients/exam_',Deceased_numbers{subj},'/FD_Olga.mat'],'Hurst');%
changed FD_masked with FD
    Hurst = Hurst.('Hurst');
    Hurst(Hurst==1/2) = nan;
    FD_Autism = 2 - Hurst;
    FD_Autism(isnan(FD_Autism)) = 0;
    [a, b, c] = size(FD_Autism);
    % if a == 47
    % FD_TBI_resized = FD_TBI;
```

```
% %    FD_TBI_padded = FD_TBI;
% %else FD_TBI_padded = padarray(FD_TBI,[7 8 6],'post');
% else FD_TBI_resized = resize(FD_TBI,[47 56 44]);
%
% end
[mean_FD, std_FD, mask_all] = ControlValues(Controls);

FD_Zmaps = zeros(size(FD_Autism));
for i = 1 : size(FD_Autism, 1)
   for j = 1 : size(FD_Autism, 2)
      for k = 1 : size(FD_Autism, 3)

         % Check two things: 1) FD value exists
         %                   2) mask exists
         current_fd = FD_Autism(i, j, k);
         if(mask_all(i, j, k) == 1 && current_fd >= 1 && current_fd <= 2)
            FD_Zmaps(i, j, k) = (current_fd - mean_FD(i, j, k)) / std_FD(i, j, k);
         end
      end
   end
end
%FD_TBI_masked_all = FD_TBI .* mask_all;
%FD_Zmaps = (FD_TBI_masked_all - mean_FD) ./ std_FD;
[~,GMmask,~,~] =
BrikLoad(['Patients/exam_',Deceased_numbers{subj},'/GM_resampled+tlrc']);
FD_Zmaps_GMmasked = double(GMmask .* FD_Zmaps);

%WRITE BRIK Z_MAPS
[err1,Info] = BrikInfo('FD_Zmaps_1569+tlrc');
bold_mean_wb = FD_Zmaps_GMmasked (:,:,:) ;
%bold_mean_wb = FD_Zmaps(:,:,:) ;
InfoBold.RootName = ''; %that'll get set by WriteBrik
InfoBold.DATASET_RANK(1) = 3; % must be 3 spatial dimensions
InfoBold.DATASET_RANK(2) = 1; % one sub brick
InfoBold.DATASET_DIMENSIONS(1) = 47;%Info.DATASET_DIMENSIONS(1);
InfoBold.DATASET_DIMENSIONS(2) = 56;%Info.DATASET_DIMENSIONS(2);
InfoBold.DATASET_DIMENSIONS(3) = 44; %Info.DATASET_DIMENSIONS(3);
%write out 3 slices
InfoBold.TYPESTRING = '3DIM_HEAD_ANAT';
InfoBold.TypeBytes = 4; % to allow 4 bytes per voxel
InfoBold.SCENE_DATA(1) = Info.SCENE_DATA(2); % value is 0: orig view
InfoBold.SCENE_DATA(2) = Info.SCENE_DATA(1); % value is 2: labels it as EPI
although any type will work
InfoBold.SCENE_DATA(3) = Info.SCENE_DATA(3); % value is 0:
3DIM_HEAD_ANAT
```

```
   InfoBold.ORIENT_SPECIFIC(1) = Info.ORIENT_SPECIFIC(1); % Value is 3: X axis
Ant to Post
   InfoBold.ORIENT_SPECIFIC(2) = Info.ORIENT_SPECIFIC(2); % Value is 0: Y axis
Right to Left
   InfoBold.ORIENT_SPECIFIC(3) = Info.ORIENT_SPECIFIC(3); % Value is 5: Z axis
Sup to Inf
   InfoBold.ORIGIN(1) = Info.ORIGIN(1);
   InfoBold.ORIGIN(2) = Info.ORIGIN(2);
   InfoBold.ORIGIN(3) = Info.ORIGIN(3);
   InfoBold.DELTA(1) = Info.DELTA(1); % Voxel size 3.75 X 3.75 X 5
   InfoBold.DELTA(2) = Info.DELTA(2);
   InfoBold.DELTA(3) = Info.DELTA(3);
   InfoBold.BRICK_TYPES = 3; % 1 store data as shorts, 3 single precision floating
point
   InfoBold.BYTEORDER_STRING = 'MSB_FIRST';
   InfoBold.BRICK_STATS= [min(FD_Zmaps_GMmasked(:)),
max(FD_Zmaps_GMmasked(:))]; %is set by writebrik
   InfoBold.BRICK_FLOAT_FACS = []; %" "
   %InfoBold.TAXIS_NUMS(1) = 1;

   %Define options:

   %OptBold.Prefix = ['FD_Zmaps',Deceased_numbers{subj}];
   OptBold.Prefix = ['FD_Zmaps',Deceased_numbers{subj}];
   OptBold.verbose = 0;
   OptBold.View = '+tlrc' ;
   OptBold.OverWrite = 'y';

   % run the WriteBrik command:
   [err, ErrMessage, InfoBold] = WriteBrik (bold_mean_wb, InfoBold, OptBold);
end
```

```
function [ mean_FD, STD_FD, mask_all, h, kt, sk] = ControlValues( Controls )
%CONTROLVALUES Calculate mean and std per voxel of control patients
%   Given a series of directories with control patients, this function will
%   mask all of the FD_masked variables to only calculate the mean and std
%   values for non-zero voxel locations across ALL patients.
%
%   Inputs:        subject_numbers
%
%   Outputs:       mean_FD
%                  STD_FD
%                  h - normality test (Kolmogorov-Smirnov)
%                  kt - kurtosis
%                  sk - skewness
% Data sizes
N = size(Controls, 2);
size_x = 47;
size_y = 56;
size_z = 44;

% Load each FD_mask and and create a logical mask where values are NOT
% zero. Store in a N x 47 x 56 x 44 matrix
zero_mask = zeros(N, 47, 56, 44);
for i = 1 : N

    % Grab the filename and load the .mat file
    filename = sprintf('Controls/%s/FD_Olga.mat', Controls{i});
    load(filename, 'Hurst');
    %FD(FD==1/2) = 0;
    Hurst(Hurst==1/2) = nan;
    FD = 2 - Hurst;
    FD(isnan(FD)) = 0;
    A = FD >= 1;
    B = FD <= 2;
    C = A .* B;
    zero_mask(i, :, :, :) = C;

end
% Create a mask to calculate mean only when minimun number of significat
% voxels is achieved
mask_all = zeros(47, 56, 44);
for i = 1 : N
    current_zero_mask = squeeze(zero_mask(i, :, :, :));
    mask_all = mask_all + current_zero_mask;
  end
  mask_all(mask_all < 2) = 0; % sample size for pwr =0.9 is 11 subjects
  mask_all(mask_all >= 2) = 1;
```

```
% Go through each control and store the entire FD_masked matrix
FDs = zeros(N, 47, 56, 44);
for i = 1 : N

   % Grab the filename and load the .mat file
   filename = sprintf('Controls/%s/FD_Olga.mat', Controls{i});
   load(filename, 'Hurst');% changed FD_masked with FD
   %FD(FD==1/2) = 0;
   Hurst(Hurst==1/2) = nan;
   FD = 2 - Hurst;
   FD(isnan(FD)) = 0;
   current_zero_mask = squeeze(zero_mask(i, :, :, :));
   FDs(i, :, :, :) = (FD .* current_zero_mask);
end

mean_FD = zeros(47, 56, 44);
STD_FD = zeros(47, 56, 44);
h = zeros(47, 56, 44);
kt = zeros(47, 56, 44);
sk = zeros(47, 56, 44);

for i = 1 : size_x
   for j = 1 : size_y
      for k = 1 : size_z
         FD1 = squeeze(FDs(:, i, j, k));
         mean_FD(i, j, k) = mean(FD1(FD1 ~= 0));
         mean_FD(isnan(mean_FD)) = 0;
         mean_FD = mean_FD .* mask_all;
         STD_FD(i, j, k) = std(FD1(FD1 ~= 0));
         STD_FD(isnan(STD_FD)) = 0;
         STD_FD = STD_FD .* mask_all;
         h(i, j, k) = kstest(FD1);
         h(isnan(h)) = 0;
         kt(i, j, k) = kurtosis(FD1);
         kt(isnan(kt)) = 0;
         sk(i, j, k) = skewness(FD1);
         sk(isnan(sk)) = 0;
      end
   end
end

end
```

Bibliography

Bär, K.-J., Boettger, M. K., Koschke, M., Schulz, S., Chokka, P., Yeragani, V. K., and Voss, A. (2007). Non-linear complexity measures of heart rate variability in acute schizophrenia. *Clinical neurophysiology*, **118**(9), 2009–2015.

Bassingthwaighte, J. B. and Raymond, G. M. (1995). Evaluation of the dispersional analysis method for fractal time series. *Annals of biomedical engineering*, **23**(4), 491–505.

Benedict, R. and Brandt, J. (2001). Hopkins verbal learning test-revised (hvlt-r): Professional manual. *Lutz: Psychological Assessment Resources*.

Bentley, L. P., Stegen, J. C., Savage, V. M., Smith, D. D., von Allmen, E. I., Sperry, J. S., Reich, P. B., and Enquist, B. J. (2013). An empirical assessment of tree branching networks and implications for plant allometric scaling models. *Ecology letters*, **16**(8), 1069–1078.

Bezo97 (2016). Mandelbulb3D, Fractal surface.

Broadbent, D. E., Cooper, P. F., FitzGerald, P., and Parkes, K. R. (1982). The Cognitive Failures Questionnaire (CFQ) and its correlates. *The British journal of clinical psychology*, **21 (Pt 1)**, 1–16.

Bullmore, E. and Sporns, O. (2009). Complex brain networks: graph theoretical analysis of structural and functional systems. *Nature Reviews Neuroscience*, **10**(3), 186–198.

Bullmore, E., Brammer, M., Williams, S. C., Rabe-Hesketh, S., Janot, N., David, A., Mellers, J., Howard, R., and Sham, P. (1996). Statistical methods of estimation and inference for functional mr image analysis. *Magnetic Resonance in Medicine*, **35**(2), 261–277.

Bullmore, E., Long, C., Suckling, J., Fadili, J., Calvert, G., Zelaya, F., Carpenter, T. A., and Brammer, M. (2001). Colored noise and computational inference in neurophysiological (fmri) time series analysis: resampling methods in time and wavelet domains. *Human brain mapping*, **12**(2), 61–78.

Cohen, N. (2002). Fractal antennas and fractal resonators.

Cox, R. W. (1996). AFNI: software for analysis and visualization of functional magnetic resonance neuroimages. *Computers and biomedical research, an international journal*, **29**(3), 162–173.

Eickhoff S, Stephan KE, Mohlberg H, Grefkes C, Fink GR, Amunts K, Z. K. (2005). A new SPM toolbox for combining probabilistic cytoarchitectonic maps and functional imaging data. *NeuroImage*, **25**(4), 1325–1335.

Eke, A., Herman, P., Bassingthwaighte, J. B., Raymond, G. M., Percival, D. B., Cannon, M., Balla, I., and Ikrenyi, C. (2000). Physiological time series: distinguishing fractal noises from motions. *Pflugers Archiv : European journal of physiology*, **439**(4), 403–415.

Eke, A., Herman, P., Kocsis, L., and Kozak, L. R. (2002). Fractal characterization of complexity in temporal physiological signals. *Physiological measurement*, **23**(1), R1–38.

El Boustani, S., Marre, O., Béhuret, S., Baudot, P., Yger, P., Bal, T., Destexhe, A., and Frégnac, Y. (2009). Network-state modulation of power-law frequency-scaling in visual cortical neurons. *PLoS Comput Biol*, **5**(9), e1000519.

Fox, M. D. and Raichle, M. E. (2007). Spontaneous fluctuations in brain activity observed with functional magnetic resonance imaging. *Nature reviews. Neuroscience*, **8**(9), 700–711.

Friston, K. J., Zarahn, E., Josephs, O., Henson, R., and Dale, A. M. (1999). Stochastic designs in event-related fmri. *Neuroimage*, **10**(5), 607–619.

Goldberger, A. L. (1996). Non-linear dynamics for clinicians: chaos theory, fractals, and complexity at the bedside. *The Lancet*, **347**(9011), 1312–1314.

Goldberger, A. L., Amaral, L. A. N., Hausdorff, J. M., Ivanov, P. C., Peng, C.-K., and Stanley, H. E. (2002). Fractal dynamics in physiology: alterations with disease and aging. *Proceedings of the National Academy of Sciences of the United States of America*, **99 Suppl 1**, 2466–2472.

Herman, P., Sanganahalli, B. G., Hyder, F., and Eke, A. (2011). Fractal analysis of spontaneous fluctuations of the bold signal in rat brain. *Neuroimage*, **58**(4), 1060–1069.

Kannathal, N. and Puthusserypady, S. (2004). Complex dynamics of epileptic EEG. In *Conf Proc IEEE Eng Med Biol Soc*, pages 604–607.

Lazar, N. (2008). *The statistical analysis of functional MRI data*. Springer Science & Business Media.

Lord, C., Rutter, M., and Le Couteur, A. (1994). Autism Diagnostic Interview-Revised: a revised version of a diagnostic interview for caregivers of individuals with possible pervasive developmental disorders. *Journal of autism and developmental disorders*, **24**(5), 659–685.

Lord, C., Risi, S., Lambrecht, L., Cook, E. H. J., Leventhal, B. L., DiLavore, P. C., Pickles, A., and Rutter, M. (2000). The autism diagnostic observation schedule-generic: a standard measure of social and communication deficits associated with the spectrum of autism. *Journal of autism and developmental disorders*, **30**(3), 205–223.

Mandelbrot, J. W. V. and B., B. (1967). Fractional Brownian Motions, Fractional Noises and Applications. *SIAM Rev.*, **10**(4), 422–437.

Maxim, V., Şendur, L., Fadili, J., Suckling, J., Gould, R., Howard, R., and Bullmore, E. (2005). Fractional gaussian noise, functional mri and alzheimer's disease. *Neuroimage*, **25**(1), 141–158.

Meyers, J. E. and Meyers, K. R. (1995). *Rey Complex Figure Test and recognition trial professional manual*. Psychological Assessment Resources.

Nair, D. G. (2005). About being bold. *Brain Research Reviews*, **50**(2), 229–243.

Nan, X. and Jinghua, X. (1988). The fractal dimension of eeg as a physical measure of conscious human brain activities. *Bulletin of Mathematical Biology*, **50**(5), 559–565.

Oldfield, R. C. (1971). The assessment and analysis of handedness: the edinburgh inventory. *Neuropsychologia*, **9**(1), 97–113.

Pauling, L. and Coryell, C. D. (1936). The magnetic properties and structure of hemoglobin, oxyhemoglobin and carbonmonoxyhemoglobin. *Proceedings of the National Academy of Sciences*, **22**(4), 210–216.

Peters, R. (2006). Ageing and the brain.

Roy, C. S. and Sherrington, C. S. (1890). On the regulation of the blood-supply of the brain. *The Journal of physiology*, **11**(1-2), 85.

Scahill, R. I., Frost, C., Jenkins, R., Whitwell, J. L., Rossor, M. N., and Fox, N. C. (2003). A longitudinal study of brain volume changes in normal aging using serial registered magnetic resonance imaging. *Archives of neurology*, **60**(7), 989–994.

Sharma, V. (2009). Deterministic chaos and fractal complexity in the dynamics of cardiovascular behavior: perspectives on a new frontier. *Open Cardiovasc Med J*, **3**, 110–123.

Simson, P. E., Criswell, H. E., and Breese, G. R. (1993). Inhibition of NMDA-evoked electrophysiological activity by ethanol in selected brain regions: evidence for ethanol-sensitive and ethanol-insensitive NMDA-evoked responses. *Brain research*, **607**(1-2), 9–16.

Smirnov, N. (1948). Table for Estimating the Goodness of Fit of Empirical Distributions. *The Annals of Mathematical Statistics*, **19**(2), 279–281.

Smits, F. M., Porcaro, C., Cottone, C., Cancelli, A., Rossini, P. M., and Tecchio,

F. (2016). Electroencephalographic Fractal Dimension in Healthy Ageing and Alzheimer's Disease. *PloS one*, **11**(2), e0149587.

Szeliski, R. and Terzopoulos, D. (1989). From splines to fractals. In *ACM Siggraph Computer Graphics*, volume 23, pages 51–60. ACM.

Tsubokawa, T., Katayama, Y., Kondo, T., Ueno, Y., Hayashi, N., and Moriyasu, N. (1980). Changes in local cerebral blood flow and neuronal activity during sensory stimulation in normal and sympathectomized cats. *Brain research*, **190**(1), 51–64.

Warsi, M. A., Molloy, W., and Noseworthy, M. D. (2012). Correlating brain blood oxygenation level dependent (BOLD) fractal dimension mapping with magnetic resonance spectroscopy (MRS) in Alzheimer's disease. *Magma (New York, N.Y.)*, **25**(5), 335–344.

Weber, A. M., Soreni, N., and Noseworthy, M. D. (2014). A preliminary study on the effects of acute ethanol ingestion on default mode network and temporal fractal properties of the brain. *Magma (New York, N.Y.)*, **27**(4), 291–301.

Wechsler, D. (2014). Wechsler adult intelligence scale–fourth edition (wais–iv).

Wink, A. M., Bernard, F., Salvador, R., Bullmore, E., and Suckling, J. (2006). Age and cholinergic effects on hemodynamics and functional coherence of human hippocampus. *Neurobiology of aging*, **27**(10), 1395–1404.

Zarahn, E., Aguirre, G. K., and D'Esposito, M. (1997). Empirical analyses of BOLD fMRI statistics. I. Spatially unsmoothed data collected under null-hypothesis conditions. *NeuroImage*, **5**(3), 179–197.